JÜLICH
Forschungszentrum

Development, calibration and deployment of an airborne chemical ionization mass spectrometer for trace gas measurements

Dissertation
zur Erlangung des Grades
Doktor der Naturwissenschaften (Dr. rer. nat.)
von
Talat Khattatov

Vorgelegt im
Januar 2019
Bergische Universität Wuppertal

**BERGISCHE
UNIVERSITÄT
WUPPERTAL**

Contents

List of Figures

List of Tables

Acronyms

AC Alternating Current.

ACE Atmospheric Chemistry Experiment.

ADC Analog-to-digital Converter.

AMA Asian Monsoon Anticyclone.

ATAL Asian Tropopause Aerosol Layer.

BB Biomass Burning.

CI Chemical Ionization.

CIMS Chemical Ionization Mass Spectrometry(er).

CLaMS Chemical Lagrangian Model of the Stratosphere.

DBD Dielectric Barrier Discharge.

DC Direct Current.

EMC Electromagnetic Compatibility.

EOS Earth Observing System.

FTS Fourier Transform Spectrometer.

FWHM Full Width Half Max.

FZJ Forschungszentrum Jülich (Research Center Juelich).

GIL Global Interpreter Lock.

GLORIA Gimballed Limb Observer for Radiance Imaging of the Atmosphere.

GPU Ground Power Unit.

GUI Graphical User Interface.

HV High Voltage.

IAGOS In-service Aircraft for a Global Observing System.

IEK-7 Institute of Energy and Climate Research, Stratosphere.

IMR Ion-molecule Reaction.

m/z Mass-to-charge ratio.

MCP Multi Channel Plate.

MDB Myasishchev Design Bureau.

MIPAS Michelson Interferometer for Passive Atmospheric Sounding.

MLS Microwave Limb Sounder.

MPS Main Power Supply.

MS Mass Spectrometry(er).

NICI Negative Ion Chemical Ionization.

OEM Original Equipment Manufacturer.

OOP Object-oriented Programming.

QMS Quadrupole Mass Spectrometry(er).

RF Radio Frequency.

TOF Time-of-flight.

TOFMS Time-of-flight Mass Spectrometry(er).

TPS TOF Power Supply.

UTLS Upper Troposphere and Lower Stratosphere.

UV Ultraviolet.

WMO World Meteorological Organization.

ZEA-1 Central Institute for Engineering, Electronics and Analytics; Engineering and Technology.

ZEA-2 Central Institute for Engineering, Electronics and Analytics; Electronic Systems.

Abstract

Some ultra trace gas species present in the upper troposphere and lower stratosphere (UTLS) region at low part-per-billion and part-per-trillion mixing ratios are known to have a major effect on atmospheric chemistry and climate. Chlorine and bromine species causing strong ozone depletion and sulfur dioxide (SO_2) driving aerosol formation processes of high relevance to the global radiative budget are prominent examples. Nitric acid (HNO_3) is another species, which is quite important for particle formation and denitrification processes. In order to fully understand and reliably model the involved processes for climate predictions, spatially highly resolved in-situ measurements of these species are needed. Therefore robust instruments are required that can perform very sensitive and accurate measurements of ultra-trace species in the extremely challenging UTLS environment from balloons or favorably high-flying aircraft, which impose stringent mechanical and electrical constraints.

Here I describe the set-up, test, characterization, deployment, data analysis, and preliminary results of the new FunMass instrument tailored to the deployment on the high-flying research aircraft M-55 Geophysica. FunMass utilizes the established techniques of chemical ionization mass spectrometry (CIMS) in an unprecedented package pairing measurement sensitivity and accuracy with high versatility at reasonable instrumental weight and dimensions.

FunMass was set up based on a laboratory prototype [1]: the concept of its transfer stage with an ion funnel and its dielectric barrier discharge (DBD) ion source was adapted for the airborne version of the instrument. The ion funnel improves the sensitivity of the instrument at least by one order of magnitude and the DBD ion source is an excellent replacement for the logistically very challenging radioactive ion source, which is widely used for CIMS. A big advantage of the TOF-MS technique for airborne measurements is that it is capable of fast and simultaneous acquisition of full mass spectra and therefore measurements of many different ion species, which is very important since flight hours of research aircraft are a very limited resource.

FunMass has been characterized in detail for measurements of HNO_3, SO_2 and HCN with CO_3^- as the reagent ion, showing outstanding sensitivity. For SO_2 and HCN we report detection limits very close to the best published, and for HNO_3 almost one order of magnitude better than any other CIMS. FunMass was fully tested in the climate chamber at relevant stratospheric temperatures and pressures before its first fully operational deployment on board of M-55 Geophysica.

FunMass is calibrated in the laboratory for all targeted species employing a setup with high accuracy permeation devices. Due to the complications with the CIMS technique, it also has an in-flight calibration for at least one species to ensure accurate measurements.

A new software was developed for FunMass to take full control over the instrument during the flight and autonomously conduct measurements, as well as to handle abnormal situations, preventing possible instrument failures and damage of the equipment.

The first deployment of the FunMass instrument happened in Kathmandu, Nepal in July/August 2017 within the aircraft campaign of the STRATOCLIM project, which aimed to investigate the transport processes between the troposphere and the stratosphere during the Asian summer monsoon (ASM).

During its first campaign, FunMass successfully measured HNO_3 and HCN. First intercomparisons of these measurements with the data from other in-situ instruments on board of M-55 Geophysica and with measurements from remote sensing satellite-based

instruments are presented in this work, emphasizing the high quality and resolution of the FunMass measurements.

Further measurements of HNO_3 and HCN in the UTLS region with FunMass can aid to improve the atmospheric models. The obtained HNO_3 and HCN data reveal several very interesting features that remain to be fully refined in further studies, which can help to improve the chemical and dynamical models of the atmosphere. FunMass has a great potential to contribute further high-quality data on the established and several additional chemical species of high relevance in the UTLS first of all SO_2 but also many nitrogen, chlorine, and bromine species employing alternate ionization schemes.

Chapter 1

Introduction

An accurate interpretation of the future of the Earth's climate could help to deal better with the derived changes in fresh water distribution, sea level and natural catastrophes as well as with their relevant geopolitical, economical and social consequences. In order to make reliable long term climate predictions, all chemical and dynamical processes in the atmosphere have to be better understood and quantified. Existing atmospheric models can be improved by including a larger number of atmospheric processes. Accurate in-situ measurements can significantly contribute to the required data base. For example, a major breakthrough in the understanding of the polar winter ozone chemistry was achieved thanks to in-situ measurements of ClO and BrO in the lower stratosphere [2] over the Antarctic continent. Despite measured mixing ratios of ClO and BrO being in the low ppb and even ppt range, such low concentrated species (also termed ultra trace gases) showed to be the main drivers of the ozone hole formation in the Southern hemisphere. Thus, sensitive measurements are advised, with a special focus on processes of high relevance for climate and the ozone balance.

This work describes the development of a versatile innovative sensitive airborne chemical ionization time-of-flight mass spectrometer (FunMass) for ultra trace gas measurements in the upper troposphere lower stratosphere (UTLS), which was first deployed in a campaign over the Asian monsoon region.

1.1   Trace gases in the atmosphere

A trace gas is a gas that is present in the atmosphere at a concentration lower than 1 %. In spite of their scarcity, trace gases have a substantial influence on many processes in the atmosphere (as already shown above for active bromine and chlorine species in the stratosphere). Changes in their concentration can have direct and indirect impacts on the Earth's climate.

For example, the rise in the concentration of CO_2 and CH_4, which together with H_2O are the main drivers of the greenhouse effect, is the main contributor to global warming [38].

The importance of a few other trace gases in the UTLS region will be defined in some more detail below, as the instrument described in this work is focusing on measuring them in particular.

1.1.1   Sulfur dioxide SO_2

One of the main sources of SO_2 in the stratosphere (among other sulfur compounds) are volcanic eruptions [4, 30, 67]. Depending on the intensity of the eruption, SO_2 can be directly injected to the UTLS region. Another pathway of sulfur compounds to the stratosphere is tropical convection [46], including the one during the Asian monsoon season, when highly polluted tropospheric air from Southeast Asia penetrates into the stratosphere [73]. A significant non-volcanic source of SO_2 in the stratosphere is UV photolysis of OCS with following oxidation [13, 44]. In the UTLS most of SO_2 is converted to H_2SO_4 (sulfuric acid) by the following reactions:

$$SO_2 + OH \longrightarrow HSO_3 \tag{1.1}$$
$$HSO_3 + O_2 \longrightarrow SO_3 + HO_2 \tag{1.2}$$
$$SO_3 + 2\,H_2O \longrightarrow H_2SO_4 + H_2O \tag{1.3}$$

By clustering with H_2O, H_2SO_4 forms aerosol particles and plays an important role in the Junge layer [41] formation (although it is still not quantitatively understood). The aerosols in the Junge layer partially block, scatter and absorb incoming sun radiation, causing a global cooling effect. According to IPCC [38] the aerosol layer reduced the radiative forcing by more than $0.5\,Wm^{-2}$ since 1750.

The mixing ratios of SO_2 in the UTLS are very low down to a few hundred ppt [33], which requires sensitive measurement techniques.

1.1.2   Nitric acid HNO_3

HNO_3 is an important stratospheric nitrogen containing species and it is a member of the group of reactive odd nitrogen known as NOy (NOy=HNO_3, NO_2, NO, N_2O_5, $ClONO_2$, ...). Sources of NO_2 and NO, which are precursors of other NOy compounds, include lightning [82], biomass burning [18] and traffic. By convection in the tropics they can be introduced to the UTLS, if they are not washed out before by rain. To emphasize the importance of HNO_3 in stratospheric chemistry, some of the NOy reactions are discussed below. The main formation reaction of HNO_3 is

$$NO_2 + OH + M \longrightarrow HNO_3 + M \tag{1.4}$$

The main loss of HNO_3 in the stratosphere consists of the two following reactions [8]:

$$HNO_3 + h\nu \longrightarrow OH + NO_2 \tag{1.5}$$
$$HNO_3 + OH \longrightarrow NO_3 + H_2O \tag{1.6}$$

NO_2 and NO_3 (and other NOy species) are involved in catalytic ozone loss reactions [64, 66]. For example NO_2 and NO drive the following simple ozone loss cycle:

$$NO_2 + O \longrightarrow NO + O_2 \tag{1.7}$$
$$NO + O_3 \longrightarrow NO_2 + O_2 \tag{1.8}$$
$$O_3 + h\nu \longrightarrow O + O_2 \tag{1.9}$$
$$\text{Net: } 2\,O_3 \longrightarrow 3\,O_2 \tag{1.10}$$

The complete picture of the NOy chemistry is much more complex [66, 70], and good in-situ measurements of HNO_3 and other NOy will contribute to the improvement of the existing atmospheric chemistry models. Accurate in-situ measurements of HNO_3 are challenging because of its low mixing ratios (from ppt to ppb [26]) and its "stickiness".

1.1.3 Hydrogen cyanide HCN

HCN is mostly produced by biomass burning (BB). Other sources like fossil fuel combustion are neglectable [51], which makes it a good tracer of BB [31]. This, together with the fact that HCN has a strong sink from contact with the ocean, makes HCN data very useful for the development and verification of transport models of the atmosphere [50, 73]. Tereszchuk et al. [88] highlighted advantages of HCN as a BB tracer over CO, which has additional anthropogenic sources. HCN measurements can be used to quantify exchange between the troposphere and stratosphere. Mixing ratios of HCN vary in the range from 200 ppt to 700 ppt in the UTLS [22].

1.2 Platforms for measurements in the UTLS region

1.2.1 Satellites

Satellites can be equipped with remote sensing instruments to measure trace gases in the Earth's atmosphere. Some examples of remote sensing instruments which operate from satellites capable of measuring HNO_3 among many other species are:

- MIPAS (Michelson Interferometer for Passive Atmospheric Sounding) was on board of the European satellite Envisat (Environmental Satellite). It was a Fourier transforming infrared spectrometer which observed the Earth's limb emission (6 km to 68 km) in range from 4.15 μm to 14.6 μm. 2002-2012.

- ACE-FTS (Atmospheric Chemistry Experiment - Fourier Transform Spectrometer) is the main instrument on the Canadian mini satellite SciSat (Science Satellite). It is an infrared solar occultation spectrometer and covers the range of the atmosphere between 10 km and 50 km and the IR spectrum from 2.4 μm to 13.3 μm. 2003 - present.

- MLS (Microwave Limb Sounder) is one of the four instruments on the American EOS (Earth Observing System) Aura satellite. MLS observes the faint microwave emissions (118 GHz, 190 GHz, 240 GHz, 640 GHz and 2.5 THz) from rotating and vibrating molecules in the limb (11 km to 55 km) of the Earth's upper atmosphere. 2004 - present.

The main drawback of current satellite instruments is their low resolution, which is usually in the range of 2 km to 6 km. Future instruments will have much better resolution by deploying improved and new techniques like, for instance, the instrument GLORIA (Gimballed Limb Observer for Radiance Imaging of the Atmosphere), commonly developed in the Karlsruhe Institute of Technology (KIT) and the Research Center Jülich (FZJ).

1.2.2 Scientific Balloons

Balloons are the only available platform for in-situ measurements on altitudes above 21 km, where no research aircraft can fly. For example, NASA's zero pressure balloons can lift payloads as heavy as 2700 kg up to 38 km [61]. The high carrying capacity of balloons allows them to host several comparably heavy instruments simultaneously. In addition, they don't constrain the dimensions and size of the scientific payload as much as other platforms do, because it is placed in a freely hanging gondola. The main drawback of balloons for atmospheric studies is the unreliable predictability of their flight trajectory,

due to changing winds. Therefore, interesting atmospheric regions may be hard to reach by balloons. Among all the platforms for in-situ measurements, balloons can fly the highest, which is clearly their big advantage. But on the other hand, the instruments carried on them are exposed to the biggest pressure changes, which can be a challenging issue to deal with for many measurement techniques.

1.2.3 Aircraft

Scientific equipment can be also placed on aircraft, both commercial and research.

Projects like IAGOS (In-service Aircraft for a Global Observing System, [37]) enroll commercial airlines for measurements of different atmospheric parameters at altitudes up to 12 km (Service ceiling of Airbus A321 is around 12 km). Unfortunately, that means that in the tropics they fly well below the tropopause. They are very efficient to make frequent measurements, which allow to determine trends in the atmospheric composition. However, data are mostly collected at fixed routes.

On the other hand, scientific research aircraft like the German HALO or the Russian M-55 Geophysica can fly higher (up to 15 km and 21 km respectively) and be scheduled to do scientifically interesting routes, e.g. flying over and around convective systems, which would not be possible with commercial airlines. The scientific payload of the M-55 Geophysica can weight up to 2000 kg, which is significantly more than what typically could be deployed within projects like IAGOS, allowing it to accommodate highly sophisticated complex instruments. Measurements from research aircraft are usually done within dedicated campaigns, which have to be carefully planned and organized, especially if the campaign has to be based in countries, where flight clearances are hard to obtain. Those campaigns are usually motivated by lack of data about specific atmospheric process and research aircraft are almost never deployed to do measurements on the regular base.

The institute IEK7 (Institute of Energy and Climate Research: Stratosphere, Research center Jülich), where this work was done, participates in the STRATOCLIM project (STRATOspheric and upper tropospheric processes for better CLIMate predictions). The FunMass instrument developed within this work was built to participate in the Asian Monsoon aircraft campaign of STRATOCLIM on board of the M-55 Geophysica.

1.3 Chemical ionization time-of-flight mass spectrometry

Chemical ionization mass spectrometry (CIMS) was developed as a versatile measurement tool in the past 50 years [58]. Some of its advantages include:

- high sensitivity,

- selectivity,

- minimal sample preparations,

- good linearity,

- high temporal resolution.

Negative ion CIMS with different reagent ions can be used to measure HNO_3, HCN, SO_2 and many other relevant atmospheric species [26, 34, 35, 36]. There are already several airborne CIMSs developed for measurements of trace gases. Most of them are quadrupole mass spectrometers (QMS) [9, 42, 74, 81], although in the last years the use of time-of-flight
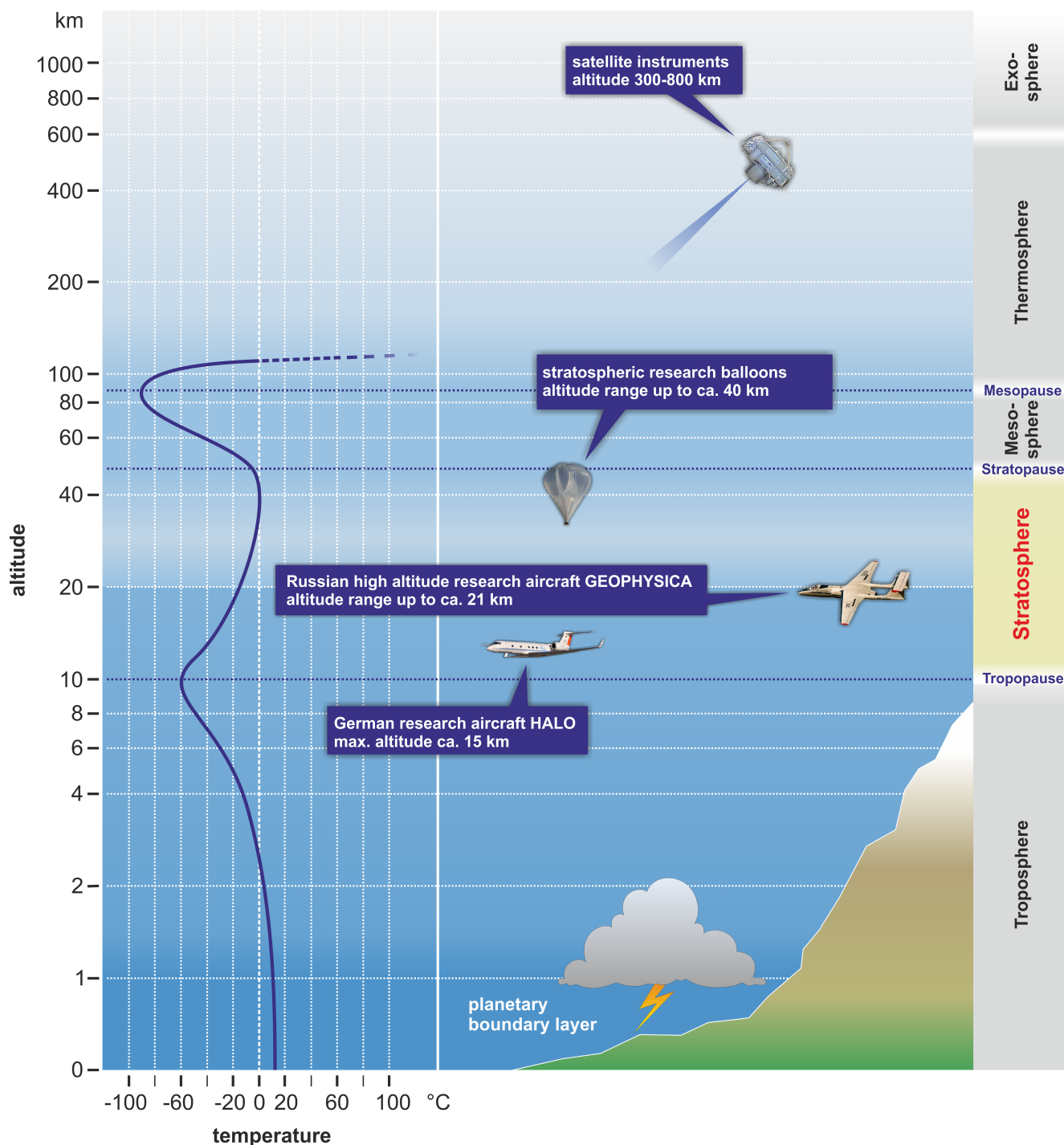
Figure 1.1: Schematic of the stratosphere structure. Overview of the different measurement platforms for stratospheric research. Source: Karlheinz Nogai, IEK-7.

mass spectrometers (TOF MS) is spreading [49, 57]. The main advantage of the TOF mass analyzer over the quadrupole technique is that a wide range of different ions is analyzed simultaneously and high mass resolution is possible.

On the other hand, the main drawback of TOF MS is that its mass analyzer operates at pressure below 5.0×10^{-6} hPa, whereas QMS may operate at around 1.0×10^{-4} hPa. This requires an additional ion transfer stage and more pumping capacity for the TOFMS.

1.4   Structure of the thesis

This thesis describes the development of the airborne CI TOF MS called FunMass for ultra trace gas measurements in the UTLS. In Chapter 2, an introduction to the topics of CIMS and TOF-MS is given. Chapter 3 shows analysis of the potential overlaps in the mass spectrum for the chosen TOF mass analyzer with CO_3^- as the reagent ion. Chapter 4 discusses critical aspects of the ion chemical kinetics involved in the CI process. A detailed description of FunMass together with its development history and its performance during the STRATOCLIM campaign in July/August 2017 in Kathmandu are given in Chapter 5. Full characterization of FunMass follows in Chapter 6 together with the calibration for HNO_3, HCN and SO_2. Chapter 7 comprises a full description of the laboratory software, data acquisition and the flight control program, specifically developed for the autonomous performance of the instrument on board. First results from the STRATOCLIM campaign are discussed in Chapter 8, before a summery is given in Chapter 9.

Chapter 2

Fundamentals of CI TOF MS

In this chapter, a short introduction to the topics of chemical ionization (CI) and time-of-flight (TOF) mass spectrometry (MS) is given.

2.1 Mass spectrometry

"The basic principle of mass spectrometry is to generate ions from either inorganic or organic compounds by any suitable method, to separate these ions by their mass-to-charge ratio (m/z) and to detect them qualitatively and quantitatively by their respective m/z and abundance" [24] .

All MS instruments follow the same basic structure and consist of an inlet stage, an ion source, a mass analyzer (separates ions by m/z) and a detector. The mass analyzer and detector operate under high vacuum. If other parts of the mass spectrometer need to operate at higher pressure, transfer stages (and a proper pumping system) to reduce the pressure between them and the mass analyzer are needed. Mass spectrometers differ in the types of used mass analyzers and ionization procedures. Further sections focus on CI TOF MS (Figure 2.1) since it is the technique used in the instrument developed within this work.

2.2 Negative-ion chemical ionization

Chemical ionization uses a positively or negatively charged reagent ion $R^{-(+)}$ to ionize an analyte molecule A and form a corresponding product ion P^-, as shown schematically in the following chemical reaction:

$$A + R^{-(+)} \longrightarrow P^{-(+)} + B. \tag{2.1}$$

Chemical ionization consists of two separate stages: the reagent ion formation taking place in the ion source ("hot" zone), and the ionization reactions (Equation 2.1) in the ion-molecule reaction (IMR) zone. The further discourse will focus only on negative ion chemical ionization (NICI), which has been successfully used for the measurement of relevant atmospheric trace gases including HNO_3, SO_2 and HCN [36, 95].

2.2.1 Reagent ion formation

Negative ions can be formed through one of the following processes [14, 24]:
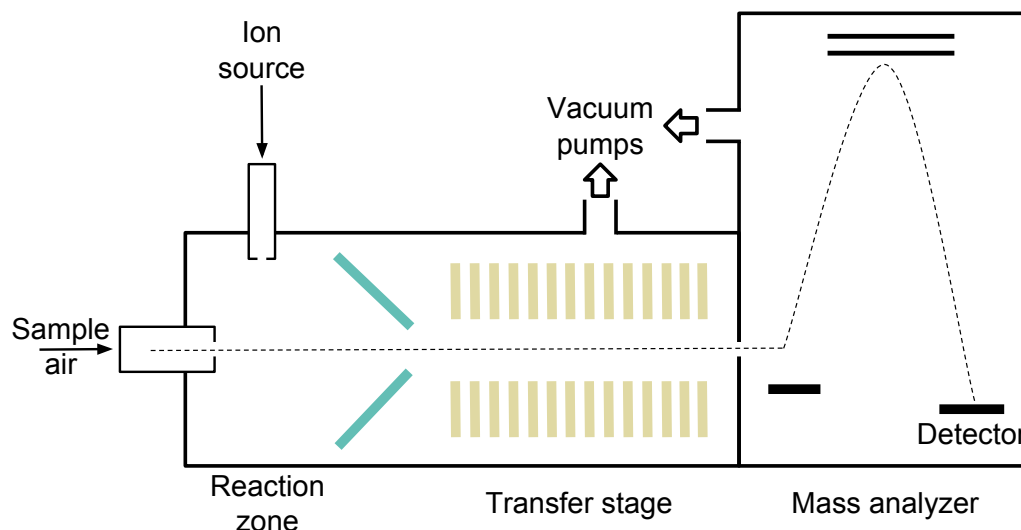
Figure 2.1: A basic schematic of CI TOF mass spectrometer.

- Resonance electron capture: $X + e^- \longrightarrow X^{-\bullet}$.

- Dissociative electron capture: $MX + e^- \longrightarrow M^{\bullet} + X^-$.

- Ion-pair formation: $MX + e^- \longrightarrow M^+ + X^- + e^-$.

- Dissociation: $MX \longrightarrow M^+ + X^-$.

The free electrons needed for the negative ion formation can be produced in many different ways, e.g. photo ionization, $\alpha/\beta-$ radiation or any kind of discharges etc. In the ionization processes always both positive and negative ions are actually formed, and it is only a matter of the polarity of the applied voltage which ions will be guided and used further.

2.2.2   Ion molecule reaction

After the reagent ions are formed, they are mixed with the analyte in the IMR region. The corresponding analyte ions P^- or clusters of analyte with the reagent ion, generally termed product ions, can be formed.

$$A + R^- \longrightarrow P^- + B \tag{2.2}$$

$$A + R^- \longrightarrow R\,A^- \tag{2.3}$$

Usually the analyte is not exposed to the hot zone to avoid e.g. unwanted dissociation of the analyte molecules and keep ions identification more predictable. This is of course just a very simplified description of chemical ionization. In the dielectric barrier discharge (DBD) ion source employed in this work, in CO_3^- mode, the ion source produces O^-, O_2^- by electron capture in a first step. Then directly in the ion source chemical ionization of CO_2 takes place (Equations 5.2 - 5.5) to produce the reagent ions.

2.3   The TOF mass analyzer

TOF mass analyzers separate ions by their m/z ratios causing them to have different "time of flight" within the flight tube and therefore reaching the detector at different times. The TOF
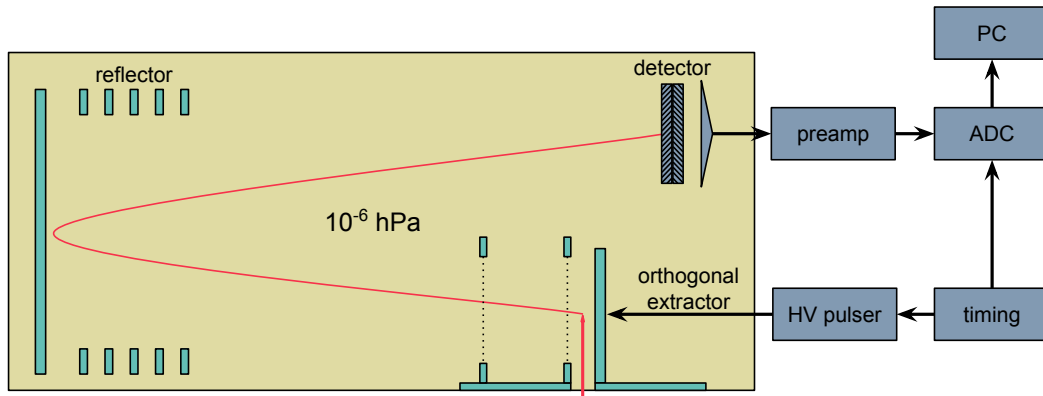
Figure 2.2: Schematic of a TOF mass analyzer with orthogonal extraction.

MS operational principal is explained below based on a TOF mass analyzer with orthogonal extraction (Figure 2.2), similar to the one used in the FunMass instrument.

After entering the mass analyzer, ions are accelerated orthogonally by an extractor as shown in Figure 2.2. After moving through the extractor with voltage U, all potential energy of the ion E_{el} is converted into kinetic energy E_{kin}.

$$E_{kin} = \frac{m_i v^2}{2} = qU = zeU = E_{el}, \tag{2.4}$$

where m_i - mass of the ion, v - attained velocity, q - electric charge of the ion, z - charge state of the ion, e - electric charge of a single electron.
From Equation 2.4 the attained velocity is:

$$v = \sqrt{\frac{2zeU}{m_i}}. \tag{2.5}$$

After the extraction, ions will fly the defined distance s before being detected by the micro channel plate (MCP) detector. With the assumption that ions just drift to the detector in a field-free space with a constant velocity, they will reach the MCP after time t:

$$t = \frac{s}{v} = s\sqrt{\frac{m_i}{2zeU}}. \tag{2.6}$$

From Equations 2.5 and 2.6 it follows that lighter ions leave the extractor with higher velocity and therefore reach the detector faster than heavier ions with the same charge, which is the basic operational principle in TOF MS.
From Equations 2.6, a direct relationship between the mass-to-charge ratio m_i/z and the time of detection t can be inferred, allowing us to "identify" the ion (mass calibration):

$$\frac{m_i}{z} = 2Ue\left(\frac{t}{s}\right)^2. \tag{2.7}$$

The time interval Δt between the detection of two ions with different mass-to-charge ratios m_1/z_1 and m_2/z_2 can be calculated as follows:

$$\Delta t = \frac{s}{\sqrt{2eU}}\left(\sqrt{\frac{m_1}{z_1}} - \sqrt{\frac{m_2}{z_2}}\right). \tag{2.8}$$

In order to increase this time interval for ions with close mass-to-charge ratios, i.e. being able to distinguish them in the mass spectra, the most obvious solution is to increase the flight distance s. To do so and keep the analyzer compact, often one (Figure 2.2) or several reflectors ([52]) are used. The TOF MS in Figure 2.2 operates in the so called "V-mode", while other TOF mass analyzers with three reflectors can operate in "W-mode", therefore increasing the resolution.

A micro channel plate (MCP) or several of them stacked together are used to detect ions. An MCP consists of millions of tiny linear channel electron multipliers. A high voltage (from few hundreds Volts up to 3 kV) is applied between the front and the back part of the plate. Therefore any arriving ion causes an avalanche of electrons inside the micro channel where it impacts. The subsequent output current of secondary emitted electrons from the MCP is proportional to the number of arrived ions. This signal is processed and converted to the mass spectrum by an analog to digital converter (ADC) and recorded on to the hard drive. One mass spectrum is generated by a single extraction. The next one can be done not earlier than the heaviest ion from the previous extraction is expected to reach the detector. The typical extraction frequency for the FunMass instrument is 20 kHz (every 50 μs) for the mass range of 0 Th to 800 Th (around 100 000 data points). Normally, spectra get averaged before being stored on the PC, therefore the acquisition frequency is much lower being currently set to 2 Hz.

The operational principle of TOF mass analyzers requires the kinetic energy of the ions to stay unchanged during the drift after the extraction, thus they should face almost no collisions, i.e. the mean free path inside the TOF mass analyzer should exceed its dimensions. The mean free path l can be calculated with the following formula:

$$l = \frac{kT}{\sqrt{2}\pi d^2 p},$$
(2.9)

where

p - pressure,

d - kinetic diameter of the molecule,

k - Boltzmann constant $1.38 \times 10^{-23}\,\mathrm{J\,K^{-1}}$,

T - temperature.

In order to have a mean free path longer than 0.5 m (which exceeds the dimensions of FunMass TOF 265 mm × 175 mm × 115 mm) for a comparably large molecule $d = 500$ pm at room temperature $T = 300$ K, the TOF mass analyzer should be operated at pressures lower than 3.73×10^{-5} hPa. Usually they are operated at pressures 5×10^{-6} hPa and lower.

Chapter 3

Overlapping peaks in a mass spectrum

Mass spectrometry is based on the separation of ions by their mass-to-charge-ratios m/z. A general problem of mass spectrometry is that due to limited resolution of the mass analyzer, peaks of two or more ions with close m/z ratio may overlap. That could affect the interpretation of a mass spectrum. This chapter briefly describes the development of a python function to predict all potential overlaps in mass spectra for the chemical ionization with CO_3^- as reagent ion, to aid the qualitative analysis of mass spectra. To solve this problem, the open source python library `Pyteomics` was used. A function to return all isotopologues of a given molecule was developed during the research and now it is a built-in function of the `Pyteomics` framework.

3.1 Theory

3.1.1 Resolution

Mass resolution is the observed m/z divided by the smallest difference $\triangle(m/z)$ for two ions that can be separated:

$$R = \frac{m}{\triangle m} = \frac{(m/z)}{\Delta(m/z)}.$$

(3.1)

Two neighbor peaks of the same size are resolved when the valley between them decreases to 50% of their intensity (Figure 3.1). This definition is known as full width half maximum (FWHM) definition of resolution, R_{FWHM}. It's widely used in TOF MS. For FunMass, the mass spectrometer CTOF from TofWerk AG was chosen because its resolution ($R_{FWHM} = 700$) is sufficient to fulfill most of the measurement objectives, as shown in Section 3.3. Two peaks m and $m + \triangle m$ of similar intensity can be separated by an instrument with resolution R if

$$\Delta m > \frac{m}{R}.$$

(3.2)

3.1.2 Typical MS for chemical ionization with CO_3^- as a reagent ion.

All abundant ions expected in CO_3^- CIMS mass spectra of stratospheric air are shown in Table 3.1. Together with the reagent ion CO_3^- the ion source produces ions like O^-, O_2^- and O_3^-. In case of a leak of ambient air into the ion source, it would also form NO_2^- and NO_3^-. In the presence of water vapor, ion clusters start forming [83]. At a pressure of 30 hPa in the funnel for the most abundant ion CO_3^-, ion clusters with up to two water
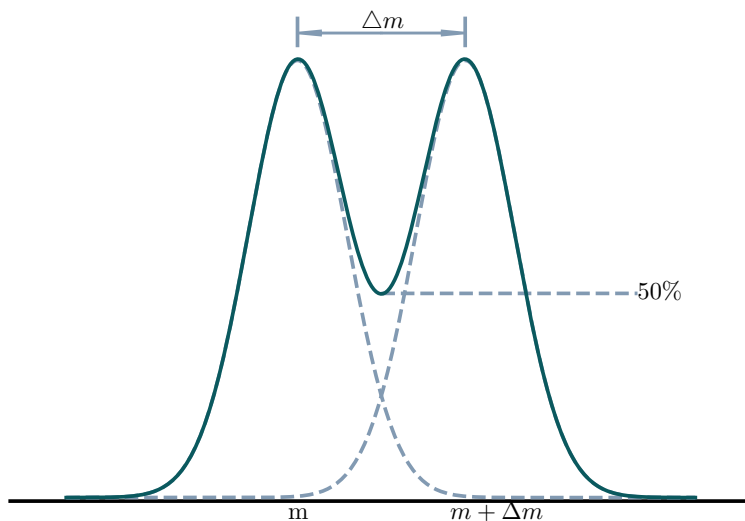
Figure 3.1: Full width half maximum (FWHM) definition of resolution.

molecules were observed for our main setup. In addition to the ions listed in Table 3.1, their water clusters, with up to two molecules of H_2O, will also be included in calculations to find all potential overlaps.

Origin	Ion	Nominal monoisotopic mass	Reference
SO_2	SO_3^-, SO_5^-	80, 112	[56], [83], [26]
HNO_3	$CO_3^-(HNO_3)$	123	[26], [86]
HO_2NO_2	$CO_3^-(HO_2NO_2)$	139	[86]
H_2O_2	$CO_3^-(H_2O_2)$	94	[86]
HCN	$CO_3^-(HCN), CN^-$	87, 26	[80], [this work]
SO_3	SO_4^-	96	[76]
H_2SO_4	$HSO_4^-, CO_3^-(H_2SO_4)$	97, 158	[76]
OH	HCO_3^-	61	[1]
O_2	O^-, O_2^-, O_3^-	16, 32, 48	[1], [this work]
N_2, O_2	NO_3^-	62	[1], [this work]

Table 3.1: List of ions observed in a mass spectrum using CO_3^- as reagent ion.

3.1.3 Isotopologues in a mass spectrum

Isotopes are atoms which have the same number of protons in the nuclei but differ in the number of neutrons. Isotopologues are molecules which differ only in their isotopic composition, therefore they do in mass as well. The ions from Table 3.1 are represented not by a single peak in the spectrum but by an isotopic pattern of peaks. The relative

abundance of isotopes can be found in the NIST database [12]. The exact mass of the most abundant isotope is called monoisotopic mass. The same term is used for the exact mass of the most abundant isotopologue of a molecule. The isotopic distribution of a molecule can be described with the following formula from Gross [24]:

$$(a_{1,1} + a_{1,2} + ... + a_{1,n_1})^{k_1}(a_{2,1} + a_{2,2} + ... + a_{2,n_2})^{k_2}(a_{3,1} + a_{3,2} + ... + a_{3,n_3})^{k_3}... \qquad (3.3)$$

where $a_{1,1}$, $a_{1,2}$, etc. represent isotopes of the first element, $a_{2,1}$, $a_{2,2}$, etc. represent isotopes of the second element and so on until all elements are included. The exponents k_1, k_2, etc. give the number of atoms of these elements as in the sum formula. After the equivalent terms in Equation 3.3 are combined, the number of isotopologues of a molecule is equal to the number of terms in it. A different approach can be used to calculate this number. It consists of two steps. First, a number of isotopic combinations for each element is calculated, then these numbers are multiplied. The number of isotopic combinations of k atoms of a chemical element with n isotopes is equal to the number of k-combinations with repetitions from a set of n different items. In combinatorics, the following notation $\left(\binom{n}{k}\right)$ (n multichoose k) is used for it [5], and it is equal to

$$\left(\binom{n}{k}\right) = \frac{(n + k - 1)!}{k!(n - 1)!}. \qquad (3.4)$$

Then the number of isotopologues is equal to

$$\left(\binom{n_1}{k_1}\right) \left(\binom{n_2}{k_2}\right) \left(\binom{n_3}{k_3}\right) ..., \qquad (3.5)$$

where n_i is a number of isotopes of the ith element, and k_i is the number of its atoms as in the sum formula.

For example, carbon has two stable isotopes (^{12}C and ^{13}C) and oxygen has three (^{16}O, ^{17}O and ^{18}O), therefore the number of CO_3 isotopic configurations is equals to 20 $\left(\left(\binom{2}{1}\right) \left(\binom{3}{3}\right) = 20\right)$. The abundance of the monoisotopic molecule may be by a huge factor higher than the abundance of the most scarce one. For CO_3 this factor is about 10^{12}. The magnitude of expected variations in peaks intensities for the ions from Table 3.1 are of the order 10^6. Considering isotopologues with relative abundance below 10^{-8} is not necessary, since in case of the overlap with the main monoisotopic peak of another ion they will not contribute more than 1% to the intensity of that peak. This is true even for overlapping isotopologues of abundant reagent ion water clusters, with low concentration product ions. Nevertheless here all isotopologues were considered, due to the low computational costs of the procedures.

3.2 Calculations

3.2.1 Short overview of the Pyteomics 3.4 framework

To calculate ion masses and their abundances in Python, the opensource library `Pyteomics` was chosen. For a brief discussion of why Python was chosen, see Section 7.1. `Pyteomics` was developed by Goloborodko et al. [23] to address the needs of data analysis in mass spectrometry-based proteomics. For the overlap problem, the following functions of the module `mass` were used:

- `Composition` - this class stores the chemical composition of a substance

```
>>>mass.Composition('H2O')
Composition({'H': 2, 'O': 1}) # shows composition of water: two atoms of
    hydrogen and 1 atom of oxygen
```

- `nist_mass()` - this function returns a dictionary with the exact masses and abundances of all isotopes of the element

```
>>>mass.nist_mass['H']
{0: (1.00782503207, 1.0), # 0 always the most abundant isotope
 # for others
 # nominal mass: (exact mass, abundance)
 1: (1.00782503207, 0.999885),
 2: (2.0141017778, 0.000115)}
```

- `isotopic_composition_abundance()` - this function calculates the relative abundance of a given isotopic composition

```
>>>mass.isotopic_composition_abundance('H[2]2O[16]')
1.319286325e-08   # relative abundance of heavy water
```

- `calculate_mass()` - this function calculates the exact mass of a given isotopic composition

```
>>>mass.calculate_mass('H[2]2O[16]')
20.02311817516     # exact mass of heavy water
```

3.2.2   Function to return all isotopologues

To find all possible overlaps in the spectrum, all isotopologues of the ions from Table 3.1 should be considered. There was no function to return all isotopic combinations for a given molecule in Pyteomics before the version 3.4.1. Partly this functionality is available in the online tool ChemCalc [65]. But ChemCalc only returns the most abundant isotopologues. The threshold of abundance is greater than the necessary 10^{-8} described above, and it cannot be set by the user. For this purpose an additional function had to be created.

For example, to iterate through all isotopologues of H_2O, all oxygen isotopes (('O[16]'[1], 'O[17]', 'O[18]') should be individually attached to all the possible combinations of two hydrogen atoms ('H[1]H[1]', 'H[1]H[2]', 'H[2]H[2]'). Writing a script to list or iterate through all isotoplogs of a specific molecule is relatively straightforward, especially for small molecules. For a water molecule only two for-loops are needed:

```
for h2 in ['H[1]H[1]', 'H[1]H[2]', 'H[2]H[2]']:    # iterating through all possible
    combinations of hydrogen isotopes in H2O
  for o in ['O[16]', 'O[17]', 'O[18]']:            # iterating through all possible
    combinations of oxygen isotopes in H2O
    print(h2 + o)
```

---

[1]In [] stands nominal mass of the isotope

The challenge is to create a versatile routine which could list all istopologues of any given molecule. To solve this problem, two aspects had to be addressed:

- automatically generate all isotopic combinations for k atoms of the same element;

- ensure that the algorithm will consider all atoms independent of how complex the molecule is.

The first one is a well known combinatorial problem and already implemented in the function `combinations_with_replacement()` from the built-in Python module `itertools` [19]. This function takes two arguments: a set of items (any iterable Python object) and an integer number k. It returns all possible k length combinations of elements from the set allowing individual elements to be repeated more than once. Example from the Python documentation [19]:

```
# combinations_with_replacement('ABC', 2) --> AA AB AC BB BC CC
```

In the present case the first argument will be a list of all isotopes of a given element, and the second one is the number of atoms of this element in the sum formula of the molecule.

The second problem is solved with the function `product()` from the same module `itertools` [19]. This function is roughly equivalent to nested for-loops like in the example with water above. Example from the Python documentation [19]:

```
# product('ABCD', 'xy') --> Ax Ay Bx By Cx Cy Dx Dy
```

This function takes an arbitrary number of iterable sets. Taking only one element from each set, it returns all possible chains of elements. In our case, the sets are lists of isotopic combinations of k atoms for each unique element in the formula, where k is the index of this element.

Based on the functions described above, a function `all_isotopologues()` to return all isotopologues of a given molecule was written. The full implementation of the function `all_isotopologues()` can be found in C.1.

3.3 Results

3.3.1 Unresolved peaks

All overlaps in the spectrum of chemical ionization with CO_3^- as a reagent ion were calculated for mass spectrometers with resolution $R \leq 700$. For the quantitative analysis of a mass spectrum, preferably monoisotopic peaks should be used, especially for the ions from Table 3.1, because of the significant predominance of their monoisotopic peaks. Unresolved peaks were filtered to find overlaps which involve at least one monoisotopic peak. These results are shown in Table 3.2 sorted in descending order of total relative abundances.

The monoisotopic peak of HSO_4^- could not be resolved neither from the monoisotopic peak of $HCO_3^-(H_2O)_2$, nor from $CO_3^-(H_2O)_2$ with one ^{13}C or one ^{17}O. Also the overlap of the monoisotopic peaks of SO_4^- and $CO_3^-(H_2O)_2$ cannot be resolved. A mass spectrometer with resolution higher than 2000 is needed to resolve these peaks. Therefore FunMass is not able to measure H_2SO_4 and SO_3 in CO_3^- mode, however it could do H_2SO_4 in NO_3^- mode [103], which is much more selective.

3.3.2   Contribution to open source

The source code (shown in C.1) of the function `all_isotopologues()`, which returns all isotopologues of a given molecule, was submitted to the authors of the `Pyteomics` library, and since version 3.4.1 it is a built-in function. It can be found in the module `mass` under the name `isotopologues()`.

Nominal mass	Peak 1	Peak 2	Minimum resolution R
96	$^{16}O_4{}^{32}S$ SO_4 9.41E-01	$^{12}C^{16}O_5{}^1H_4$ $CO_3(H_2O)_2$ 9.77E-01	1773
97	$^{16}O_4{}^{32}S^1H$ HSO_4 9.41E-01	$^{12}C^{16}O_5{}^1H_5$ $HCO_3(H_2O)_2$ 9.77E-01	1792
97	$^{16}O_4{}^{32}S^1H$ HSO_4 9.41E-01	$^{16}O_5{}^{13}C^1H_4$ $CO_3(H_2O)_2$ 1.06E-02	1953
96	$^{12}C^{16}O_4{}^{18}O^1H_2$ $CO_3H_2O_2$ 1.00E-02	$^{16}O_4{}^{32}S$ SO_4 9.41E-01	2246
97	$^{16}O_4{}^{32}S^1H$ HSO_4 9.41E-01	$^{16}O_4{}^{33}S$ SO_4 7.43E-03	11492
97	$^{16}O_4{}^{32}S^1H$ HSO_4 9.41E-01	$^{12}C^{16}O_4{}^{17}O^1H_4$ $CO_3(H_2O)_2$ 1.86E-03	1920
97	$^{16}O_4{}^{32}S^1H$ HSO_4 9.41E-01	$^{16}O_3{}^{32}S^{17}O$ SO_4 1.43E-03	26874
97	$^{16}O_4{}^{32}S^1H$ HSO_4 9.41E-01	$^{12}C^2H^{16}O_5{}^1H_3$ $CO_3(H_2O)_2$ 4.49E-04	1844
97	$^{16}O_4{}^{13}C^{18}O^1H_2$ $CO_3H_2O_2$ 1.09E-04	$^{16}O_4{}^{32}S^1H$ HSO_4 9.41E-01	2535

Table 3.2: Unresolved peaks and minimum resolution needed to resolve the given ions. For each peak, the following parameters are specified: isotopic composition, empirical formula and relative abundance.

Chapter 4

Chemical kinetics simulations

Chemical ionization mass spectrometry employs the ionization of analyte molecules through gas-phase ion-molecule reactions with selected reagent ions. Such reactions are among the fastest chemical reactions known. At the same time, the residence time in the ion-molecule-reaction (IMR) region for chemical ionization (CI) to take place is very limited. Chemical kinetics can help to address this problem, and clarify if the design of the instrument is sufficient for CI.

In the first part of this chapter some basics of chemical kinetics are introduced, together with an approach to the numerical solution of the system of chemical kinetic equations. The kinetic simulations of the chemical ionization with CO_3^- as the reagent ion and the estimate of the residence time in the IMR region of the FunMass instrument are presented in the second part of this chapter.

4.1 Theory

Chemical kinetics studies the reaction rates and changes in the concentrations of reactants and products with time [93].

4.1.1 Reaction rates

Reaction rate is the speed of a chemical reaction, i.e. the rate at which reactants are used or equivalently the rate at which products are formed. For the general reaction

$$aA + bB \longrightarrow cC + dD, \tag{4.1}$$

the instantaneous reaction rate R equals

$$R = -\frac{1}{a}\frac{d[A]}{dt} = -\frac{1}{b}\frac{d[B]}{dt} = \frac{1}{c}\frac{d[C]}{dt} = \frac{1}{d}\frac{d[D]}{dt}, \tag{4.2}$$

where the brackets [ ] indicate concentrations of the corresponding reactant/product.

4.1.2 Rate law

Typically, the reaction rate depends on the concentration of reactants. The reaction rates generally increase when reactant concentrations are increased and decrease when their concentrations are decreased. The relationship between the instantaneous reaction rate

and the reactant concentrations is described by a mathematical expression called differential rate law. For the reaction in Equation 4.1 the rate law can be written in the following form:

$$R = k[A]^\alpha [B]^\beta, \tag{4.3}$$

where k is the rate constant of the reaction and the values of α and β are derived from laboratory measurements. The constants α and β are not necessary but often equal to the stoichiometric coefficients of the reactants. The reaction order is the sum of all the exponents in the rate law: $\alpha + \beta$. All reactions considered in this chapter (Table 4.2) are 2nd order reactions with $\alpha = \beta = 1$ as they are assumed to be elementary reactions. A reaction rate constant k strongly depends on the temperature.

4.1.3 Change of concentration with time

The rate law Equation 4.3 essentially is an ordinary differential equation (ODE). Resolving it gives concentrations of reactants and products as a function of time.

For a 2nd order reaction as Equation 4.1 with $\alpha = \beta = 1$

$$A + B \longrightarrow C + D \tag{4.4}$$

the concentrations of reactants and products at the time t can be expressed by the following formulas: $[A] = A_0 - x(t)$, $[B] = B_0 - x(t)$, $[C] = C_0 + x(t)$, $[D] = D_0 + x(t)$, where A_0, B_0, C_0, D_0 are the corresponding initial concentrations and $x(t)$ is a function expressing the amount of product formed in the reaction in the time interval t. In the beginning of the reaction when no products are formed, $x(0) = 0$. From the definition of the function $x(t)$, follows the reaction rate $R = \frac{dx}{dt}$. Then, the rate law 4.3 can be written in the following way:

$$\frac{dx}{dt} = k(A_0 - x)(B_0 - x), \tag{4.5}$$

where k is the rate constant.

For a more general reaction Equation 4.1 ($\alpha + \beta$ order and with one or more stoichiometric coefficients $\neq 1$) the auxiliary function $x(t)$ will be defined using a reversed approach. If $x(t)$ is a function with the properties $x(0) = 0$ and $\frac{dx}{dt} = R$, then from Equation 4.2 the concentrations of reactants and products at the moment t can be derived as $[A] = A_0 - ax(t)$, $[B] = B_0 - bx(t)$, $[C] = C_0 + cx(t)$, $[D] = D_0 + dx(t)$. Then, the rate law 4.3 can be written in the following way:

$$\frac{dx}{dt} = k(A_0 - ax)^\alpha (B_0 - bx)^\beta, \tag{4.6}$$

where k is the rate constant.

Equations 4.5 and 4.6 have analytical solutions. A system of ODEs for several simultaneous concurrent reactions (see e.g. Table 4.2) usually can be resolved only numerically. There are already many existing and effective scientific packages for the numerical solution of systems of ordinary differential equations (ODEs) for all popular programming languages. The function `integrate.LSODA()` from the scientific Python package `SciPy` [40] was used for the calculations in this chapter.

4.1.4 Algorithm for solving systems of ordinary differential equations

A system of n chemical reactions with m unique reactants and products is represented in the matrix form as

$$Ay \longrightarrow By, \tag{4.7}$$

where y is a $m \times 1$ vector containing all empirical formulas of all unique reactant and product species, A and B are $n \times m$ matrices containing the stoichiometric coefficients of the reactions in the following way: $a_{i,j}$ is the coefficient in the ith reaction before y_j if it is an reactant in this reaction and 0 otherwise. $b_{i,j}$ is the coefficient in the ith reaction before y_j if it is a product in this reaction and equals 0 otherwise.

If $x(t)$ is a $n \times 1$ vector function with the following properties $x_i(0) = 0$ and $R_i = \frac{dx_i}{dt}$ for $i = 1, ..., n$, where R_i is the rate of ith reaction, then the $m \times 1$ vector of concentrations y can be calculated in the following way:

$$y = y_0 - Ax + Bx, \tag{4.8}$$

where y_0 is a $n \times 1$ vector with the initial concentrations of reactants and products. Some compounds can be an reactant in one reaction and a product in another. The term Ax in Equation 4.8 is representing its usage in the reactions where it is an reactant and Bx is representing its formation as a product.

The system of ODEs for the 2nd order reactions (type Equation 4.4) can be written as follows:

$$\frac{dx_i}{dt} = k_i \prod_{j=1}^{m} y_j^{a_{i,j}} \tag{4.9}$$

where i is the number of the reaction, $i = 1, ...n$ (where n is the total number of reactions in the system), m is the number of unique reactants and products in the system and k_i is the rate constant of the ith reaction. Equation 4.9 can be used without any modification for the most of the reactions of any order ($\alpha, \beta, ...$ have to be equal to the stoichiometric coefficients of those reactions), including reactions of dissociation and termolecular reactions.

After the explained mathematical formalization, the systems of ODEs 4.9 can be numerically solved in Python (or other programming language) providing the time dependence of the reactant and product species.

The routines to set and solve systems of the chemical kinetics ODEs were integrated into a graphical user interface that allows interactive variation of the start concentrations (mixing ratios) and rate constants and a built-in plotting routine to visualize the results. It has been programmed in order to provide a convenient tool for fast visual inspection of different ionization schemes. The program was checked by intercomparing results of a reaction scheme for the conversion of chlorine monoxide to chlorine atoms by NO molecules to those produced by the established commercial FACSIMILE package (AEA Technology, based on Gear [20]) which is proprietary, inconvenient to program, and needs external tools for visualization. Good agreement was found giving confidence in the results provided by the developed program.

4.2 Calculations

In order to check on the completion of the ionization reactions for CO_3^- CIMS, the IMR as depicted in Figure 4.1 was parameterized and the species and reactions from Tables 4.1 and 4.2 were examined.

4.2.1 Residence time in the reaction zone

The analyte gas flow and the ion source flow are mixed and reacted in the ion-molecule reaction (IMR) region of FunMass. Figure 4.1 shows a schematic diagram of the IMR. A more detailed figure is presented in Chapter 5 (see Figure 5.4).

Trace gas	Mix. ratio in the UTLS	Ref.	Mix. ratio for the calculations in the IMR region
HNO_3	1 ppt - 4 ppb	[48]	10 ppb
SO_2	1 ppt - 0.5 ppb	[32], [33]	10 ppb
HCN	200-700 ppt	[22]	5 ppb
H_2SO_4	a few ppt	[55]	1 ppb

Table 4.1: Expected mixing ratios of trace gases in the UTLS, together with their mixing ratios in the IMR region used for calculations.

To estimate the residence time t spent by the gases in the IMR region (i.e. time of chemical ionization) of the FunMass instrument, a simplified model of a cylindrical duct with appropriate volume and total flow is used:

$$t = \frac{volume}{flow} = \frac{\pi d^2 l}{4 flow} \tag{4.10}$$

where d and l are the diameter and length (geometrically, hight) of a representative cylinder. This results in an approximate residence time of 140 ms for the FunMass instrument.

4.2.2 Initial values and calculations

To start the chemical kinetics simulations for the system of reactions shown in Table 4.2, all initial concentrations of the reactants have to be given. To form the reagent ion CO_3^-, 400 sccm of O_2 and 2.5 sccm [1] of CO_2 flow through the dielectric barrier discharge (DBD) ion source (see Section 5.4). In addition, 1.4 slm [2] of ambient air (containing around 20 % of O_2) enters the IMR region through the inlet (see Figure 4.1). From that, the volume mixing ratios of O_2 r_{O_2} and CO_2 r_{CO_2} in the IMR region can be calculated:

$$r_{O_2} = \frac{1.4 \times 0.2 + 0.4}{1.8} \approx 38\% \tag{4.11}$$

$$r_{CO_2} = \frac{2.5 \times 10^{-3}}{1.8} \approx 0.139\% \tag{4.12}$$

The CO_3^- mixing ratio is estimated based on the amount of analyte, which causes a clear decrease in the measurements of the reagent ion signal. The calculated mixing ratio of CO_3^- in the IMR region is around 200 ppb, which means that approximately only 0.014 % of CO_2 gets converted to CO_3^-.

The expected mixing ratios of the trace gases in the UTLS that can be measured with CIMS using CO_3^- as the reagent ion are listed in Table 4.1. The corresponding ionization reactions are shown in Table 4.2. Nonetheless the calculations were done for higher initial concentrations (right column Table 4.1) to ensure that the mixing ratios of the trace gases in the UTLS are in the range that can be completely chemically ionized during the residence time in the IMR region.

---

[1] 1 sccm = 1 standard cubic centimeter per minute = $\frac{p_n}{T_n}\frac{T}{p}$cm^3/min, where T_n = 273.15 K and p_n = 10×10^5 Pa are temperature and pressure at standard conditions.

[2] 1 slm = 1 standard liter per minute = $\frac{p_n}{T_n}\frac{T}{p}$L min^{-1}, where T_n = 273.15 K and p_n = 10×10^5 Pa are temperature and pressure at standard conditions.
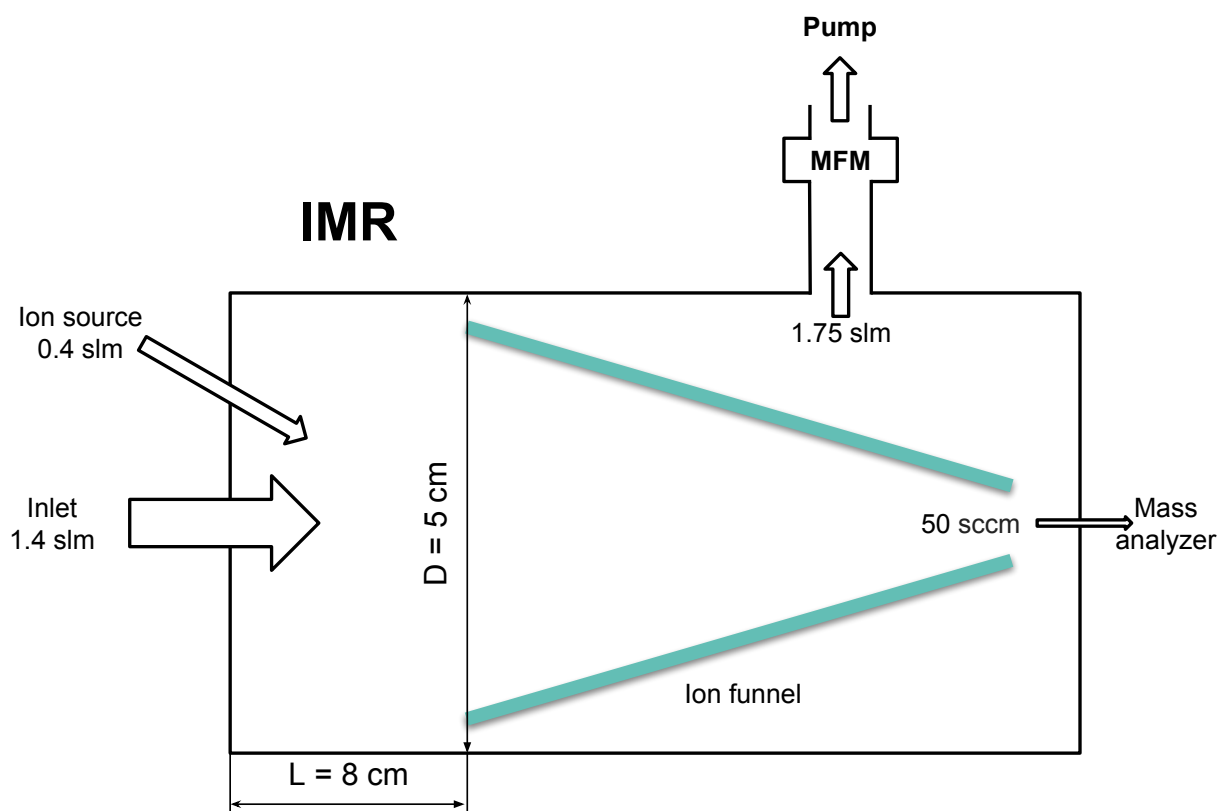
Figure 4.1: Schematic drawing of the flows in the IMR region of the FunMass instrument.

The calculations were done assuming that the reactants are well mixed in the IMR region. This is an idealized model, but since no strong dependence of the product ion signal on variations of the flows was found, this seems to be a reasonable assumption.

The results of the simulations for a pressure of 30 hPa and temperature of 300 K for the parameters given in Tables 4.1 and 4.2 are summarized in Figure 4.2. At values higher than the maximum expected concentrations, analyte molecules are fully converted to the corresponding ions in less than 100 ms, which is less than the estimated residence time in the IMR. Simulations show that reactions with the actual smaller concentrations of analytes (mixing ratios down to 0.1 ppt) have almost identical conversion curves to those shown in Figure 4.2 resulting in the full conversion of the analytes within the whole range of the expected concentrations. As shown later in Chapter 6, the linearity of the FunMass

Reaction	Rate constant $\times 10^{-9}\,\mathrm{cm^3/s}$	Reference
$HCN + CO_3^- \longrightarrow CO_3^-(HCN)$	3.17	[80]
$HNO_3 + CO_3^- \longrightarrow CO_3^-(HNO_3)$	0.8	[17]
$SO_2 + CO_3^- \longrightarrow SO_3^- + CO_2$	0.37	[83]
$SO_3^- + O_2 \longrightarrow SO_5^-$	0.0005	[3]
$H_2SO_4 + CO_3^- \longrightarrow HSO_4^- + HCO_3$	2.39	[94]

Table 4.2: Chemical ionization with CO_3^- as the reagent ion. The rate constants are given at 300 K.
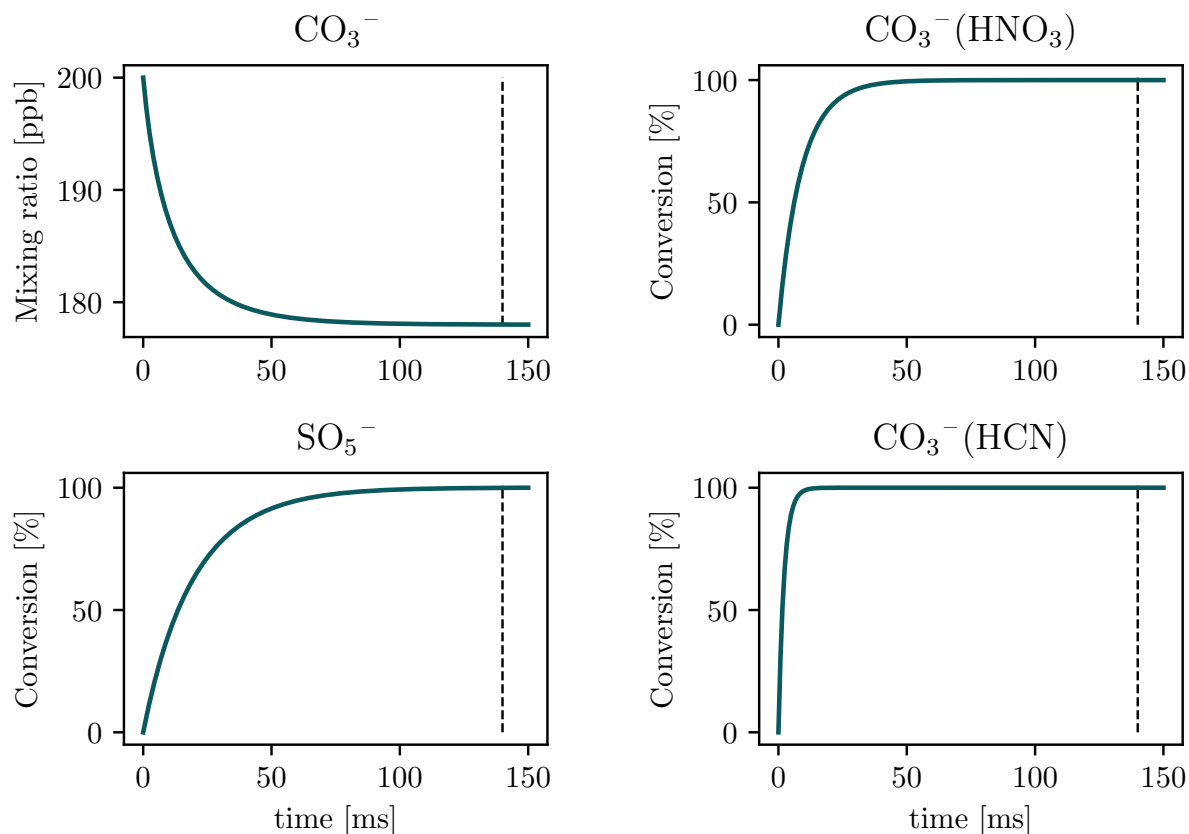
Figure 4.2: Kinetics simulations of the temporal evolution of the chemical ionization reactions of HNO_3, SO_2 and HCN for the parameters given in Tables 4.1 and 4.2. The upper left panel shows the modeled reduction of the reagent ions $CO3^-$. The dashed vertical line indicates the expected residence time in the IMR region.

calibration curves obtained for a wide range of analyte concentrations corroborates these calculations.

4.3 Results

In order to make sure the conversion of analyte molecules at atmospherically relevant concentrations by the CI reactions in the FunMass IMR is complete, calculations have been performed on the chemical reaction system for the ionization employing CO_3^- as the reagent ions. The results prove the FunMass ionization setup sufficient for the full conversion of UTLS concentrations of HNO_3, SO_2, and HCN. Similar calculations have been done for other systems such as I^- ionization.

For that purpose a Python program has been set up allowing the reliable and convenient study of such chemical reaction kinetics systems and providing a graphical user interface including online plotting routines. This tool replaces an old proprietary system which is rather inconvenient to use.

Chapter 5

FunMass development and deployment

FunMass is an airborne chemical ionization time-of-flight mass spectrometer. The name FunMass is derived from the terms *ion **Funnel*** (an important part of the transfer stage) and ***Mass** spectrometer*.

FunMass was developed to measure multiple trace gases in the upper troposphere and lower stratosphere (UTLS) region on board of the research aircraft M-55 Geophysica. It has the potential to improve the understanding of nitric oxide species and sulfur chemistry and their effects on particle formation as well as diagnosing transport processes in the UTLS region.

The early laboratory prototype of FunMass was developed as part of PhD work of Dr. Sascha Albrecht [1]. The concepts of its transfer stage and the ion source were adapted to the new airborne instrument.

In this chapter, a general description of the instrument is given, as well as some important steps of its development (including component tests), and a review of the performance of the FunMass instrument during the Stratoclim campaign.

5.1   M-55 Geophysica

The M-55 Geophysica is a high-altitude aircraft developed by Myasishchev Design Bureau (MDB) in the Soviet Union in the 1980s. Designed originally as a high-altitude reconnaissance aircraft, it underwent a series of modifications between 1996 and 2001 (the most noticeable being the addition of two wingpods and a dome behind the cabin) to be used as a research aircraft capable of hosting up to 27 scientific instruments simultaneously. The M-55 has a service ceiling of 21 500 m (55 hPa), a maximum range of approximately 5000 km and an endurance of 6.5 h at 17 000 m. The M-55 has been used as measurement platform for many successful scientific campaigns all around the world (in South America, Northern Australia, Seychelles, West Africa, many places across Europe up to Northern Sweden, and lately the Indian subcontinent).

5.2   Overview

FunMass (Figure 5.1) was built to replace an instrument to measure halogen oxides (mainly ClO and BrO) named HALOX [96, 97]. It was mounted in the left wingpod of M-55 Geophysica. The characteristics of the wingpod determined the dimensions of FunMass. The instrument is 145 cm long, 56 cm wide and 56 cm high (Figure 5.1) with a total mass of

175 kg. The existing windows on the side of the wingpod (Figure 5.16(b)) determined the positioning of the power plugs and the gas supply system of the instrument, which should be accessible after the instrument has been mounted.

Three institutes of Forschungszentrum Jülich (IEK7, ZEA1, ZEA2, see Figure 5.2) and the Swiss company Tofwerk AG took part in the development of FunMass. A schematic of the instrument with the distribution of tasks is shown in Figure 5.2.

A short description of the main FunMass components is given here:

- **Main Power Supply** (MPS). It redistributes the power supplied from the aircraft (115 V AC, 400 Hz and 27 V DC) to every other part of FunMass. FunMass can also be powered with 230 V AC, 50 Hz and 27 V DC, in the laboratory. Besides housekeeping data, the MPS control board can manage up to 22 Pt1000 temperature sensors (although only 16 of them are currently used), conducting measurements in different parts of the instrument, and contains a sensor for measuring the ambient pressure in the wingpod (0.01 bar to 1 bar, CTE7002, First sensor AG, Germany).

- ADQ acquisition unit. This unit is responsible for processing up to 100 000 TOF spectra per second. It converts the analog signal from the TOF and averages the converted data (up to 100000 data points for each spectrum) at a given rate and sends it to the PC via USB interface. More about the purpose of this unit can be found in the description of a comparable system [28].

- **TOF Power Supply** (TPS). It supplies DC voltages to all ion optics of the instrument and high voltages to the TOF. The original housing supplied by Tofwerk was modified by ZEA-2 to make it pressure-tight to avoid sparking.

- **Ion- Funnel and Ion Source** power supply (IFS). High voltage for the ion source is generated by GBS Minipuls 2.1 electronic, with an operating frequency of 10 kHz and an amplitude up to $10\,kV_{pp}$. A newly developed setup (see Figure 5.11(b)) is used to generate the voltage of $200\,V_{pp}$ with up to 10 MHz frequency for the ion funnel.

- Inlet system. It regulates the amount of ambient air sampled into FunMass. See Section 5.3 for further details.

- Pumping system. It consists of two dry scroll pumps (IDP3, Agilent Technologies, Germany) and a turbomolecular pump (multi-stage split flow turbomolecular pump, SF270, Pfeiffer Vacuum, Germany). The first IDP3 pumps air from the first part of the transfer stage (ion funnel), the second one pumps the turbomolecular pump. The turbomolecular pump is responsible for the vacuum in the second and third part of the transfer stage and in the TOF.

- Heating system. It consists of dozens of thermofoil heaters (Minco Products Inc., Minneapolis, MN, USA) to control the temperature of all sensitive parts of the instrument during the extreme cold flight conditions (down to $-90\,°C$). In addition, the instrument is covered by a thermal insulation case made of flame resistant Nomex® sheets (DuPont, 3 mm thickness).

- Ion Source. It produces the reagent ions, used for the chemical ionization of the analyzed air. For further details see Section 5.4.

- Transfer stage: ion funnel, RF only quadrupole and an ion lens system. They focus ions and guide them to the mass analyzer. For further details see Section 5.5.

- **Compact Time-Of-Flight (CTOF)** mass spectrometer. For further details see Section 5.6.

- **Giraffe (GRF)** is the TOF control system. It manages all pumps of the instrument and monitors their housekeeping data as well as the housekeeping data of the TOF, including crucial parameters for the experiment such as pressure in the funnel (0 - 100 hPa, UNIK 5000, GE Measurement & Control, USA) and in the TOF (down to 1.0×10^{-9} hPa, Pfeiffer, Germany). It shares a housing with the instrument control computer.

- **Instrument control computer:** Intel Core i7-3517UE 1.7 GHZ, 8 GB RAM DDDR3, NANDrive 32 GB, Microsoft Windows 7, anaconda 2 (Python 2.7.14 x64). It runs the control and data acquisition software.

- **Gasdeck.** Gas and calibration supply. For further details see Section 5.7.

- **Rack and Baseplate.** All parts of the instrument are integrated into these structural parts. They were developed in the ZEA-1, and allow for the convenient installation of the FunMass instrument within the wingpod. It can be lifted from a cart and fixed in the wingpod using four screws and the help of two people. It is worth to mention that a pressure-tight housing for the whole instrument would be desirable, but due to the space limitations of the M-55 wingpod it is nearly impossible.

5.3 The inlet system

The inlet system of the FunMass instrument consists of three different stages:

- the front opening of the wingpod. The fluid dynamics simulations (Figure 5.3(a)) show that air entering during the flight slows in the wingpod down to approximately $30 \, \mathrm{m \, s^{-1}}$.

- the primary inlet: a bent tubing attached to the back wall of the wingpod opening (Figure 5.3), its main purpose is to prevent sampling of large particles (FunMass is designed to only measure analyte in the gas phase). The design of the primary inlet was adapted from the HALOX instrument.

- the secondary inlet: the flow regulating inlet of FunMass itself. The fluid dynamics simulations (Figure 5.3(b)) show that the pressure gradient ensures that the air flowing to the secondary inlet will be sampled through the primary inlet and will originate from the opening of the wingpod, not from the inside. Its operational principle is described below.

A cut through the secondary inlet is shown in Figure 5.4 and a 3D model of its front is shown in Figure 5.5. The secondary inlet consists of two steel parts: an inner tube (length: 220 mm; inner diameter: 8 mm; outer diameter: 10 mm), and an outer cylinder (length: 63 mm, inner diameter: 16 mm; outer diameter: 22 mm) covering the front of the inner tube (see Figure 5.4). Both of these parts are fully open only on their rear sides and have 2 mm wide orifices shifted 2 mm from the axis on the fore side. The outer cylinder can be accurately rotated by a motor and by doing so the overlap of the orifices can be varied. The inlet is fully open when the orifices are entirely overlapped and closed when they do

Figure 5.1: FunMass. Photograph by Ralf-Uwe Limbach.

FunMass Schematical Diagram
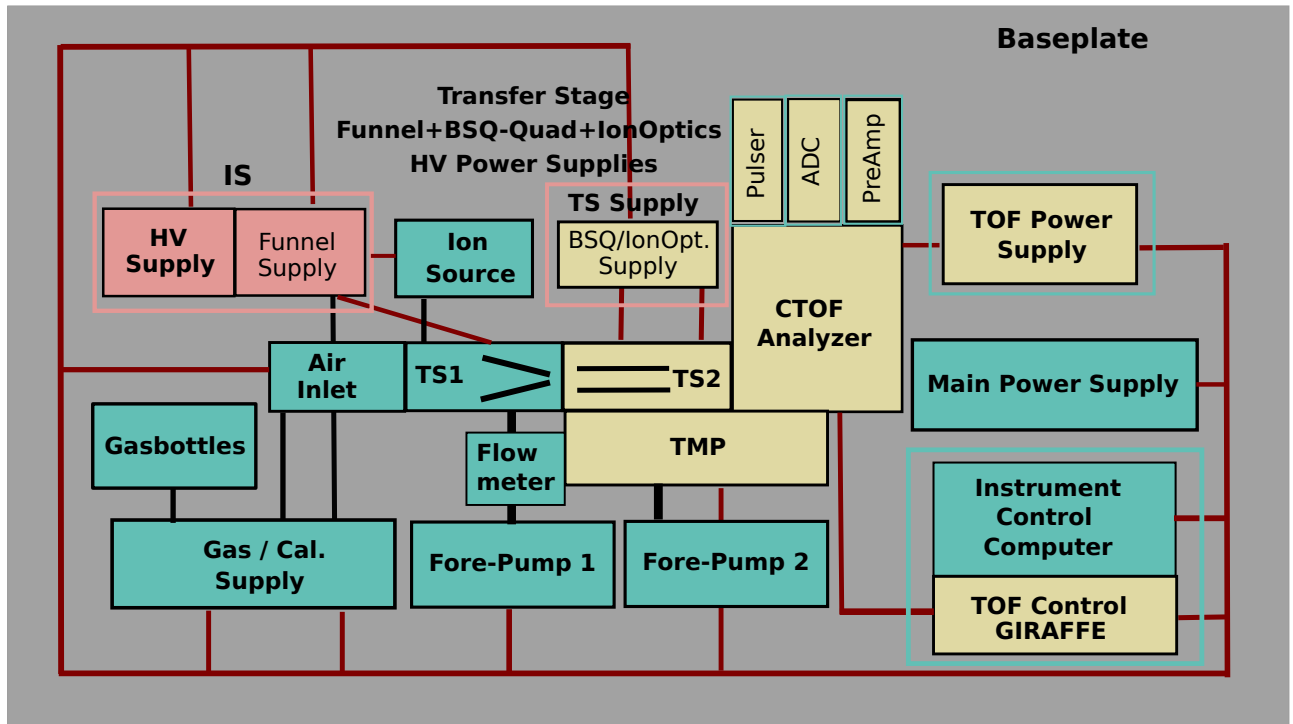
- IEK-7: Institut für Energie- und Klimaforschung; Stratosphäre (Institute of Energy and Climate Research; Stratosphere), Forschungszetrum Jülich Gmbh (FZJ), Germany.

- Tofwerk: Tofwerk AG, Thun, Switzerland

- ZEA-1: Zentralinstitut für Engineering, Elektronik und Analytik; Engineering und Technologie (Central Institute for Engineering, Electronics and Analytics; Engineering and Technology), FZJ.

- ZEA-2: Zentralinstitut für Engineering, Elektronik und Analytik; Systeme der Elektronik (Central Institute for Engineering, Electronics and Analytics; Electronic Systems), FZJ.

Figure 5.2: Detailed schematic of FunMass. Colorcoded distribution of the tasks during development.
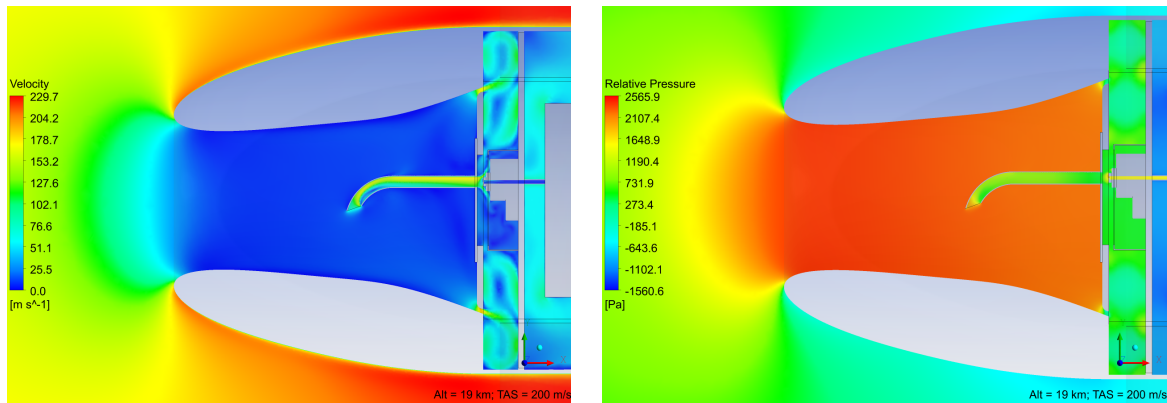
(a) Air velocity distribution in the wingpod during the flight.

(b) Pressure distribution in the wingpod during the flight.

Figure 5.3: The fluid dynamics calculations were performed by Armin Afchine (IEK-7, Forschunszentrum Jülich GmbH) using Ansys CFX 14 (Ansys Inc., USA). Parameters: $Alt = 19\,\mathrm{km}$, $T = 217\,\mathrm{K}$, $v = 200\,\mathrm{m\,s^{-1}}$. Schematic position of the primary and secondary inlet.
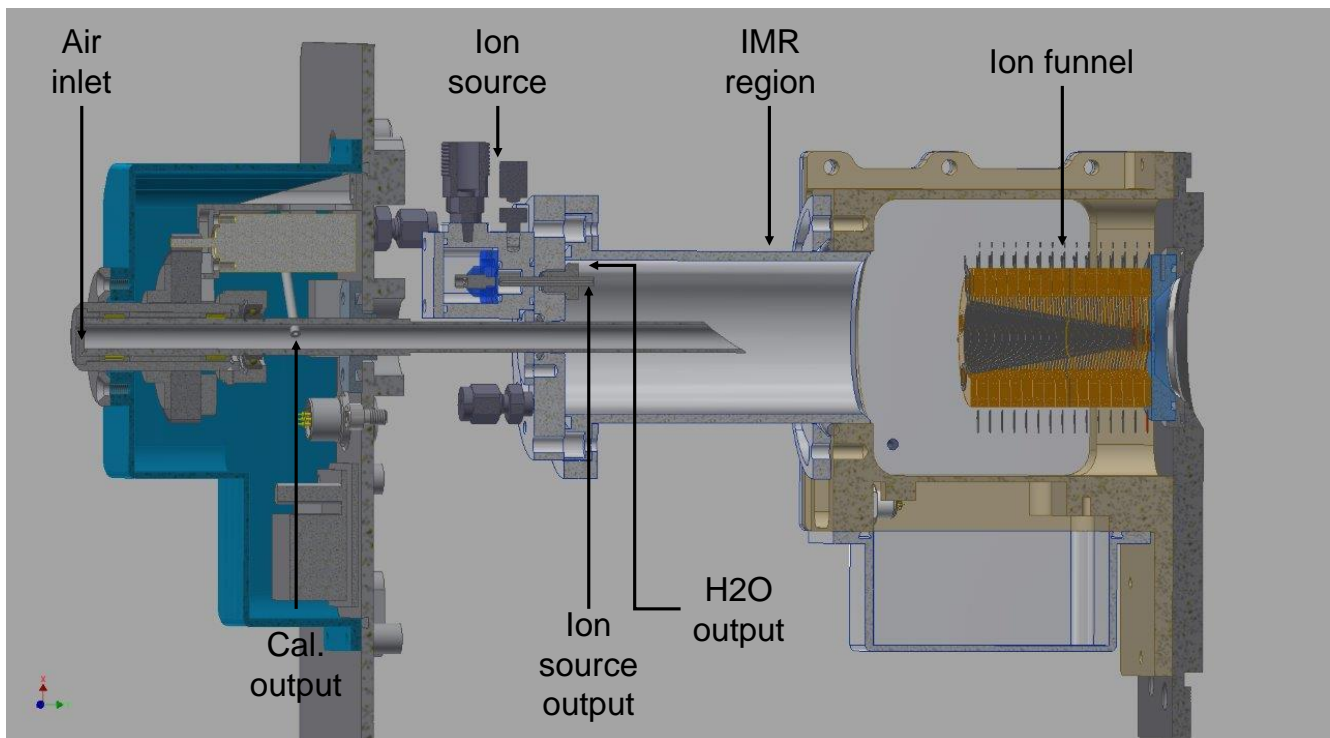
Figure 5.4: Cut through the front part of the instrument: inlet, ion-molecule reaction (IMR) region and ion funnel.
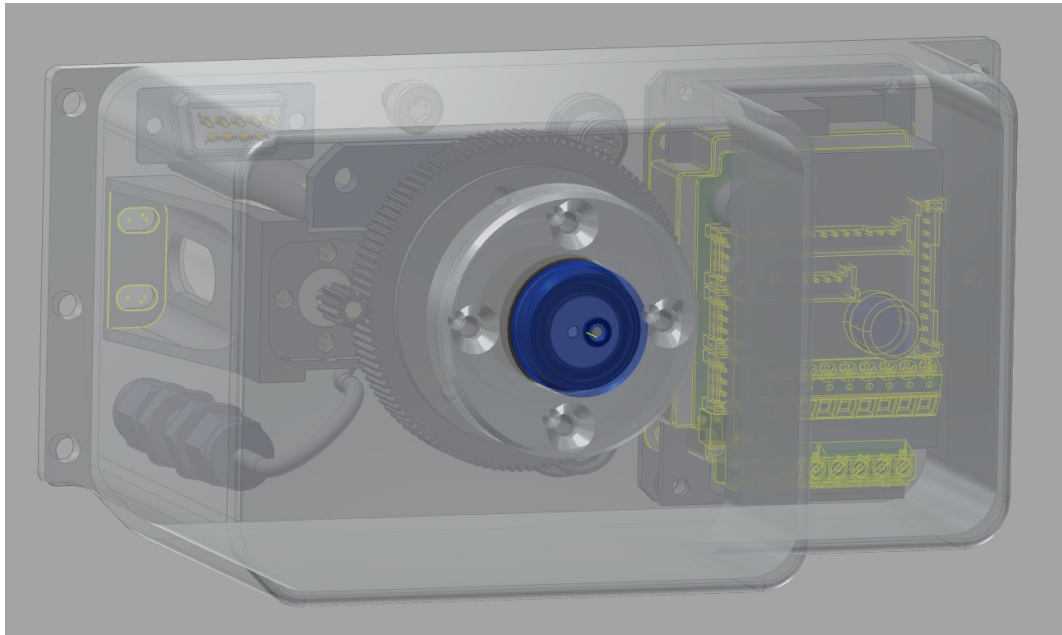
Figure 5.5: 3D schematic of the inlet.

not overlap at all (Figure 5.6(a)). The area S of the overlap (Figure 5.6(b)) can be calculated with the following formula:

$$S = 2 \left(\arccos \left(\frac{R}{r} \sin \frac{\phi}{2} \right) r^2 - R \sin \frac{\phi}{2} \sqrt{r^2 - R^2 \sin^2 \frac{\phi}{2}} \right). \tag{5.1}$$

Figure 5.7 shows the dependence of the area S on the angle ϕ, which is very close to the linear dependence. At fixed pressure difference on both sides of the inlet, the flow through it is proportional to the area. Thus, at a given pressure condition, the incoming flow can be almost linearly regulated from zero to the maximal possible one by varying the voltage applied to the motor. The drive motor system was implemented by the IEK-7 electronics department. It consists of a motor (DCX19S EB KL 24V, Maxon motor, Switzerland) and two meshed gears: a small one rotated directly by the motor and a big one connected to the outer cylinder (Figure 5.5).

In operation, the pressure in the funnel is maintained within the range (30 ± 3) hPa. The inlet regulation follows a simple pattern: every 5 s, the pressure is compared to the set point. If it is out of the desired range, the motor makes a small step in order to increase the overlap or in the opposite direction to decrease it if the pressure is too low or too high respectively. If the pressure is inside the aforementioned range, no action is taken.

To decrease wall losses for "sticky" gases (e.g. HNO_3, SO_2 etc.) a coating from SilcoNert (r) [92] was used on the inner tube. To prevent possible leaks in the closed position, the inner tube has a Teflon o-ring around the orifice.

The motor and the inner tube are heated, keeping the temperature between $0\,°C$ and $10\,°C$.

5.4   The ion source

Different types of ^{210}Po and ^{241}Am radioactive ion sources are widely used in CIMS [77], [54], [15], including the airborne instruments described in [49], [9]. The international deployment
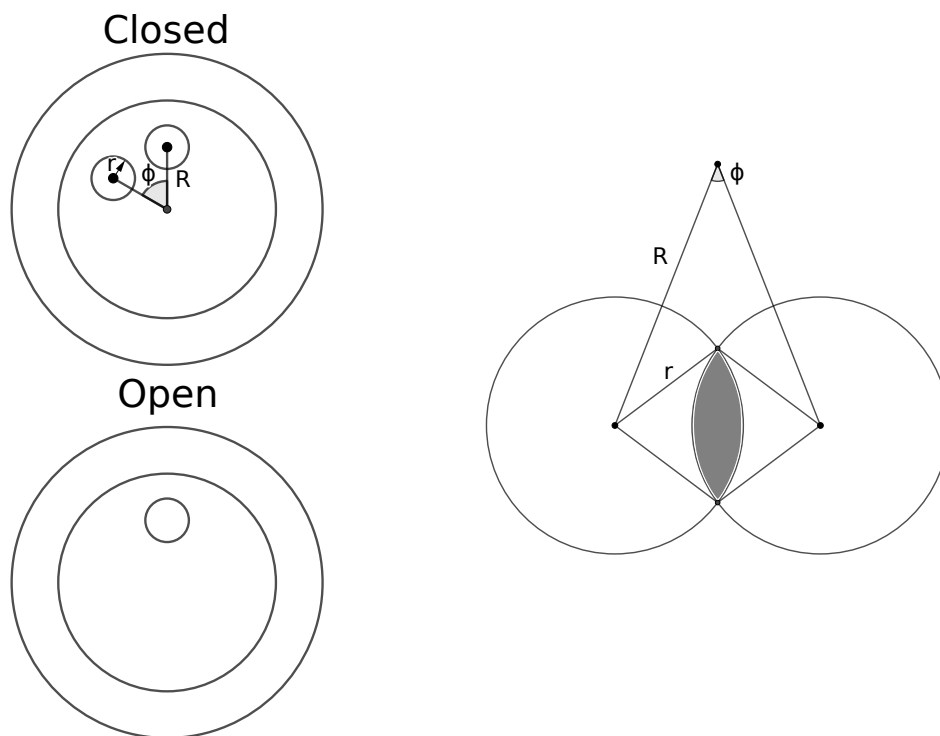
(a) Utmost positions of the inlet.   (b) Geometry of the inlet, partially open.

Figure 5.6: Regulation principle of the inlet.
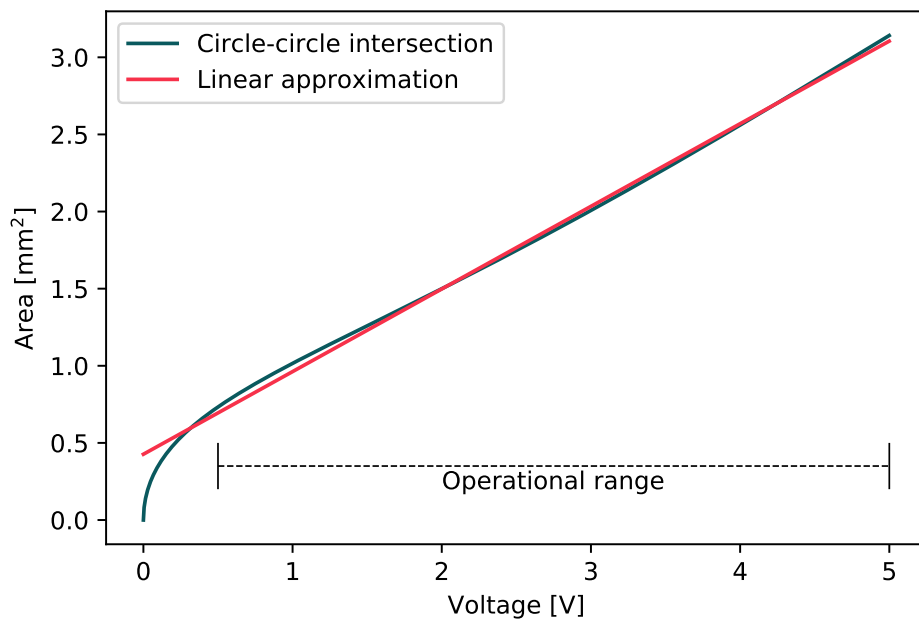
Figure 5.7: Opening area of the secondary inlet as a function of the applied voltage.
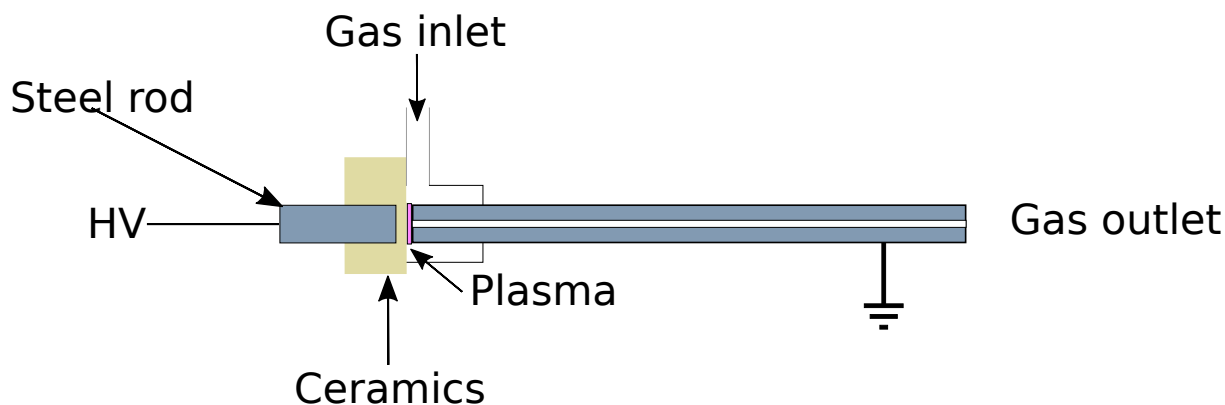
Figure 5.8: A schematic of the DBD ion source of FunMass.

of an instrument with such a radioactive ion source is logistically very challenging due to the strict rules applying to radioactive devices. Therefore, a dielectric barrier discharge (DBD) ion source was developed for FunMass. The detailed design of the ion source is described in Albrecht [1]. It was adapted to FunMass with minor modifications. A schematic of the FunMass ion source is shown in Figure 5.8. In order to produce the reagent ions, the gases supplied by the gasdeck are led through a RF plasma, which ionizes them before they pass the capillary in a fast flow into the IMR region. This plasma is formed in the 1 mm gap between a ceramic (Macor, machineable glass-ceramic) dielectric and the gas outlet capillary (length: 20 mm, inner diameter: 0.8 mm, outer diameter: 4 mm) by radio frequency (RF) high voltage (HV) (10 kHz, 3 kV to 10 kV) applied to a steel rod insulated in the ceramic.

FunMass was designed to operate in two different modes: with CO_3^- or I^- as reagent ions. In order to produce CO_3^-, a mixture of O_2 (99%) and CO_2 (1%) is passed through the plasma, where O_2^- and O^- ions are generated via three body electron attachment and dissociative electron attachment. The possible ways of CO_3^- formation are shown in Reactions 5.2 - 5.5 [1, 84]. Figure 5.9 shows a typical mass spectrum of the ion source output in CO_3^- mode. If, instead, FunMass is to be operated in I^- mode, CH_3I or I_2 diluted with N_2 is passed through the plasma, where I^- ions are generated mostly via dissociative electron attachment. In this work, the focus was on the CO_3^- mode.

$$O^- + CO_2 + M \longrightarrow CO_3^- \tag{5.2}$$

$$O^- + O_2 + M \longrightarrow O_3^- \tag{5.3}$$

$$O_2^- + O_3 \longrightarrow O_3^- + O_2 \tag{5.4}$$

$$O_3^- + CO_2 \longrightarrow CO_3^- + O_2 \tag{5.5}$$

5.5 The transfer stage

The transfer stage of FunMass is composed of an ion funnel, a segmented quadrupole (called big segmented quadrupole - BSQ by TofWerk) and an ion lens system. A schematic of the transfer stage is shown in Figure 5.10. Besides the ion funnel, which was built in ZEA-2, the other parts of the transfer stage belong to the delivered TofWerk setup.
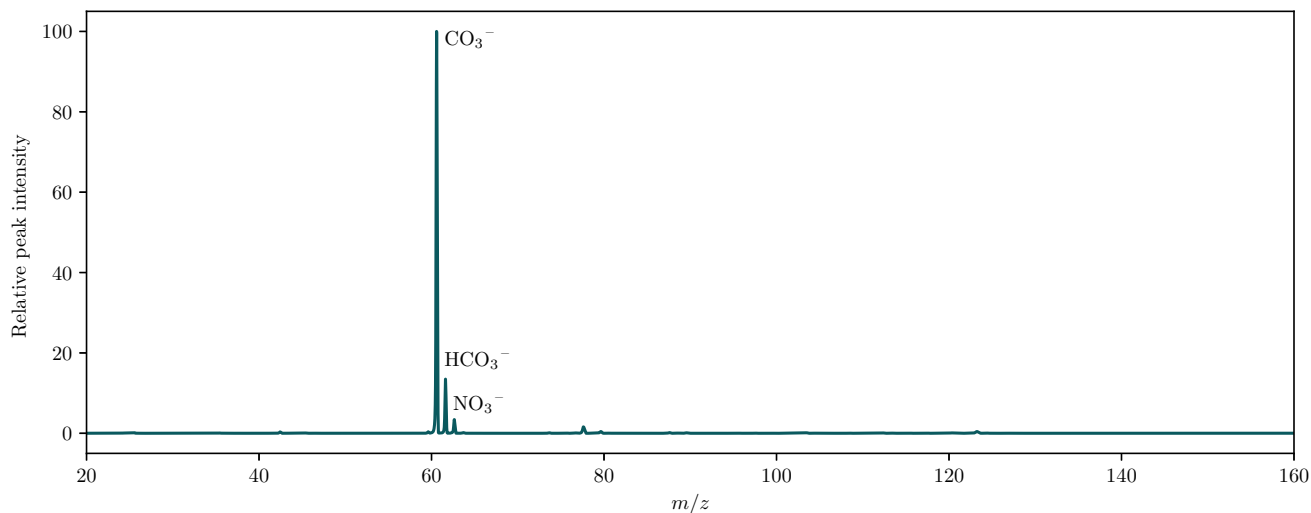
Figure 5.9: Mass spectrum of CO_2 and O_2 flowing through the DBD with a CO_2 mixing ratio of 0.6%. Mass spectrum is scaled to the most abundant signal.
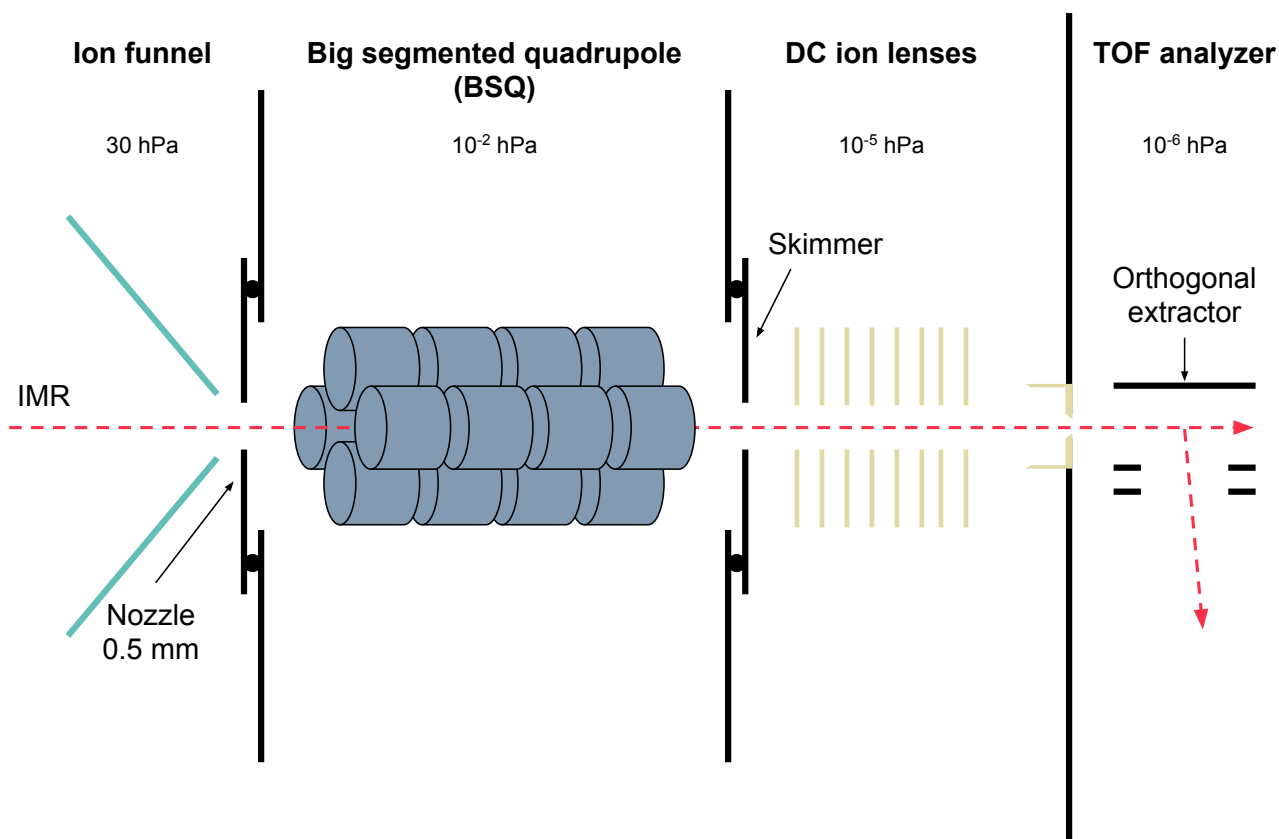
Figure 5.10: Schematic of the transfer stage of FunMass. Adapted from the TofWerk reference guide [90].
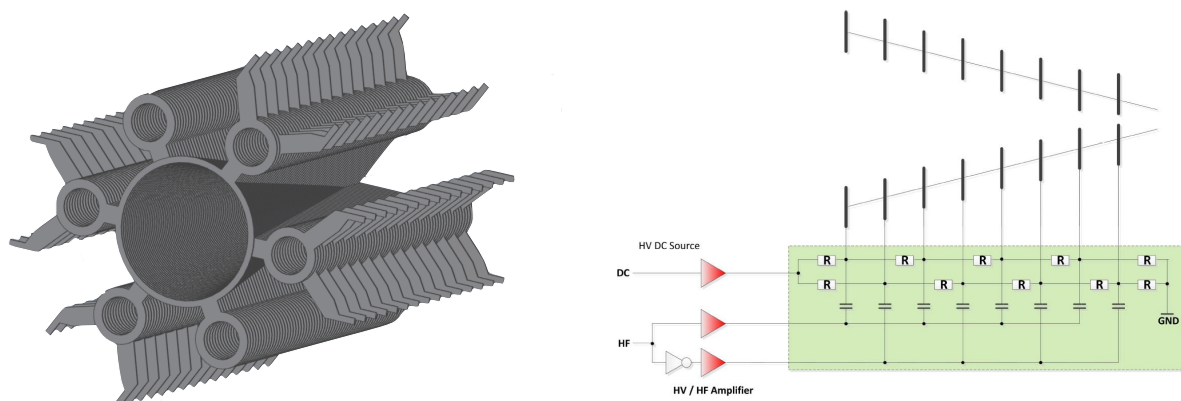
(a) 3D representation of the ion funnel electrodes. (b) Schematic of the ion funnel electronics. Source:
Source: Jochen Barthel   Heinz Rongen, ZEA-2. Taken from Albrecht [1].

Figure 5.11: The ion funnel

5.5.1 The ion funnel

Ion funnels can be used to focus ions without mass discrimination in the range of pressures where quadrupoles and electrostatic lenses are not that efficient (1 hPa to 100 hPa) [1], [43].

The funnel consists of a sequence of ring metal electrodes with decreasing inner diameter in the direction of flow. Radio frequency potentials of opposite polarities are applied to neighboring electrodes, creating an effective potential (pseudo potential) towards the axis of the funnel that confines ions inside of it (Figure 5.2) [21].

At first a transfer stage with two funnels was developed for the prototype, one operating at 100 hPa and another at 5 hPa [1]. Further tests showed that the final version of the transfer stage could work with just only one funnel operating at 30 hPa without losing much ion transmission. The latest version of the transfer stage includes only one funnel consisting out of 120 electrodes (0.25 mm thick stainless steel, gold coated) separated by 0.5 mm gaps (Figure 5.11(a)). The funnel is driven at a frequency up to 10 MHz and at a voltage up to 200 V.

In order to keep the flow and the pressure at the original values in the next part of the transfer stage (quadrupole), the diameter of the orifice between the funnel and the quadrupole had to be decreased from 1 mm to 0.5 mm.

5.6 CTOF

Compact TOF (CTOF) by Tofwerk AG was selected to be the mass analyzer of the FunMass instrument for different reasons:

- TofWerk AG (Thun, Switzerland) is one of very few companies supplying TOF mass spectrometers in OEM configurations tailored to the customers needs.

- The analyzer is provided with all power supplies etc. and a versatile modular driving software.

- The laboratory prototype of FunMass was based on the High-Resolution-TOF (HTOF) by the same company.

- The instrument response to ions is very linear over a large dynamical range of 1×10^6 [16].

- In order to fit the wingpod of Geophysica a compact and light-weight analyzer was needed.

The CTOF has a resolution of 700, a mass of 9 kg and is 265 mm long, 175 mm wide and 115 mm high. It is one of the most compact TOF mass analyzers on the market, what makes it perfect for the airborne instrument. Using the HTOF (R_{FWHM} = 2000, $665 \times 250 \times 102$ mm, 12 kg) would not lead to a critical increase in the overall mass of the instrument, but would require a complete redesign of the transfer stage in order to fit within the M-55 wingpod. As shown in the calculations of Chapter 3, CTOF is able to resolve most of the targeted species and still provides reasonable resolution for the UTLS measurements compared to the traditional quadrupole mass analyzers employed in UTLS in-situ studies with resolutions mostly below 300 [89].

5.7   Gasdeck

The gasdeck supplies the gases needed to run the instrument. It is fixed on the left side of the instrument (Figure 5.1, Figure 5.13). The gasdeck is split into two connected boxes. One is located above the baseplate (upper gasdeck) and the other one directly under the first one below the baseplate (lower gasdeck). A detailed schematic of the gasdeck is shown in Figure 5.12. The gasdeck has three outputs (Figure 5.4):

- an output into the ion source, to supply the gases needed for the generation of reagent ions;

- a humidified air output to create water clusters with reagent ions before reacting with analyte air (if it is needed);

- an output to supply calibration gases and/or synthetic air to replace the ambient air from the inlet.

To operate all mass flow controllers and solenoid valves as well as temperature measurements in the gasdeck two control boards (CHM1 and CHM2) were developed by ZEA-2 and placed into the upper gasdeck. All mass flow controllers are listed in the table in Figure 5.12. Solenoid valves are used to isolate the gas lines not being used at the moment and prevent leaks through the flow controllers. For instance, leaks of unwanted gases to the ion source can dramatically change the ion chemistry. The valves were tested and showed no leaks larger than 1.0×10^{-8} hPa/(Ls).

With the current configuration of the gasdeck, FunMass can work in two different ion modes: CO_3^- and I^- as a reagent ion, and can switch between them during the flight. Two 4.7 L cylinders (Worthington industries, USA) with N_2 and O_2 (purity 6.0, Linde Group, Germany) correspondingly and one 2.37 L cylinder (SCI, USA) with CO_2 (purity 5.5, Linde Group, Germany) are mounted on the back of the instrument and connected to the upper gasdeck. They are rated to 450 bar, but are filled to 200 bar (O_2, N_2) and 68 bar (CO_2). That would allow the instrument to run for over 30 hours. Two bottles with calibration gases are fixed under the lower gasdeck. As calibration gas for the CO_3^- mode a mixture of 100 ppb SO_2 in nitrogen at 90 bar is used. For the I^- mode a home made mix of 685 ppb Br_2 in nitrogen at 4.5 bar was used. The mixture was prepared via pressure measurements employing high quality sensors.
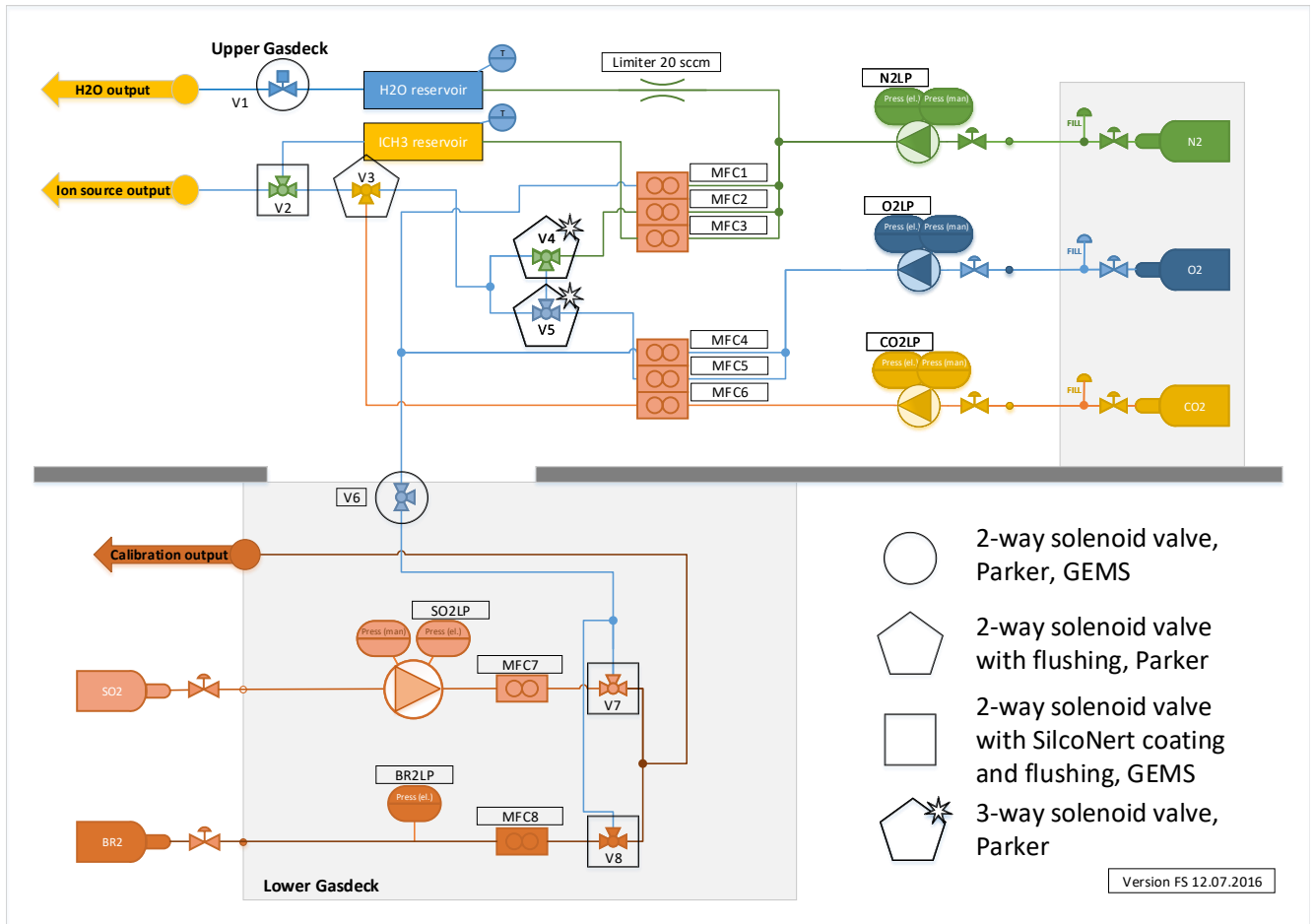
Name	Max flow	Type	Comment
MFC1	1 slm	Bronkhorst	N_2 for calibration
MFC2	1 slm	Bronkhorst	N_2 for the ion source
MFC3	50 sccm	Bronkhorst	N_2 through ICH_3 reservoir for the ion source
MFC4	1 slm	Bronkhorst	O_2 for calibration
MFC5	1 slm	Bronkhorst	O_2 for the ion source
MFC6	50 sccm	Bronkhorst	CO_2 for the ion source
MFC7	10 sccm	Bronkhorst with SilcoNert coating	SO_2 mixture for calibration
MFC8	10 sccm	Bronkhorst with SilcoNert coating	Br_2 mixture for calibration

Figure 5.12: Schematic of the gasdeck and gas flow plan.

5.8 Problems of high voltage devices in airborne instruments

The FunMass instrument is supposed to operate at low pressure (down to 50 hPa) since a pressurized tank could not be realized due to spatial constraints of the wingpod. At such low pressures voltages, as low as a few hundred volts may cause sparks that can destroy electronic equipment and are a fire hazard.

Paschen's law shows the dependence of breakdown voltage between two flat electrodes

Figure 5.13: Gasdeck. Photograph by Ralf-Uwe Limbach.
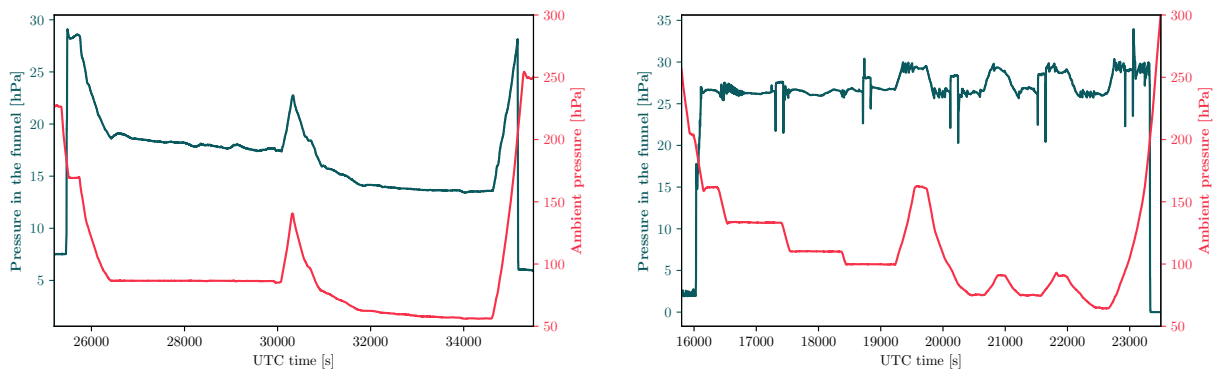
(a) Flight on 06.09.2016. Kalamata campaign.

(b) Flight on 08.08.2017. Kathmandu campaign.

Figure 5.14: Pressure in the funnel and ambient pressure during two measurement flights.

as a function of pressure of the gas and the width of the gap (Equation 5.6) [72]:

$$V_B = \frac{Bpd}{\ln(Apd) - \ln\left(\ln\left(1 + \frac{1}{\gamma}\right)\right)},$$ (5.6)

V_B : breakdown voltage,
p : pressure,
d : distance between electrodes,
A and B : experimentally determined constants,
γ : the secondary-electron-emission coefficient, depends on electrode's material.
This function reaches its minimum at

$$pd_{min} = \frac{e \cdot \ln\left(1 + \frac{1}{\gamma}\right)}{A},$$ (5.7)

e : Euler's number.

For air and steel electrodes $A = 11.28\,(\text{Pa} \cdot \text{m})^{-1}$, $B = 274.44\,(\text{Pa} \cdot \text{m})^{-1}$ and $\gamma = 10^{-2}$ from Raizer [72], therefore $pd_{min} = 1.1\,\text{Pa} \cdot \text{m}$. FunMass has four high voltage units: TPS, IFS, the BSQ power supply and the pulser. For the distances inside of these high voltage units ($> 1\,\text{mm}$) and working condition pressures (0.05 bar to 1 bar), possible pd values are higher than the minimum point pd_{min}. Therefore the breakdown voltage is lower at lower pressure (in the FunMass operating range). Paschen's curves for 50 hPa and 700 hPa are shown in Figure 5.15. it is important to emphasize that Paschen's law quantifies the breakdown voltage in the DC fields. The right part of the Paschen's curve is applicable for the AC fields at the relevant ambient conditions for the FunMass instrument (pressure $\geq$50 hPa, temperature inside of the wingpod $\geq$$-30\,°\text{C}$), where the mean free path ($\leq$ ~0.5 µm) is much shorter than the distance between the electrodes (discharge surfaces) ($\geq$1 mm) [72].

The IFS generates up to 10 kV AC for the ion source. At 50 hPa, this voltage can break down for distances up to approximately 5 cm, which exceeds the distance between the high voltage contacts and IFS housing (or to any other conductor in general). Although the high voltage contacts are insulated with rubber coating, this cannot ensure reliable operation under low pressure conditions, since this insulation could be damaged or get loose, for example, during the reattachment of the ion source cables.

To prevent potential damage to the instrument or even damage to the aircraft, it was decided to keep all high voltage units pressurized. The pressures inside of them are monitored during the flight and if a leak is detected, the leaking unit will be shut down by the control program as a precaution before pressure reaches dangerous levels. The threshold pressure is set to 700 hPa (Figure 5.15).

5.9 Test flights and climate chamber tests

5.9.1 Test of components in the climate chamber

The TofWerk MS components were delivered in late June 2016. Therefore we had less than two months before the beginning of the test campaign (August/September 2016) to assemble the complete instrument and make first tests. For this purpose IEK-7 owns a climate test chamber (WK 500/70-100/D, Weiss Umwelttechnik GmbH, Germany) that can simulate in-flight conditions with temperatures down to $-80\,°\text{C}$ and pressures down to 10 hPa.

Figure 5.15: Breakdown voltage in air at 50 hPa and 700 hPa according to Equation 5.6.

The chamber dimensions are $77 \times 75 \times 75$ cm. Unfortunately, FunMass in its flight configuration exceeds these dimensions and therefore a full test of the instrument was impossible without rearranging the components to fit the chamber. Due to lack of time those necessary rearrangements could not be done before the campaign. The decision was made to test only the main critical components separately in the climate chamber:

- After standard sniffing tests employing a leak detector the pressurized components the TPS, pulser, BSQ power supply and IFS were separately kept in the climate chamber for 10 hours at pressure down to 50 hPa and temperature down to $-20\,°C$. No major leaks were found.

- The IDP-3 pumps were characterized in terms of pumping power and power consumption at the relevant pressures and temperatures in order to ensure that the standard TofWerk power supplies housed inside the Giraffe were appropriate. No problems were found. A maximum power consumption of the funnel pumping unit of 180 W under operating conditions was found.

- The original high voltage cables delivered with CTOF by Tofwerk AG employing standard HV connectors (coax high voltage connectors, Fischer connectors, Switzerland). They were found to develop internal sparking in the backshells at relevant flight pressures. Therefore all plugs were redone employing a special high-vacuum glue (Torr Seal, Kurt J. Lesker Company, USA) applied inside the backshells. Each of these home-made cables was qualified in the the climate chamber at 50 hPa and $-20\,°C$ for 4 kV applied from a special DC voltage supply while maximum operational voltages were less than 3 kV.

Summarizing no in-flight HV problems were encountered due to low pressures and temperatures for the tested units.

(a) Geophysica M55 in the hangar in Kalamata Airport (KLX) during the test campaign 2016.

(b) FunMass mounted in the left wingpod of the aircraft.

Figure 5.16: Photographs from the test campaign 2016, Kalamata, Greece

5.9.2 Instrument certification tests

In order to be integrated on the aircraft, an electromagnetic compatibility (EMC) test along the specification RTC-DO160E (category M) as well as a mechanical certification along the specification RTCA/DO-160G has to be supplied for each instrument to the aircraft operator.

The EMC test ensures that the running instrument does not interfere with the aircraft electronics and other instruments. The EMC test for FunMass was carried out at the EMC chamber at ZEA-2, Forschungszentrum Jülich GmbH [102]. FunMass directly passed the test.

The mechanical certification was supplied based on a finite element method (FEM) stress analysis performed by ZEA-1, Forschungszentrum Jülich GmbH. This analysis ensures the instrument hardware will stand mechanical stress up to 10g in each direction [101]. The FunMass design passed the test.

5.9.3 Results of the test campaign in Kalamata, Greece

Despite the fact that all airborne instruments are certified beforehand to meet the electromagnetic requirements of the aircraft, the EMC test has to be run on the ground with all instruments on board before the first measurement flight. This is done to check if simultaneous operation of all instruments causes any problems as well as to test the power system of the aircraft.

Since the inlet and the flow system could not be tested in the climate chamber due to time constrains, we decided to first test them in-flight. Since failure of the inlet could have led to excessive pressures within the TOF MS this could not be activated before proper inlet operation had been ensured.

During the test campaign we faced a number of complications for FunMass, which are described in a short summary of the test campaign:

- 1st test flight (30.08.2016): the main program lost connection with gasdeck control boards at the moment when power was switched from the ground power unit (GPU) to the aircraft engines. The program failed to reconnect and communication with the inlet was lost. This problem was solved on the ground before the next flight.

- 2nd test flight (01.09.2016): the inlet did not open because of a defect in its motor. The motor was replaced before the next flight.

- 3rd test flight (06.09.2016): the inlet regulation worked as desired. The instrument was deemed fully operational during the 4th test flight. Unfortunately, the 4th and final flight had to be canceled due to severe flooding of the Kalamata region with closure of the airport for 3 days. This left us without a test in full measurement mode.

Some data from the 3rd test flight (as the most complete for FunMass at the time) are shown in Figure 5.17. While the air temperature inside the instrument insulation cover went down to $-20\,°C$, it did not cause any issues as all temperature sensitive units were also heated using thermofoil heaters with temperature switches. Pressure in the funnel stayed in acceptable range, see Figure 5.18. The housings of TPS, IFS and pulser also stayed pressurized during the entire flight. That would have allowed us to activate full measurement mode (with all high voltages switched on) for the 4th flight.

Although FunMass was operational, as any new instrument being developed, it had room for improvement. During the test campaign three obvious problems were identified:

- Figure 5.17 shows that the pressure in the pressurized IFS housing was low from before the flight. Here a small crack in the ceramic of the ion source was found. It caused a leak from the IFS housing through the pressurized HV connector into the pumped IMR region. The drop from around $1000\,hPa$ to $800\,hPa$ happened during a few days, caused by the FunMass pumps being operated 24/7. Fortunately, the leak was small and within the flight it did not cause a critical drop of the pressure. In Jülich the ceramic was exchanged and this problem was solved;

- in order to operate the MS the pressure in the TOF housing should be below 5×10^{-6} hPa. Figure 5.18 shows that the necessary pressure was achieved only after about 30 min from the moment the inlet was open. This results in at least 30 min (could vary) of measurements being lost. The in-flight variation of the TOF pressure with ambient pressure gave us the hint that there was a leak on the TOF housing. Back in Jülich, this leak was located at the mounting flange of the pressure sensor and the problem was eliminated. In regular operation FunMass is switched on shortly before the pilot gets into the cabin, approximately 45 min - 60 min before take-off, which is sufficient to reach the pressure threshold well before start of the measurements;

- in order to achieve good measurement sensitivity and accuracy, FunMass should be operated around the optimum funnel pressure (25 hPa - 35 hPa) where also calibrations are done. During the 3rd test flight the pressure stayed within a range of 15 hPa - 30 hPa which should be improved by revising the inlet regulation.

5.9.4 Full-up climate chamber tests

In April/May 2017, after resolving the problems discussed in the last section FunMass was temporarily rearranged to fit into the climate chamber (Figure 5.19).

Full flights were simulated in terms of ambient pressure and wingpod temperature by a computer-based control of the climate chamber. During those flight simulations:

- the instrument's performance was monitored at close to in-flight conditions (pressure down to 50 hPa, temperature down to $-30\,°C$); first fully operational manual and autonomous run of the instrument at low pressure and temperature;

- the FunMass autonomous control program was fully tested and optimized.

Figure 5.17: Data from the 3rd test flight (06.09.2016), Kalamata, Greece. The ambient temperature and pressure were taken from the Geophysica avionic data.

Several major and minor problems were identified and solved. The inlet regulation logic was revised and established as already described in Section 5.3. The latest version of the regulation is based on the data from the pressure sensor in the funnel and now managed by the main program on the FunMass computer. The previous one was using the data from the mass flow meter (MFM, see Figure 4.1), because it was managed by a task on the CHM2 board in the gasdeck, which did not have access to the data of the pressure in the funnel. Figure 5.14 clearly shows the improvement in the funnel pressure stability achieved by these modifications. Sharp spikes of the funnel pressure in Figure 5.14(b) appear at the moments of switching between different modes (Section 6.7) due to short pressure jumps and are managed within 5 s. In the end of June 2017 FunMass was assembled back to the flight configuration and shipped to Kathmandu for the main part of the StratoClim aircraft campaign (July/August 2017).

5.10 FunMass instrument performance during the campaign in Kathmandu

All critical parts of FunMass had been tested during the test campaign in Kalamata and in the climate chamber, therefore FunMass was planned to fully operate and make atmospheric measurements from the very first flight in Kathmandu.

However, one very critical component, namely the regulating inlet unfortunately did not open on the first four flights and therefore no atmospheric measurements could be acquired. However, in-spite of very low temperatures all other FunMass components performed normally and reactant ions were produced and measured over the complete flights.

During the first flight, the inlet did not open when commanded at the ambient pressure

Figure 5.18: Pressure in the funnel and in the TOF during the 3rd test flight (06.09.2016), Kalamata, Greece.

Figure 5.19: Rearranged FunMass configuration for the climate chamber in IEK-7. (a) photograph, (b) schematic by Jochen Barthel.

of 200 hPa. Even right after the flight the inlet did not work on the ground. The instrument was dismounted from the aircraft and the inlet was cleaned and the rotating parts were additionally greased. FunMass was mounted back and successfully tested on the ground before the next flight.

However in the next three flights the inlet did not open in spite of successive application of heating elements and thermal insulation to various parts of the inlet. Due to the huge ambient air flow around the inlet it is impossible to keep the inlet support structure at temperature much above the ambient temperature. This inlet problem is assumed to be a complex combination of different factors, related to mechanical stress on the inlet drive due to thermal deformations of the wingpod's front part. Therefore, when integrating FunMass again the instrument position was slightly moved backwards (as far as achievable within the mounting screws) in order to prevent stress on the inlet plate.

In the fifth flight the inlet finally opened but due to overheating on the ground before the take off, the turbo pump failed and didn't run for the whole flight, although it remained powered. Therefore the threshold TOF pressure was not reached and no measurements could be done. A new function in the main flight program was implemented to detect the unexpected failures of the turbo pump and to restart if necessary after a 10 minutes break, necessary for the pump to cool down. A definitive solution may still need to be found. The prevention of overheating of instrument components during long waiting loops before take-off with the aircraft exposed to the full sun is almost impossible without switching off components and was experienced by many instruments during the StratoClim campaign.

In the sixth flight only a minor problem with the ion source due to an hitherto unexperienced high voltage drift appeared and the last 15 minutes of the measurements were lost. After this, a small function in the program was introduced to prevent drop of the high voltage in the ion source.

During the seventh flight FunMass worked flawlessly and a full data set was acquired. Before the eighth flight the instrument was dismounted to refill water in the gasdeck and to prepare instrument for the I^- mode which we aimed to use on at least one flight to gather some halogen species data. Unfortunately, during the flight the inlet did not open. In addition to the inlet issue, overheating of the ADQ on the ground occurred. That problem led to the loss of all mass spectra during the flight. The ADQ has to remain powered from the beginning on to allow all data from all parts of the instrument to be stored in one datafile along with mass spectra. That is a requirement of the supplied software from TofWerk. This requirement can be bypassed by using a software simulator while the instrument is on the ground and no actual measurements are done, allowing the ADQ to remain off till the actual flight begins. This will eliminate the risk of ADQ overheating on the ground, and the ADQ will be powered only after the take off, and the system will return to the standard data acquisition procedures.

Table 5.1 gives an overview of the somewhat disappointing FunMass performance during the Kathmandu flights. However, for a new instrument of this complexity, such failures due to unexpected problems which also were extremely hard to diagnose and remedy in the field can happen. However, the first results of the successful flights 6 and 7 are presented and discussed in Chapter 8.

Flight #	Date	Status	Comment
Flight 1	27.07.2017	No atmospheric data	Instrument operated; inlet didn't open
Flight 2	29.07.2017	No atmospheric data	Instrument operated; inlet didn't open
Flight 3	31.07.2017	No atmospheric data	Instrument operated; inlet didn't open
Flight 4	02.08.2017	No atmospheric data	Instrument operated; inlet didn't open
Flight 5	04.08.2017	No MS	Overheating of the turbo pump
Flight 6	06.08.2017	Missing data in last 15 minutes	Drop of ion source voltage in the last 15 minutes
Flight 7	08.08.2017	Full flight data	
Flight 8	10.08.2017	No MS	Overheating of ADQ on the ground, inlet didn't open

Table 5.1: FunMass performance during the Stratoclim campaign, Kathmandu, Nepal, 2017.

Chapter 6

Characterization and calibration of FunMass

In this chapter, the calibration process of FunMass is described. Also, the characterization and the relevant specifications of the instrument are discussed. Due to the peculiarities of the CIMS technique FunMass is calibrated in the laboratory for all detected species but also has an in-flight calibration for at least one species to ensure accurate measurements. Both techniques are discussed in the following sections. Generally, calibrations should be done employing the best accuracy analyte mixing ratios that can be reasonably purchased or generated.

6.1 Signal processing

Before jumping into the instrument characterization, a short introduction to the acquisition of the TOF MS data will be given and a few terms and units will be explained. In order to simplify the reading, this discussion will just describe the current set-up employed for the TofWerk CTOF used in the FunMass instrument with its default settings, which can of course be adapted to other requirements, like faster data rates, etc.

A fast analog-to-digital converter ("ADQ") converts the preamplified MCP signal (voltage) with a temporal resolution of $0.625\,\mathrm{ns}$. The time between two consecutive ion extractions is $17\,\mathrm{\mu s}$ ($60\,\mathrm{kHz}$), while data cannot be stored at such high frequency. Data transfer from the ADQ to the host computer is set to $2\,\mathrm{Hz}$, i.e. the ADQ summarizes in its memory 30006 spectra and sends the result to the PC via an USB 2.0 port. These 30006 extractions are referred to as one "block". An example of a typical spectrum was shown before in Figure 5.9. In the data file, the sum of 30006 spectra (one block) is stored in units of mV. From that, the averaged spectrum within one block can be calculated.

So a spectrum is an array of numbers with their indexes being proportional to the time when the corresponding part of the signal from the MCP was processed by the ADQ and therefore proportional to time-of-flight of the ions which generated this part of the signal by exciting the MCP.

The index of the array (stored spectrum) is converted to the mass-to-charge ratio m ($z = 1$) by the following formula [90]:

$$m(i) = \left(\frac{(i - p_2)}{p_1} \right)^{\frac{1}{p_3}} , \tag{6.1}$$

where i is the index, p_1, p_2 and p_3 are the mass calibration parameters. These calibration parameters are derived from three or more peaks which mass-to-charge ratios have to

Figure 6.1: The peak at m/z 60, which corresponds to the reagent ion CO_3^-. The mass spectrum was averaged for 0.5 s.

be specified. The spectrum can be recalibrated post-factum using different peaks or even using a formula different from Equation 6.1. All routines for that are provided by TofWerk. An array of the converted indexes to the corresponding masses is automatically generated and stored alongside the spectrum in the datafile.

In Figure 6.1, a typical averaged peak corresponding to the reagent ion CO_3^- (60 Th) is plotted. From now on, an averaged spectrum of one block of extractions will be referred as "spectrum". The peak area is proportional to the number of ions with the corresponding mass-to-charge ratio detected by the MCP during one extraction on average for one block. This area can be converted to the number of detected ions by dividing it by the so-called "single ion signal", which is the signal generated by a single ion in mV×s [90]. The number of ions with a given mass-to-charge ratio detected by the MCP during one extraction is called "ion count rate" for this specific ion. The areas under the peaks are calculated by numerical integration using as limits the nominal mass (an integer number) ± 0.5 Th by default. These default limits can be modified if needed. These areas are calculated for all nominal masses within the range of the mass spectra, converted to ions count rates and stored alongside with the spectrum by the TofWerk software automatically. For a strong and isolated peak as in Figure 6.1, numerical integration gives accurate results of the ion count rate. If two peaks are closer than 0.5 Th or noise is comparable to the signal, then the automatic routines operating with the default integration limits will be affected by the second peak or noise and the results will not be accurate, i.e. will not just represent the ion count rate due to one specific ion. Figure 6.2 shows such a case where a yet unidentified "artifact" [68] appears close to mass-to-charge ratio 26 (CN$^-$). Here, peak fitting routines can be used to isolate the peak. However, in this work these routines were not applied, since even for m/z 26 the calibrations have shown that the default procedure provides reliable count rates. The contribution of the artifact is getting eliminated when the background is subtracted (see Section 6.3).

Figure 6.2: The peak at m/z 26 and unknown "artifact" at slightly lower m/z. The mass spectrum was averaged for 30 s. The area under the peak calculated by the default routines (yellow) and area under the fitted Gaussian peak (pink) are indicated.

6.2 Laboratory calibration

Calibration of the FunMass instrument should cover the mixing ratio range expected in the UTLS. This is rather demanding for the low mixing ratios of the target species, especially if these are reactive or sticky. For calibrating FunMass, so-called permeation tubes with HNO_3, SO_2 and HCN (Fine Metrology, Italy) were used as gravimetric standards. A permeation tube is a section of a plastic tube with an enclosed substance, which permeates out (outgases) a given substance in nanogram quantities per minute at a stable rate (at constant temperature) until the enclosed content is nearly exhausted [63].

To calculate the permeation rates, the tubes are usually weighed every one to two weeks employing a precision balance. Within this procedure, three independent weighings are averaged for each tube and a reference mass is used in order to establish the reproducibility of the balance. Typical results are summarized in Table 6.1. For the mass determination of the permeation tubes an analytical balance with readability of 0.01 mg (CPA225D, Sartorius Lab Instruments GmbH, Göttingen, Germany) is used. It should be mentioned that for HNO_3 mainly two problems for permeation devices have been reported:

- Different ratios of water vapor may be emitted from the devices. Our device contains an azeotropic mixture of HNO_3 in water (68% of the weight is HNO_3) and the tube is expected to also emit this gas ratio, which reportedly may change [39].

- HNO_3 may decompose photolytically and also thermally according to the reaction: $4\,HNO_3 \longrightarrow 4\,NO_2 + O_2 + 2\,H_2O$ which also leads to NO_2 and O_2 emission from the permeation device [75].

Both problems will make the gravimetric determination of the gas mixture obsolete. No such problems are known for devices containing (pure) SO_2 or HCN.

Name	Permeation rate & uncertainty 1σ	Mixing ratio range	Weight on 11.01.2018	Uncertainty 1σ
HNO_3	$(6.53 \pm 0.07)\,\mathrm{ng\,min}^{-1}$	64 ppt to 1290 ppt	$4.176\,66\,\mathrm{g}$	$1 \times 10^{-5}\,\mathrm{g}$
SO_2	$(6.83 \pm 0.02)\,\mathrm{ng\,min}^{-1}$	65 ppt to 1300 ppt	$24.169\,20\,\mathrm{g}$	$1 \times 10^{-5}\,\mathrm{g}$
HCN	$(68 \pm 2)\,\mathrm{ng\,min}^{-1}$	1.6 ppb to 34 ppb	$8.997\,74\,\mathrm{g}$	$3 \times 10^{-5}\,\mathrm{g}$

Table 6.1: Gravimetric permeation rates with their uncertainties determined from 17 weighings of the permeation tubes contained at 25 °C from February of 2017 to May 2018. The possible range of mixing ratios was calculated for a minimum flow of 2 slm and a maximum of 40 slm.

Figure 6.3: Schematic diagram of the calibration setup. Adapted from Kloss [44].

A home-built permeation oven is employed to stabilize the temperature of the tubes with an accuracy better than 0.1 °C [98], being 25 °C the chosen temperature for the FunMass standards and yielding the permeation rates given in Table 6.1. The oven is constantly flushed with at least 0.05 slm of dry N_2 (purity 5.0) or synthetic air (purity 5.0) to prevent accumulation of the permeated gases. When changing the flow through the oven, sticky species like HNO_3 will take minutes to hours to equilibrate to the state where the mixing ratio corresponds to the permeation rate [62]. It is extremely important that the surfaces are inert to the species under investigation, otherwise this state will never be reached [45].

During the calibration, the emitted gas from the permeation devices is diluted with synthetic air (purity 5.0). With one or two (parallel) MFCs (Mass Flow Controller MC-10SLPM-D, NATEC Sensors GmbH, Garching, Germany, accuracy is better than 1%), the dilution flow can be regulated up to 40 slm and together with the known permeation rates, the resulting mixing ratio of the produced gases are calculated. A schematic of a typical calibration setup with the permeation system is shown in Figure 6.3. The mixing ratios could be held in the ranges listed in Table 6.1. One of the advantages of the described setup is that the instrument can be calibrated to several analytes simultaneously. The response of the instrument to such multi species calibration (HNO_3 and SO_2) is shown in Figure 6.4. In order to avoid irreversible absorption to any wet surfaces (oven, valves, gas lines) the permeation oven is coated with Silconert 2000 (Restek GmbH, Bad Homburg, Germany) and PFA Teflon lines heated to 40 °C [45, 62] were used to deliver standards to the instrument. To guarantee full HNO_3 adsorption/desorption, dwell times of 10-20 minutes are needed for the surfaces to equilibrate, ensuring signal stabilization. Nevertheless, for HNO_3 wall effects give the biggest uncertainty to the calibration of all the measured species.

Figure 6.4: Simultaneous calibration of the FunMass instrument to SO_2 and HNO_3.

6.3 Sensitivity

Sensitivity is the slope of the calibration curve (analyte amount vs. signal strength), i.e. sensitivity determines the response of any analytical system for a certain analyte when operated under well-defined conditions [24, 60].

FunMass was calibrated multiple times with the described calibration setup before and after the Nepal campaign (Figures 6.5 - 6.7). Calibrations were done at slightly different pressures in the funnel (30 - 35 mbar) and with and without addition of H_2O (around 15 ppm) from the H_2O inlet (Figure 5.4). The instrument response to SO_2, HNO_3, HCN was measured at the peaks 112 Th (SO_5^-), 123 Th ($CO3^-(HNO_3)$) and 26 Th (CN^-) respectively. Schematically the chemical ionization process can be written as:

$$A + R^- \longrightarrow P^- + B, \tag{6.2}$$

where A is the analyte, R^- is the reagent ion and P^- is the corresponding product ion. The mixing ratio of analyte [A] is proportional to the following ratio

$$[A] \propto \frac{P^-}{R^-}, \tag{6.3}$$

where P^- is the count rate of the corresponding product ion and R^- is the count rate of the reagent ion CO_3^- (60 Th), both derived from the areas of the corresponding peaks. These ratios are shown in Figures 6.5(a), 6.6(a) and 6.7(a) as a function of the species mixing ratios, and will be referred from now on as "normalized count rates". The instrument response to different concentrations of analytes is a linear function as long as the reagent ion concentration is not depleted too much.

(a) Calibration of SO_2. The ion count rate at $112\,Th$ (SO_5^-) divided by the reagent ion count rate at $60\,Th$ (CO_3^-).

(b) Calibration of SO_2. The ion count rate at $112\,Th$ (SO_5^-) divided by the reagent ion count rate at $60\,Th$ (CO_3^-) minus the background.

Figure 6.5: Calibration of SO_2

(a) Calibration of HNO₃. The ion count rate at 123 Th (CO3⁻(HNO₃)) divided by the reagent ion count rate at 60 Th (CO₃⁻).

(b) Calibration of HNO₃. The ion count rate at 123 Th (CO3⁻(HNO₃)) divided by the reagent ion count rate at 60 Th (CO₃⁻) minus the background.

Figure 6.6: Calibration of HNO₃

(a) Calibration of HCN. The ion count rate at 26 Th (CN$^-$) divided by the reagent ion count rate at 60 Th (CO$_3$$^-$).
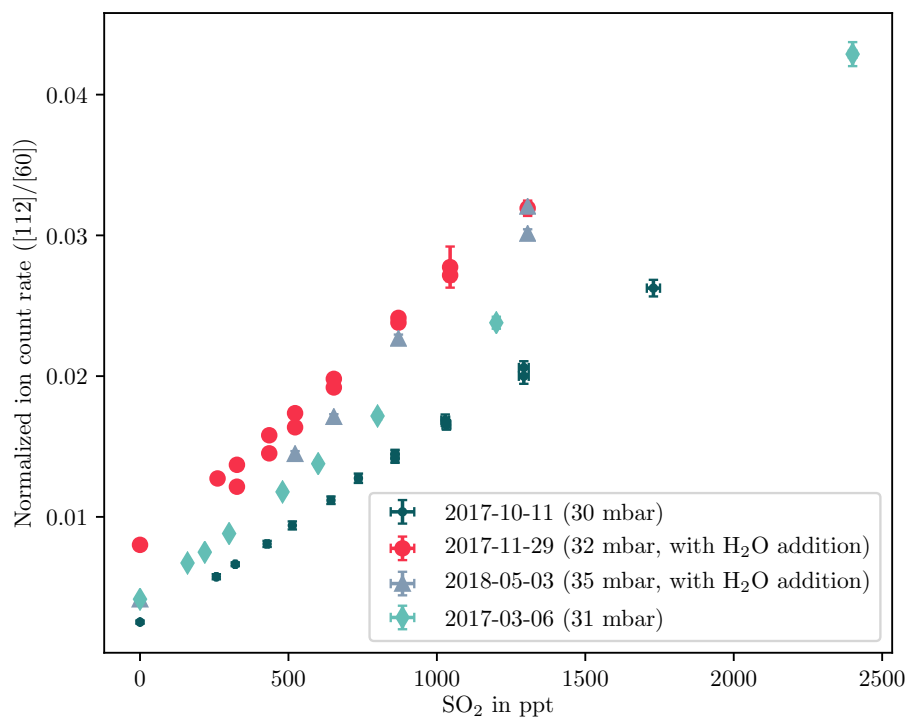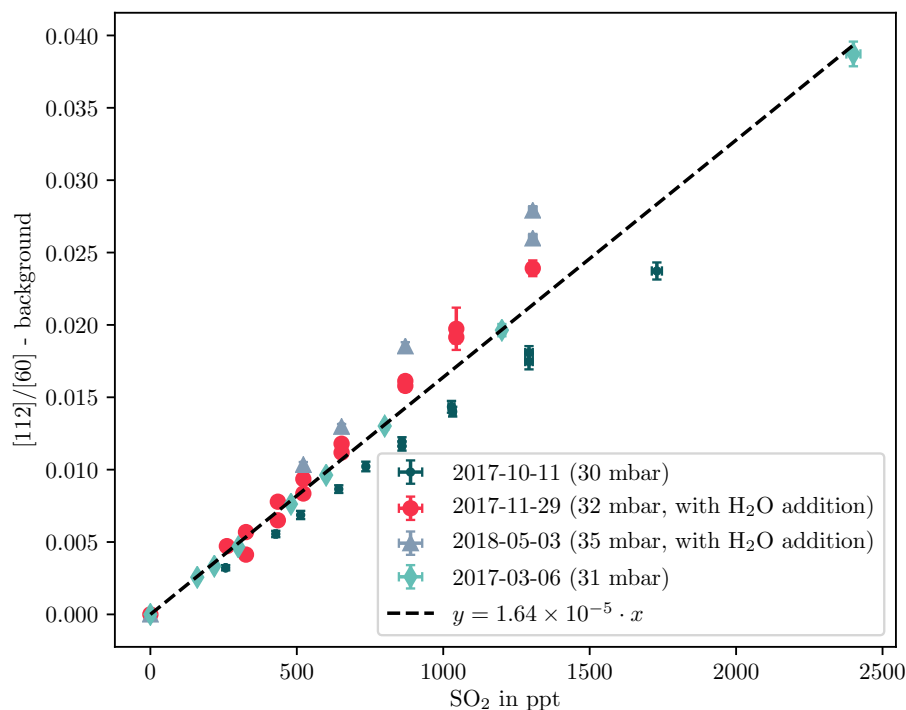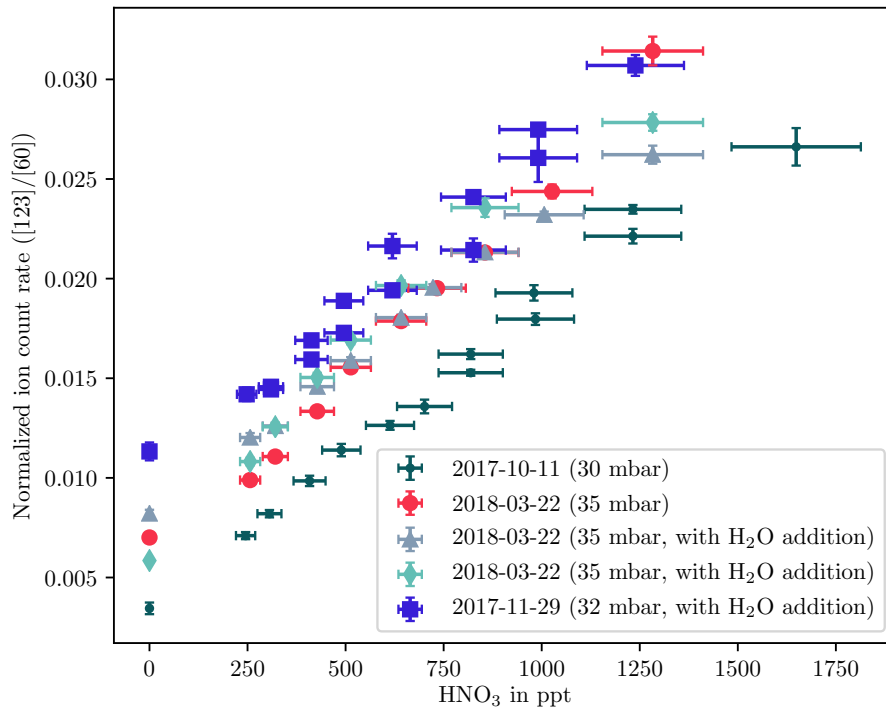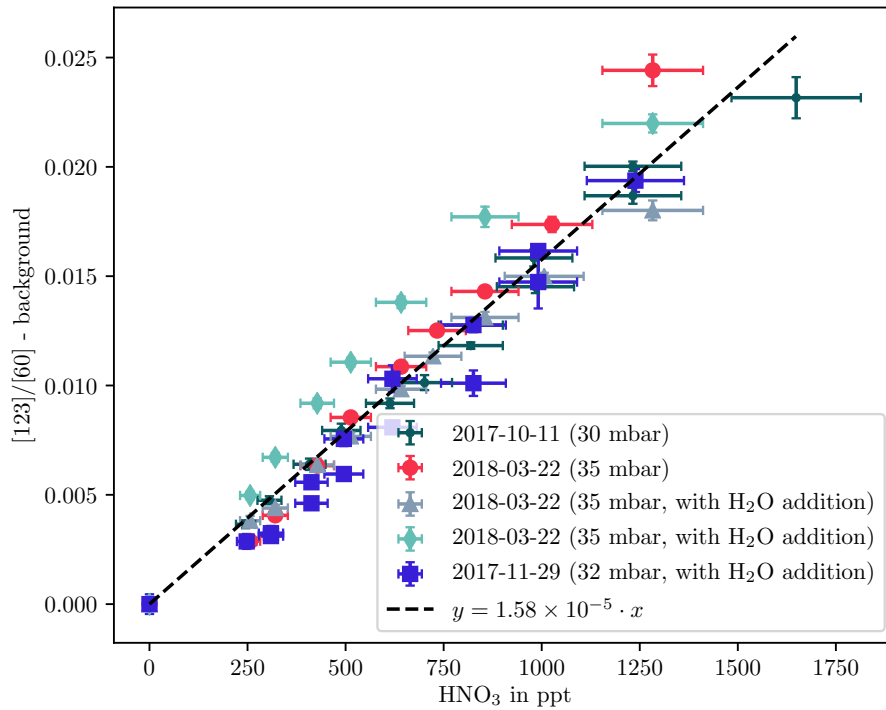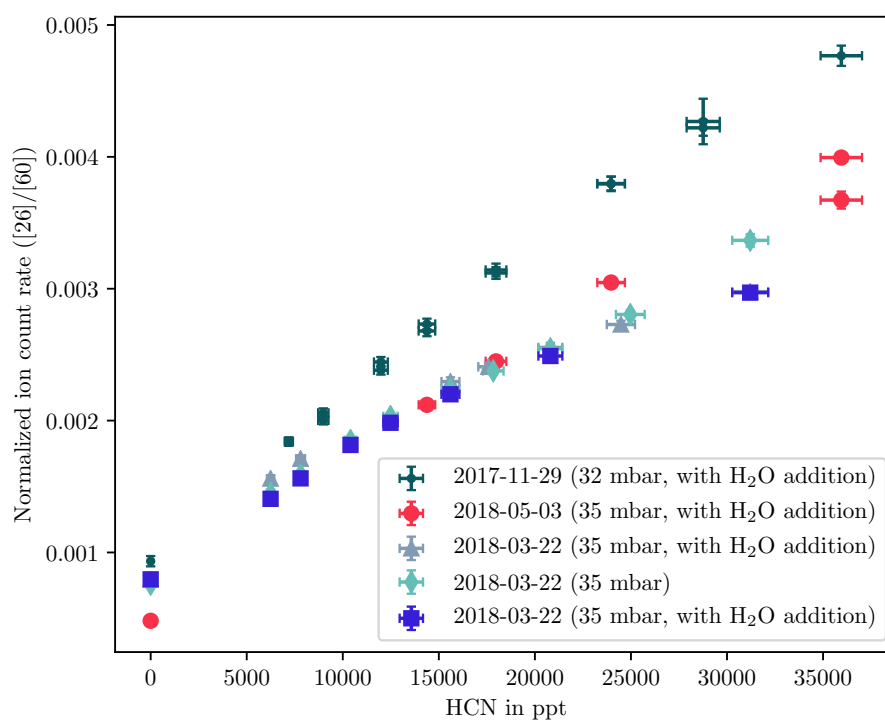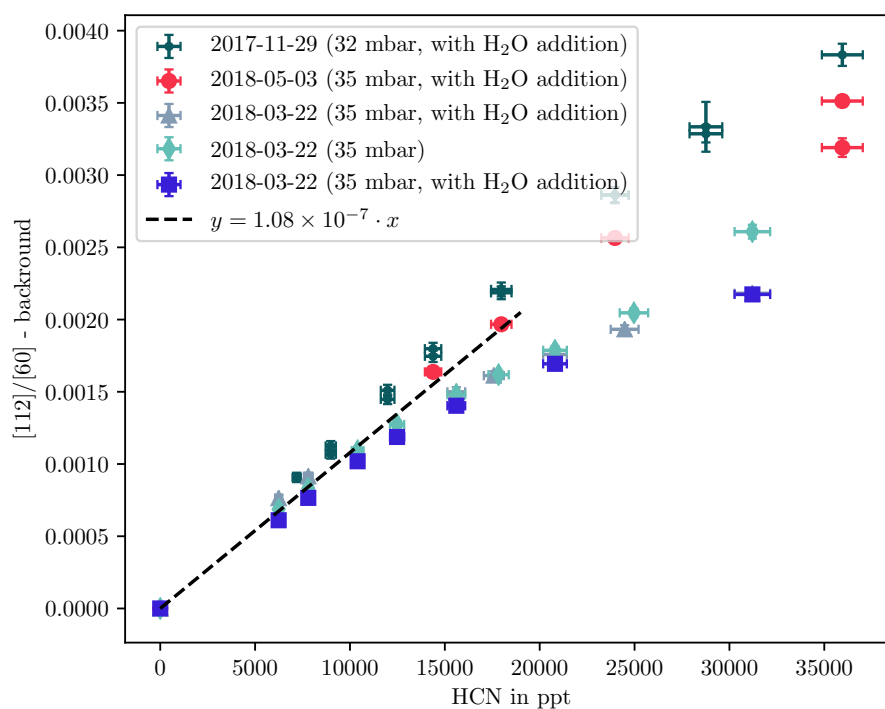
(b) Calibration of HCN. The ion count rate at 26 Th (CN$^-$) divided by the reagent ion count rate at 60 Th (CO$_3$$^-$) minus the background. Only data with mixing ratios below 20 ppb were used for the linear regression fit, e.g., for the sensitivity determination.

Figure 6.7: Calibration of HCN

As obvious from Figures 6.5(a), 6.6(a), 6.7(a) the extrapolations of the normalized signals to zero mixing ratio do not yield zero signal but a background (or blank) of different size is observed for the different species instead. This background may have several causes:

- Species absorbed by the instrument walls will cause a low permanent background concentration in the instrument. This effect will increase the more sticky a species is (HNO_3).

- For the species employed for the in-flight calibration small remainders of the species may leak out of the calibration line (SO_2).

- Other unknown isobaric ions may cause a background. However, we are not aware of any other species abundant in the UTLS generating ions on the respective m/z values.

In order to properly account for that, the background is also determined during the flight (see Section 6.7).

After the background was subtracted (Figures 6.5(b), 6.6(b), 6.7(b)), linear regression with no intercept parameter was used to determine the sensitivity factors: $1.58 \times 10^{-5}\,\mathrm{ppt}^{-1}$ for HNO_3, $1.64 \times 10^{-5}\,\mathrm{ppt}^{-1}$ for SO_2 and $1.08 \times 10^{-7}\,\mathrm{ppt}^{-1}$ for HCN. A typical count rate for the reagent ion CO_3^- in the current configuration of the FunMass instrument is about $2 \times 10^7\,\mathrm{ions\,s^{-1}}$, that allows to present sensitivity of the instrument in more physical units: $>300\,\mathrm{ions\,s^{-1}ppt^{-1}}$, $>320\,\mathrm{ions\,s^{-1}ppt^{-1}}$ and $>2\,\mathrm{ions\,s^{-1}ppt^{-1}}$ for HNO_3, SO_2 and HCN respectively.

As can be seen in Figures 6.5(b), 6.6(b), 6.7(b), the sensitivity does not show clear dependence on the humidity or funnel pressure over the relevant range.

The sensitivity for HCN in the atmospherically relevant range below 500 ppt has been extrapolated here from higher mixing ratio calibrations due to the high permeation rate of the HCN device. However, no problems of an extrapolation from mixing ratios in the ppb range down to hundreds of ppt are anticipated for a relatively stable and non-sticky species. A new permeation tube is currently being prepared for HCN and more studies on the sensitivity of the instrument in the missing range will be done.

6.3.1 Error in calibration curve results

The uncertainty of the unknown mixing ratio can be calculated with the following formula [10, 87]:

$$s_x = \frac{s_y}{m}\sqrt{\frac{1}{n} + \frac{1}{k} + \frac{(y_u - \bar{y})^2}{m^2 \sum (x_i - \bar{x})^2}}, \tag{6.4}$$

where

- s_x is the uncertainty in the unknown (predicted) mixing ratio,

- $s_y = \sqrt{\dfrac{\sum (y_i - mx_i)^2}{n - 2}}$ is the standard deviation in the residuals,

- m is the sensitivity (slope of the calibration curve),

- n is the number of points in the training dataset (calibration dataset),

- k is the count of measurements of the unknown,

Figure 6.8: Distribution of the background measurement at 123 Th ([123]/[60]) from a 4 min sampling period at 2 Hz.

- y_u is the measurement of the unknown (mean value if $k > 1$),

- $\bar{y}$ is the average measurement of the standards (training dataset),

- x_i are the true concentrations of the standards (training dataset),

- $\bar{x}$ is the average concentration of the standards (training dataset).

6.4   Limit of detection

Detection limit of the instrument corresponds to the smallest Δs that the signal $s_0 + \Delta s$ can be "reliably" distinguished from the zero measurement s_0 (background or blank). If the background measurement follows the Gaussian statistic $n(\mu, \sigma^2)$, then $\mu \pm 2\sigma$ gives the 95.4% confidence interval around the mean measurement of the background. In order to determine the limit of detection for the FunMass instrument and make it compatible with most values reported in the literature, this value of 2σ will be used.

As explained above, the detection limit of any instrument, including CI-TOFMS, depends on the variability of the instrument zero. The background measurements were done with dry synthetic air (purity 5.0). Figure 6.8 and Figure 6.9 on the example of HNO_3 show that the measurements of the background signal can be characterized with the normal distribution. Standard deviation σ for the background measurements were calculated for SO_2, HNO_3 and HCN. For these standard deviations, 2σ detection limits for 0.5 s average were calculated, being 2.6 ppt, 2.7 ppt and 200 ppt for HNO_3, SO_2 and HCN respectively. The detection limits for longer averaging times are discussed in the next section, providing much better detection limit for HCN.

Figure 6.9: Q-Q (quantile-quantile) plot, comparing distribution of the HNO$_3$ background signal to the normal distribution. 2 Hz data taken from a 4 min sampling period while sampling zero air.

6.5   Precision

Precision describes the reproducibility between two or more measurements of the same value to each other. In order to estimate the short-term precision of the FunMass instrument, the normalized difference between adjacent points for 1 h of measurement at 1.5 Hz, at constant SO$_2$, HNO$_3$ and HCN concentrations were calculated using Equation 6.5 for each analyte respectively [6].

$$NAD = \frac{[X_n] - [X_{n-1}]}{\sqrt{[X_n][X_{n-1}]}} \tag{6.5}$$

Figure 6.10 shows the standard deviation of the Gaussian fit to the normalized distribution of the normalized adjacent differences (NAD), which is a direct measure of the instrument precision. From this analysis, the upper limit to the short-term precision (1σ) is 0.95% for an HNO$_3$ concentration of 600 ppt. The short-term precision, derived from the normalized adjacent difference analysis, was calculated for a range of different concentrations of HNO$_3$, SO$_2$ and HCN. This analysis shows short-term (at around 1 s) precisions not higher than 2% for HNO$_3$, 2.5% for SO$_2$ and 5% for HCN.

Averaging the signal may reduce the variance in the background measurements by eliminating white noise, which gives better detection limits. However, other factors (e.g. instrumental drift in the calibration) often become significant on timescales 30 s - 1 min, limiting the reasonable averaging time. The Allan variance ([99], [6]) was used to determine the time period for which averaging no longer improves signal-to-noise ratio. The Allan variance was calculated using the package `allanvar` of the programming language R [11, 71]

The Allan deviation (square root of Allan variance) was calculated using the signals corresponding to SO$_2$, HNO$_3$ and HCN from one hour of continuous measurements of the blank. The results are shown in Figure 6.11. From the analyses of the Allan deviation, the

Figure 6.10: Distribution of normalized adjacent differences, calculated for normalized count rate at 123 Th ([123]/[60], HNO_3) from one hour of continuous 1.5 Hz measurements of 600 ppt of HNO_3.

optimal integration periods are 10 s for SO_2, 20 s for HNO_3 and 80 s for HCN, giving the detection limits 1.62 ppt, 0.66 ppt and 36 ppt for them correspondingly. The detection limits for a 20 s average are 1.7 ppt, 0.8 ppt and 64 ppt correspondingly.

6.6 Accuracy

The accuracy of the instrument determines how close the measured value actually is to the real (true) one. Therefore, the accuracy is closely related to the calibration process, as only when the instrument is being calibrated the true measured value is known.

Several different factors contribute to the scattering of the FunMass measurements around the calibration line in Figures 6.5(b), 6.6(b), 6.7(b):

- uncertainties in the mixing ratios of the standards, which come from:

  - uncertainties in the permeation rates of the devices;

  - uncertainties in the flow controlled by the mass flow controllers;

  - wall losses and wall outgasing. They are hard to quantify. Materials were chosen to minimize them [45];

- different conditions of the experiments, among others:

  - slightly different pressure in the IMR region;

  - different days, therefore different temperature in the lab, i.e. in the IMR;

  - different ion source settings/performance;

Figure 6.11: Allan deviation plot, calculated using SO_2, HNO_3 and HCN signals from one hour of continuous $1.5\,Hz$ measurements of the blank.

6.6.1 Uncertainties in mixing ratios of the standards

As mentioned above, the uncertainties in the mixing ratios of the standards derive from uncertainties in the permeation rates and the uncertainties of the mass flow controllers. As explained in Section 6.2, the permeation oven uses up to two NATEC flow controllers simultaneously. Each regulates flow with a relative uncertainty better than 1%. The mixing ratio r has the following dependence on the permeation rate and flows through the oven:

$$r \propto \frac{p\_rate}{f_1 + f_2},\qquad(6.6)$$

where p_rate is the permeation rate of the corresponding device, f_1 and f_2 are flows through the first and second MFCs of the calibration oven.

Each term in Equation 6.6 is associated with an error which are not correlated with each other. Therefore simple error propagation can be employed here [7, 47] The derived error budget for the mixing ratios is summarized in Table 6.2. However, the reasonable estimate for the uncertainty of the HNO_3 mixing ratio is expected to be much higher than the calculated 1.4% due to the many potential issues with HNO_3 permeation devices (briefly discussed in Section 6.2). We estimate the final uncertainty of the HNO_3 mixing ratio to not be better than 10%.

6.6.2 Accuracy of the measurements

In order to derive the accuracy of the instrument, calibration data are used. The calibration process is reduced to a linear regression problem. The linear regression fits shown in Figures 6.5(b), 6.6(b), 6.7(b) were done based on all calibration data listed in the corresponding legend.

Training the linear regression model and testing its quality both only on the same dataset is a bad practice in statistics [27], because the model can be easily overfitted to these data

	SO_2	HNO_3	HCN
Permeation rate [ng min^{-1}]	6.83	6.53	68
Uncertainty perm. rate (gravimetric) [ng min^{-1}]	0.02	0.07	2
Rel. perm. rate uncertainty (gravimetric)[%]	0.3	0.9	2.9
Rel. uncertainty, MFC [%]	1	1	1
Calc. rel. uncertainty, mixing ratio [%]	1.0	1.4	3.1
Expected rel. uncertainty, mixing ratio [%]	1.0	10	3.1

Table 6.2: Uncertainties in measurements

and show better results on the accuracy than the instrument actually has. In order to get an independent estimate of the accuracy, a second training of the linear regression was done keeping one of the calibration datasets out of the training and was used afterwards for the accuracy test. As test datasets, data from the following dates were taken: '2017-03-06', '2017-11-29', '2018-05-03' for SO_2, HNO_3 and HCN, respectively. Both linear regression models (trained on all data and on all minus one dataset) show very similar results for the slope of the calibration line (sensitivity). To calculate the relative accuracy $rel\_accuracy$ of a single measurement with a known true value (known "true" mixing ratio) the following formula was used:

$$rel\_accuracy = \frac{|x_{predicted} - x_{true}|}{x_{true}} = \frac{|y_{measured}/m - x_{true}|}{x_{true}}, \tag{6.7}$$

where x_{true} is the mixing ratio determined from the permeation rate of the standard and the flows, $y_{measured}$ is the measured normalized count rate of the corresponding ion (the blank has to be subtracted) and m is the sensitivity of the instrument (slope of the calibration line).

The relative accuracy of the instrument calculated on both the training dataset and the test dataset is shown in Figures 6.12(a), 6.13(a) and 6.14(a) for SO_2, HNO_3 and HCN respectively. The very high accuracy for SO_2 on the test dataset can be explained by the fact that the sensitivity of the instrument on that day was very close to the average (see Figure 6.5(b)), therefore this result is not considered as an upper estimate of the overall instrument accuracy for SO_2.

The relative accuracies of the instrument can be reliably estimated to be better than 30%, 35% and 18% for SO_2, HNO_3 and HCN, respectively, but not lower than the corresponding detection limits. The stated estimates of the accuracy apply for the measurements, which were converted using the averaged sensitivity. If the measurements are followed by a calibration process done exactly at the same conditions, accuracy can be much better because, in general, one calibration dataset aligns much closer to the line fitted to it.

In Figures 6.12(b), 6.13(b) and 6.14(b), the predicted mixing ratios for the test datasets with their corresponding uncertainties (Equation 6.4) were plotted versus the true mixing ratios (derived from the permeation rates). Figure 6.14(b) shows fairly large error bars for the predicted values of HCN mixing ratios in the range above $20\,000\,\text{ppt}$ because the linear regression fit was done on the data below that range, and such statistical behavior of the formula from Equation 6.4 is expected.

6.7   In-flight calibration

Due to the obvious systematic differences between different laboratory calibrations (see Figures 6.5(b), 6.6(b) and 6.7(b)) and the rough conditions during flight, an in-flight calibration procedure was established to monitor the validity of the laboratory calibration during flight. Since maintaining reliable permeation devices under field operation is close to impossible, a procedure based on a gas mixture of just one of the less sticky gases was established. Here SO_2 was selected since it also was the main species to be measured. The in-flight calibration unit was integrated into the lower gasdeck (see Figure 5.12). It includes two bottles with home-made SO_2 (100 ppb, for CO_3^- mode) and Br_2 (685 ppb, for I^- mode) calibration gas mixtures, both are prepared in N_2 of 6.0 grade purity. These gases are mixed employing two 10 sccm mass flow controllers and purged solenoid valves in order to switch on and off the flow and purge out remaining calibration gas. The total accuracy of these in-flight calibration mixtures is estimated at about 20% for SO_2 and 30% for Br_2, both for additions in the low ppb range.

The calibration done for one species can be transferred to others. Equation 6.3 can be modified to:

$$[A] \propto \frac{1}{k} \frac{P^-}{R^-}, \tag{6.8}$$

where k is the effective reaction rate of the corresponding chemical ionization reactions (Equation 6.2), P^- is the count rate of the corresponding product ion and R^- is the count rate of the reagent ion. Then sensitivities (slopes of the calibration curves) m_1 and m_2 of the instrument for two different species must have constant ratio at the given parameters of the experiment:

$$\frac{m_1}{m_2} = \frac{k_2}{k_1}, \tag{6.9}$$

where k_1, k_2 are the effective reaction rates of the corresponding ionization reactions. To use the described sensitivity propagation reliably, it should be tested for extended temperature ranges.

In order to make measurements, determine the background and calibrate the instrument during the flight, the following modes were scheduled to be sequentially repeated during the measurements:

- Measurement mode (MM) is active for 20 min. The inlet is open and measurements of ambient air are done.

- Calibration Mode A (CMA) is active for 40 s. The inlet is open. In addition to the ambient air, a small flow of calibration gas is injected through the calibration inlet (see Figure 5.4).

- Blank Mode (BM) is active for 40 s. The inlet is closed and measurements of the background are done. The flow through the inlet (a value calculated based on the measurements of the mass flow meter which is placed before IDP3/1 pump) is replaced by the same flow of dry synthetic air (mixed on board form N_2 and O_2) through the calibration inlet.

- Calibration Mode B (CMB) is active for 40 s. The inlet is closed. In addition to the synthetic air, calibration gas is injected with the same flow as for CMA.

The blank BM and calibration procedures CMA and CMB were successfully tested on the ground. However, during the flights, no clear response to the calibration gas in

CMA/CMB or the BM periods has been found at 112 Th (SO_5^-). Instead, a strong exponentially decaying signal from beginning of the flight was found without any signs of atmospheric signatures. This may be associated to a spill of calibration gas during ascent. The issue is still being checked and an analysis of the data SO_2 data cannot be done. Due to the SO_2 addition during the calibration procedures and unexpected response of the instrument to it, analysis of SO_2 data cannot be done without better understanding of the issue.

However, the background signal was successfully measured at 123 Th and 26 Th. Two full measurement cycles for a part of the 7th scientific flight (06.08.2017, Kathmandu, Nepal) are shown in Figure 6.15. The successful measurements of the background allowed the quantitative analysis of the flight data for HNO_3 and HCN based on the laboratory calibration.

6.8 Discussion

FunMass was characterized for HNO_3, SO_2 and HCN measurements. All relevant characteristics are listed in Table 6.3 together with the characteristics of some other CIMS as a reference.

For HNO_3 and SO_2 FunMass provides very good sensitivity, which translates into very low detection limits. Even at 2 Hz measurement frequency, for SO_2 we report a detection limit very similar to the best among CIMS instruments, and for HNO_3 almost one order of magnitude better. This fits the main requirements for airborne measurements of UTLS trace gases in low mixing ratios.

The CI of HCN to CN^- may occur as a side reaction of the cluster formation or as a follow-up reaction of the cluster breakdown which could not be further characterized. However, the HCN calibrations are robust and no other species in the UTLS (besides the very low abundance methyl cyanide) could produce CN^-. The comparably low sensitivity of FunMass towards HCN obviously is due to the inefficient formation of CN^-.

Name	HNO_3	SO_2	HCN	
Sensitivity [ppt^{-1}]	1.58×10^{-5}	1.64×10^{-5}	9.74×10^{-8}	
Uncert. of the sens. [ppt^{-1}]	3×10^{-7}	4×10^{-7}	2.5×10^{-9}	
Typical sensitivity [$ions\,s^{-1}ppt^{-1}$]	>300	>320	>2	
Detection limit (2σ, 0.5 s avg.) [ppt]	2.6	2.7	200	
Detection limit (20 s avg.) [ppt]	0.8	1.7	64	
Min. detection limit [ppt]	0.66 at 40 s avg.	1.62 at 10 s avg.	36 at 80 s avg.	
Short-term precision [%]	≤ 2	≤ 2.5	≤ 5	
Accuracy [%]	≈ 35	≈ 30	≈ 20	
Published characteristics of other CIMS instruments				
Name	HNO_3	SO_2	HCN	Source
Detection limit (2σ)	30-50 ppt	30-40 ppt		[26]
Accuracy	20-45%	20-30%		
Detection limit (2σ, 1 s avg.)		≤ 1 ppt		[89]
Detection limit (2σ)	17-78 ppt	15-48 ppt		[91]
Detection limit			37-83 ppt	[95]

Table 6.3: Characteristics of FunMass.
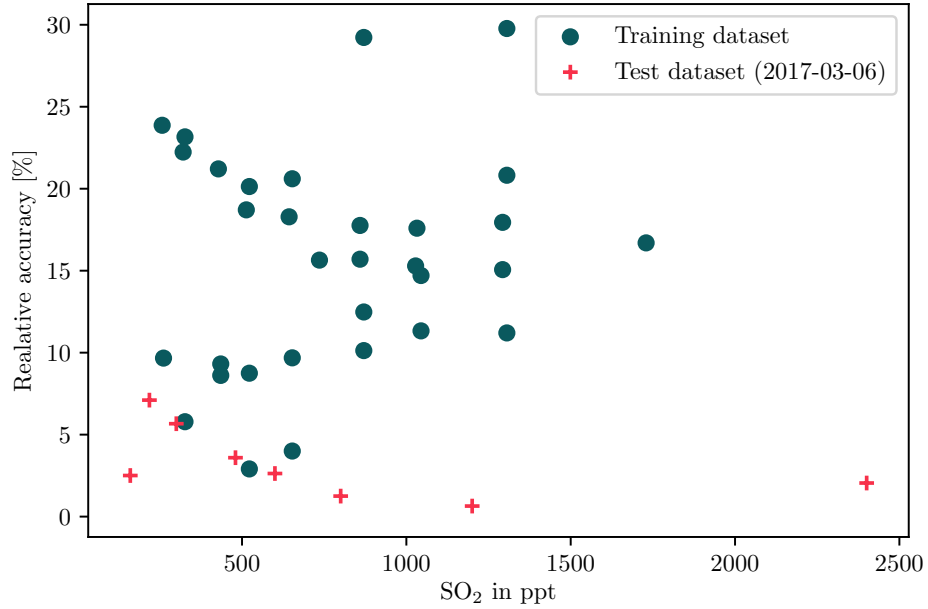
(a) Accuracy for the SO$_2$ measurements, checked on both the training and test datasets.
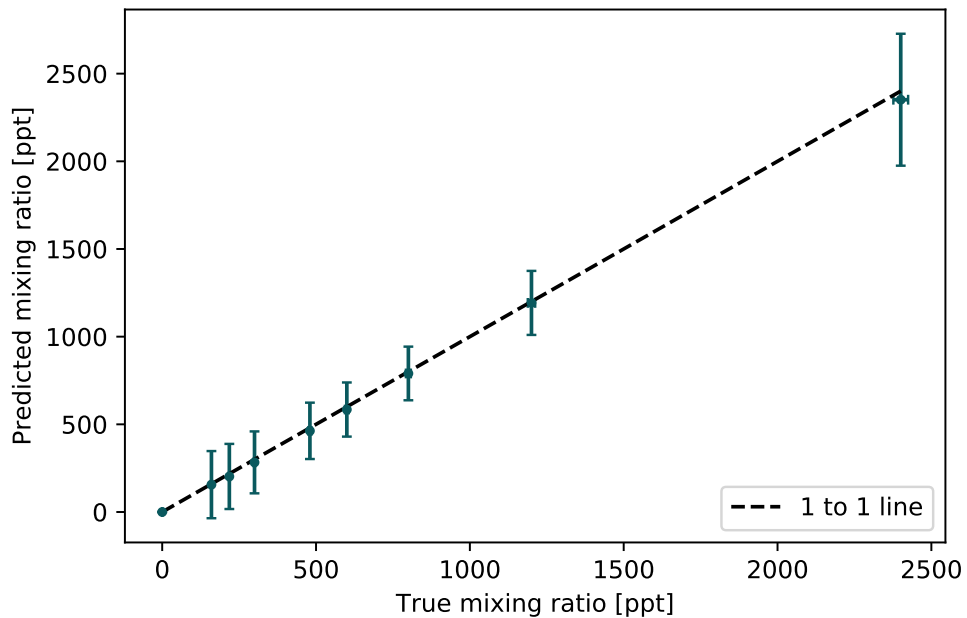
(b) Measured (predicted) mixing ratios of SO$_2$ versus true ones on the test dataset. True values were derived from the permeation rate of the corresponding permeation tube.

Figure 6.12: Accuracy for the SO$_2$ measurements.
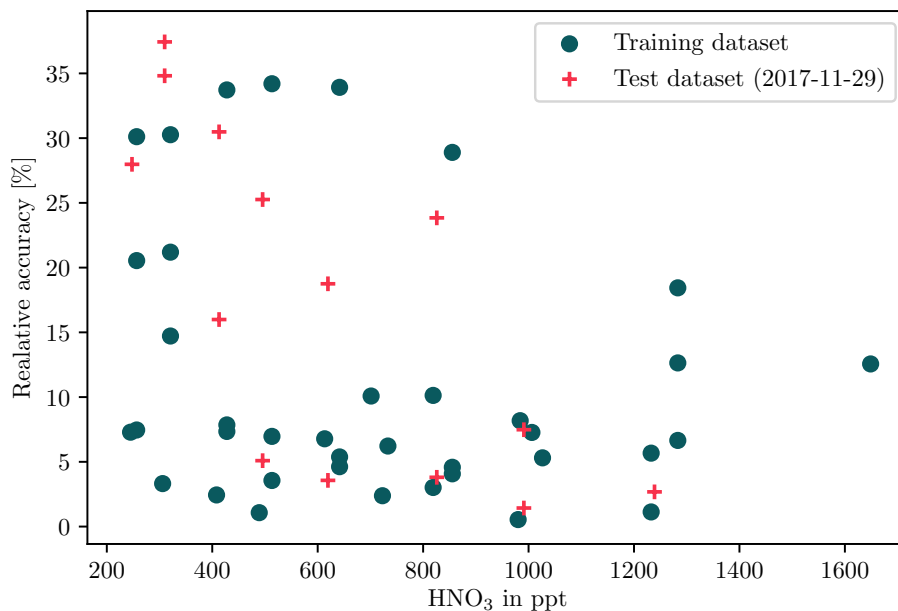
(a) Accuracy for the HNO_3 measurements, checked on both the training and test datasets.
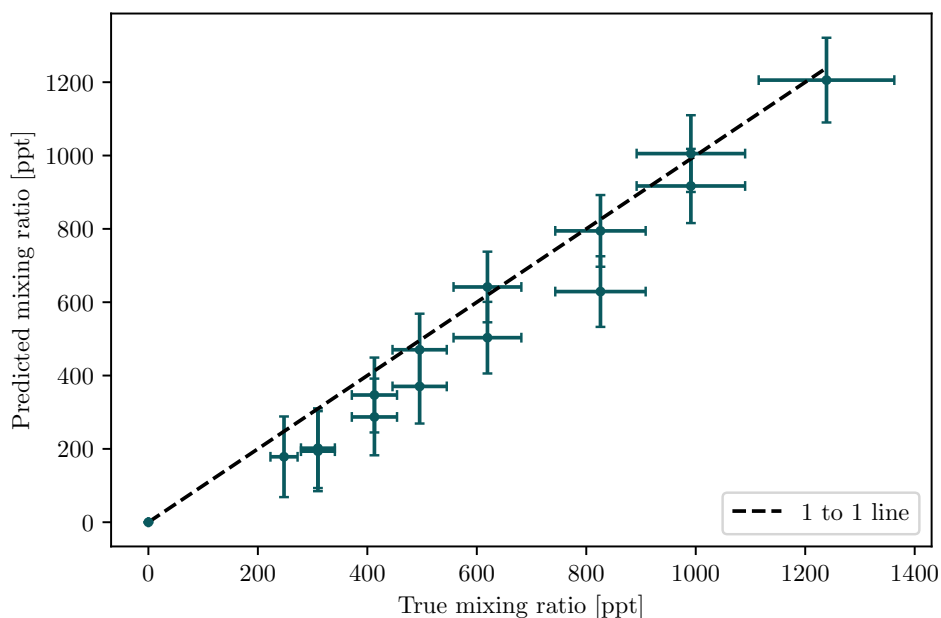
(b) Measured (predicted) mixing ratios of HNO_3 versus true ones on the test dataset. True values were derived from the permeation rate of the corresponding permeation tube.

Figure 6.13: Accuracy for the HNO_3 measurements.
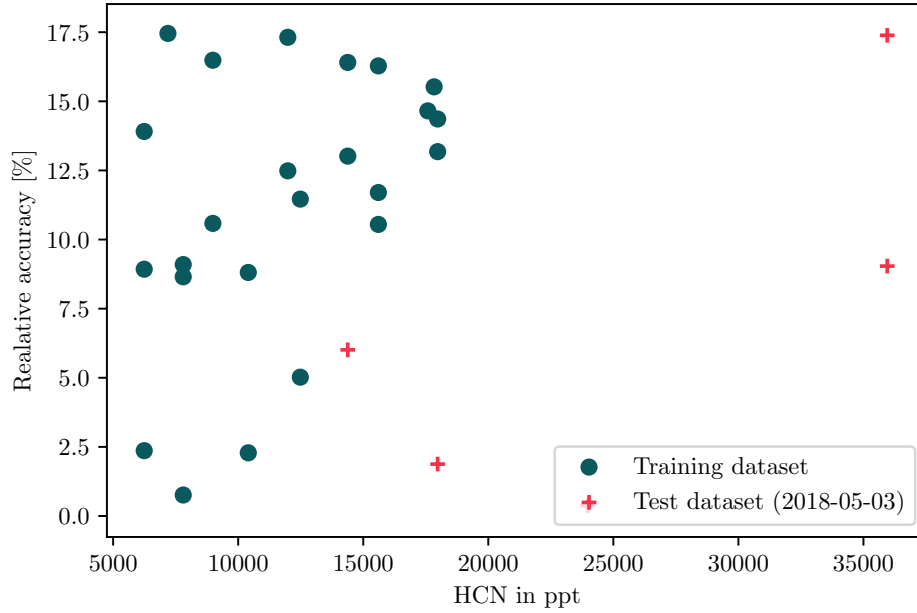
(a) Accuracy for the HCN measurements, checked on both the training and test datasets.
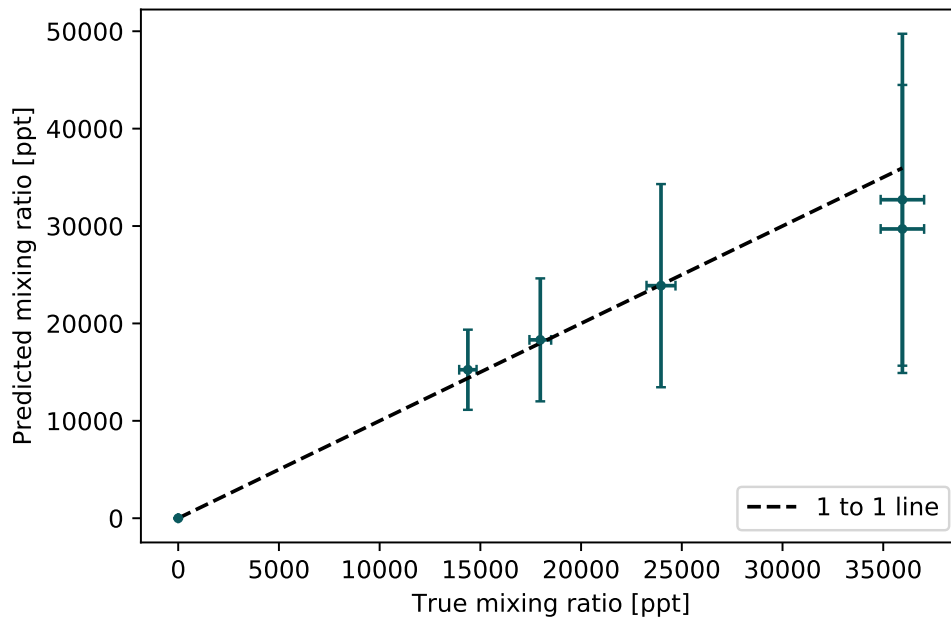
(b) Measured (predicted) mixing ratios of HCN versus true ones on the test dataset. True values were derived from the permeation rate of the corresponding permeation tube.

Figure 6.14: Accuracy for the HCN measurements.
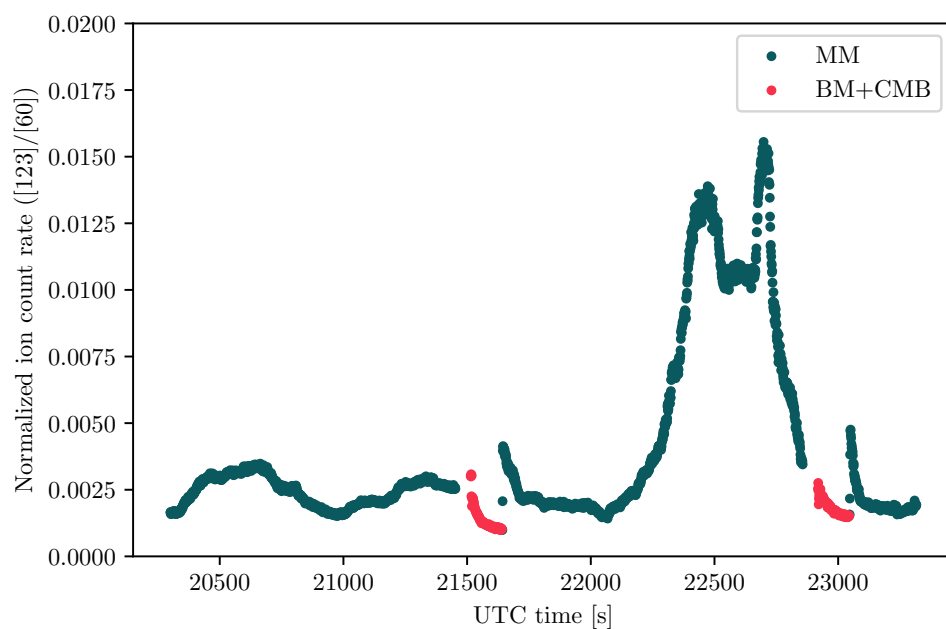
Figure 6.15: Part of the time series of the normalized ion count rate for the HNO_3 measurements ([123]/[60]) performed by the FunMass instrument during the 7th scientific flight in Kathmandu, Nepal on 08.08.2017. The sections marked in red show the decays of HNO_3 to the background (blank) values.

Chapter 7

Data acquisition and software

FunMass is a new instrument that requires individually tailored software to operate. As an airborne instrument, it has to run entirely autonomously during the measurement flight. This chapter describes the development of such software.

7.1 General requirements for software and language selection

Tofwerk AG delivers their mass spectrometers with the software package TofDaqRecorder, which has a graphical user interface (GUI) and requires the presence of a specialist to operate the TOF MS. Software which is running without supervision and contains the logic and schedule of the measurements had to be created. Besides the mass analyzer CTOF, FunMass consists of many other units, developed at Forschungszentrum Jülich. Software drivers had to be written in order to operate these units from the main program on the FunMass computer during the flight and in the lab. The development of FunMass required a variety of tests. To make all the lab tests much easier in addition to the flight program a GUI application for FunMass was developed, which allows the instrument to be operated with standard input/output (I/O) devices such as mouse and keyboard, and to monitor all important run-time parameters in real time.

FunMass is an instrument developed to perform under stratospheric conditions. Low temperature and low pressure could potentially cause many various problems. We could not solve on the hardware level all of the threats that could possibly damage the instrument. One of the examples is the high voltage power supply TPS. The housing of TPS was leak-tested on the ground, and it should stay pressurized during the entire flight. However if for some reason it starts leaking out during the operation, and pressure inside of it reaches the discharge value, the unit would burn and possibly cause a fire hazard to the aircraft. The TPS doesn't have hardware interlocks to manage this problem because it's designed for ground-based measurements where this condition could never be reached. The main flight program has to be able to detect this and other unwanted situations and prevent the instrument and the aircraft from damage.

Python was selected as the primary programming language to write all software for FunMass. The language preference is a matter of taste, but Python was chosen for the following reasons:

- A simple and easy to read syntax makes Python programs much shorter than programs, written in Java or C++, making the development time shorter.

- Python is a free open source programming language.

- Python is a flexible multiparadigm language, that supports object-oriented, procedural and functional programming styles.

- Programs written in Python can run almost on every modern platform, e.g. Windows, Unix, OSX, FreeBSD, Linux.

- Python has an extensive list of built-in and external libraries/frameworks.

- Python has a huge community of developers, offering a wide assistance for solving problems.

7.2   TofWerk software

The delivered program TofDaqRecorder allows to control and operate TOF. It provides tools in order to:

- change the data acquisition rate;

- change the ion extraction rate;

- change the mass range of the recorded spectrum;

- change the mass calibration parameters;

- visualize the mass spectrum in real time;

- calculate and visualize in real time the peak data of certain ions.

To provide control over the TPS, TofWerk approaches the matter in a slightly different manner. To operate the current generation of their power supplies, users don't need to have a separate application installed on their computers. The TPS hosts an application on its microprocessor and gives users remote access to a browser user interface (BUI) to interact with it via the controls presented within a web browser. BUIs became common for devices that have installed microprocessor and network interface, such as printers or network routers. The BUI of the TPS allows to:

- set and change HV of the TOF;

- switch on/off the turbo pump;

- monitor and display the housekeeping data (e.g. pressures in the TOF, in the funnel etc.).

Unlike the BUI of the TPS, the TofDaqRecorder application currently can run only on Windows operating system. That's the reason why the FunMass computer runs Windows 7.

TofWerk AG also provides an application programming interface (API) which allows to develop new software to interact with the TOF. The API consists of a dynamic-link library (DLL) file "TofDaq.dll", which contains all functions needed to operate the TOF (e.g. giving access to control over the running acquisitions and to recording data etc.). Actually, the TofDaqRecorder application is just a wrapper of functions from TofDaq.dll. Furthermore, the API allows to save arbitrary data synchronously or asynchronously alongside with the
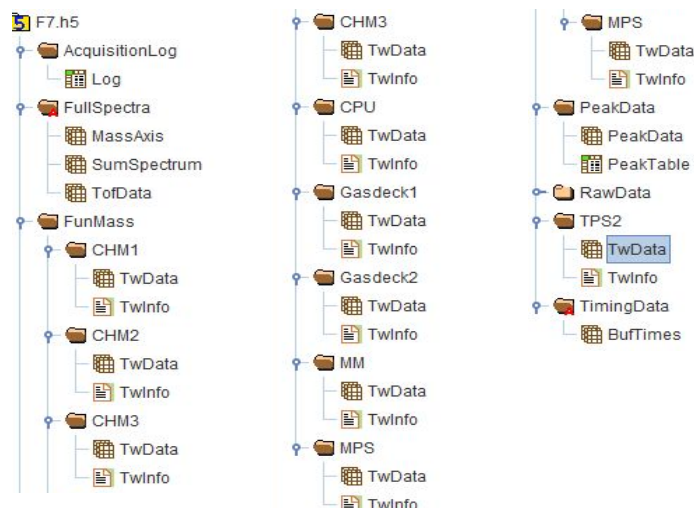
Figure 7.1: Structure of the FunMass datafile. Screenshot from HDFView 2.13

recorded spectra into the same data file. That is a key point of FunMass data acquisition, merging all data from all parts of the instrument into the same single file.

The TofWerk API is written in C++ but easily accessible from Python with the help of the built-in library `ctypes` [19].

7.3 Data format

7.3.1 HDF5 format

HDF5 is a **H**ierarchical **D**ata **F**ormat designed to store large amounts of data, originally developed at the National Center for Supercomputing Applications (NCSA) at the University of Illinois at Urbana-Champaign and currently supported by "The HDF Group" [25]. This format can store two types of objects:

- dataset: multidimensional array of data elements;

- group: a container structure which can contain itself datasets and other groups.

With these two objects almost any kind of scientific data structure can be stored, including images, arrays of vectors, structured and unstructured grids, etc. The HDF5 data format is popular and widely used among scientists and engineering communities working in high performance and data intensive computing environments (e.g. TOF MS).

7.3.2 FunMass data structure

TofWerk AG is using the HDF5 data format for their instrumentation. In the default configuration, besides periodically storing mass spectra (in `FullSpectra/TofData`), TofDaqRecorder also saves following data in a single file (see structure in Figure 7.1):

- `AcquisitionLog/Log`, contains a table with the date and time of the beginning and end of the data acquisition in a string format.

- `PeakData`, contains an automatically calculated table with the integrated peak data (`PeakData`) in ions/ex and a `PeakTable` with the corresponding integration limits for each peak.

- `RawData`, contains all housekeeping data from the ADQ unit.

- `TPS2`, contains a table with all housekeeping data from the TPS as well as data from the sensors operated from the TPS and the GRF (`TwData`) and their detailed description (`TwInfo`)

- `TimingData`, contains a table (`BufTimes`) with a timestamp for each recorded event.

- attributes of the group `FullSpectra` contain all settings of the TofDaqRecorder at which this file was generated.

The main FunMass program is responsible for the data in the group `FunMass` (see Figure 7.1). Besides the data from different parts of the instrument, the program saves numerical codes of the running mode ("0" for operation in the lab, "1" for the S/BM mode, "2" for the MM mode, "3" for CMA mode, "4" for the BM mode and "5" for the CBM mode, see Section 7.6) in the `MM/TwData` table. Having this information simplifies the later post flight data analysis. Historically, flows of mass flow controllers MFC1-6 (Figure 5.12) are saved in the Gasdeck1 and Gasdeck2 groups, not in the groups of classes where these flows are processed (CHM1, CHM2).

7.4   FunMass program

The detailed schematic of FunMass was discussed in Chapter 5. In this chapter the focus will only be on the communication logic between different units of the instrument and other software related issues.

To simplify the development of the software, principles of object-oriented programming (OOP) were used. OOP is a programming paradigm based on the concepts of "objects" (called "classes" in Python), complete modules of code with predefined purpose and functionality. In OOP, programs are built out of these written in advance classes which interact with each other [29].

The FunMass computer is in the same local network with the following units: MPS, TPS, GRF, gasdeck and IFS (Figure 7.2). In the FunMass program, classes were written for nearly each of those units. GRF and TPS were delivered from TofWerk AG. Both are accessed via the provided API and cannot really work separately from each other. Therefore, only one single class `TPS` was written to control both. On the other hand, gasdeck brings into the local network two separate control boards and two classes `CHM1` and `CHM2` were written for them. A class contains all the needed functionalities to communicate and operate with the corresponding unit. A unit could be tested and its class modified independently from the others, which was specially helpful on the early stages of the development of FunMass. `class MPS`:

- contains methods to send commands to switch on/off all other units and the main heating system;

- receives once per second a data package of 122 Bytes with housekeeping data from the MPS, breaks it down into 51 values, including among other the following data: power information of the complete instrument, twenty temperature inputs, ambient pressure, etc., and makes them available for the rest of the program.
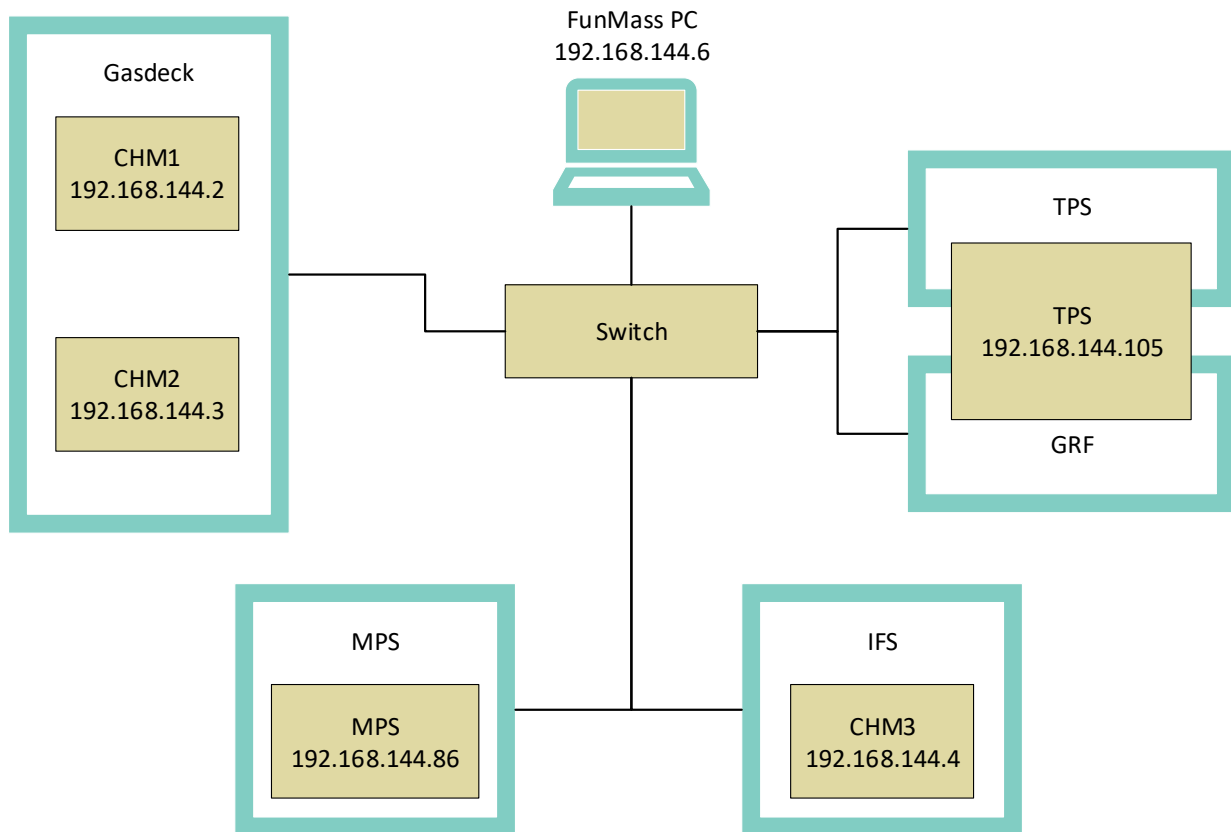
- main power supply (MPS): `class MPS`

- TOF power supply (TPS) and giraffe (GRF): `class TPS`

- gasdeck: `class CHM1` and `class CHM2`

- ion funnel and ion source power supply (IFS): `class CHM3`

Figure 7.2: Schematic of the FunMass local network. In blue frames, instrument units. In yellow filled boxes, class names of the drivers together with their IP addresses in this network.

`class` TPS:

- provides Python wrappers of the TPS BUI functions (Section 7.2);

- requests once per second selected values from the housekeeping data of the TPS and makes them globally available.

`class` CHM1:

- contains methods to send commands to set output voltages on the first board of the gasdeck (CHM1). By doing so it can open/close all eight solenoid valves in the gasdeck (V1-8, Figure 5.12) and switch on/off the heating of the H_2O and the ICH_3 reservoirs;

- receive, process and export the housekeeping data of the CHM1;

- contains methods to set and request the flow through MFC4-6 (Figure 5.12);

- requests flows through MFC4-6 every three seconds and makes them available for the rest of the program.

`class` CHM2:

- contains methods to send commands to set output voltages on the first board of the gasdeck (CHM1). By doing that it can set the position of the inlet and the flow through the MFC7 and MFC8 (Figure 5.12);

- receives, process and export the housekeeping data of the CHM2;

- contains methods to set and request the flow through MFC1-3 (Figure 5.12);

- requests flows through MFC1-3 every three seconds and makes them available for the rest of the program.

`class` CHM3:

- contains methods to send commands to switch on/off the ion source and the ion funnel, and set their parameters;

- contains methods to set new default parameters for the control board in the IFS (CHM3);

- receive, process and export the housekeeping data of the CHM3, which include but limited to temperature in the IFS, pressure in the IFS housing and parameters of IS and IF.

All code of these classes and other basic bricks for the further software development was put together in one module `funmass.py`.

7.5 Multitasking in Python

It is evident that the main program should do multiple different tasks at the same time, e.g., hold several connections, continuously monitor system parameters, etc. There are two basic concepts allowing to achieve that in programming [85]:

1. concurrency: when a computer performs several tasks seemingly at the same time. For example, the operating system on a computer with only one CPU core will rapidly switch which program is running at the moment, providing the illusion that the programs run simultaneously.

2. parallelism: when a computer is actually doing two or more things at the same time. This concept requires a CPU with multiple cores. Each core runs the instructions for a different task, allowing them to progress during the same instance.

Parallelism is a good concept when heavy calculations need to be sped up but the number of parallel tasks is limited to the number of the CPU's cores. Multitasking in the FunMass program cannot be fully managed employing only the parallelism concept, since the number of tasks which should run simultaneously exceeds the number of cores of the CPU the FunMass PC has or could be potentially acquired for it. In addition, parallelism is not really necessary for the FunMass program, as all of its independent tasks are not that "busy" and don't require a lot of CPU resources, being easily managed by only one CPU core. For example, the MPS class receives the housekeeping data once per second and after receiving that data package, the CPU processes it in less than 5 ms and this task is idle until the next data package arrives almost one second later. There are plenty of CPU resources to work on other tasks meanwhile. Python makes it easy to write concurrent programs with the built-in module `threading` by making every separate task to run in its own thread (class `Thread` from module `threading` [19]).

7.5.1 Synchronizing access to shared resources in Python

Python is an interpreted programming language. CPython is a standard Python interpreter. CPython runs a program in two steps [85]:

1. it parses and compiles the source text into bytecode instructions;

2. it runs the bytecode using a stack-based interpreter.

CPython should generate bytecode to ensure coherence of different threads while the program executes. Python enforces that with a mechanism called the global interpreter lock (GIL). Concurrency assumes that one thread takes control over the program by interrupting another thread. Such an interruption could corrupt the interpreter if it comes at an unexpected time. The GIL prevents corruption of the interpreter by not allowing to interrupt a single bytecode instruction. Operation on data structures in a thread can be interrupted between any two bytecode instructions in the Python interpreter. This is potentially dangerous and may lead to miscalculations if the same object is accessed from multiple threads simultaneously (as shown in the example B.1 in the appendix). These problems are specially difficult to debug [85]. One of the ways to solve this issue is to use a lock (class `Lock` from the module `threading` [19]) to protect some quick, sequential operations from being interrupted (as show in the example B.2 in the appendix). It is worth to mention that most operations on the built-in data structures are implemented in a thread-safe way (could not

be interrupted) and don't cause the described problem. But to guarantee thread safety and to have better control over the sequence of computations, it was decided to use a lock to protect quick sequential operations from being interrupted.

7.5.2   Queues in Python

Another tool which helps to organize multithreading in Python is the so-called queue (class `Queue` from the built-in module `queue`). Queue is an abstract data structure which is handy when you want to coordinate workflow in two threads. In the FunMass program, there are many connected threads, where one thread has often to wait for the input from another one. For example, in one thread data packages with housekeeping data from MPS are received and in another one they are processed and according to the data package structure broken down into the separate values. The second thread does not need to wake up before the data package has arrived. A queue could be used to coordinate these two threads. In the first thread, the data package is put in the queue (method `queue.put()`). In the second thread, the method `queue.get()` is used to get this data out. This keeps the second thread asleep while the queue is empty and unlocks it as soon as a data package gets into the queue. While the queue is empty, the program will never activate this thread and will work on other tasks. Using queues for these purposes is one of the most efficient ways to organize communication between two threads. In our case, it ensures that the program will process and convert all data packages from the MPS even if the data would arrive more frequently or less than expected.

7.6   Flight program

FunMass as an airborne instrument must operate fully autonomous during flight. The logic of the in-flight stand-alone mode is discussed in this section.

At the moment FunMass' MPS is powered by the aircraft, by default it powers only the PC. The PC starts up, loads Windows and launches the flight program from the autostart directory. Then the program takes full control over the FunMass instrument. It establishes a connection with the MPS, then sends the commands to the MPS to power all other units one after another and establishes connection with them. Units are powered with a small gap, about 3 s to 10 s, which experimentally showed to provide a smooth start up of the whole instrument and guarantee flawless connections between the program and all the units.

Once all units are powered and running in standby mode, the following cycling tasks are started, each in a separate thread:

- data acquisition task;

- system monitor task;

- turbo pump task;

- TOF high voltage task;

- IFS high voltage task;

- measurement task.

Flow charts of some of these tasks are given in Appendix A. The tasks are described in a few more details below.

7.6.1 Data acquisition task

In this task new data from the MPS, the TPS and CHM1-3 are periodically registered with TofDaqRecorder and synchronously stored alongside with mass spectra from the TOF in one data file. On the ground when the TOF is not fully operational, mass spectra consist of arrays of zeros.

7.6.2 System monitor task

In the system monitor task, six critical pressures are continuously checked: ambient, funnel, TOF and in the housings of the TPS, pulser and IFS. After comparing these values with the predefined thresholds, it is decided whether specific operations are allowed or forbidden. It's important to emphasize that no direct order commands (e.g. open the inlet, etc.) are given from this task. It only checks if the external and internal conditions are in the operational range of the instrument:

- For the inlet regulation there are two critical parameters: ambient pressure and pressure in the funnel. The inlet is enabled[1] if the two following conditions are met:

    1. ambient pressure is below $200\,\text{hPa}$
    2. pressure in the funnel is below $40\,\text{hPa}$

    The inlet will be kept disabled otherwise. The first condition ensures that the inlet is enabled only at suitable altitudes. The second condition ensures that the pressure in the funnel stays below the critical value, and the pumps are not under extreme load. An example of a possible scenario where the second condition is not met is briefly discussed below. The inlet is supposed to regulate the pressure in the funnel within $(30 \pm 3)\,\text{hPa}$ range, so if it is higher than $40\,\text{hPa}$ it may indicate that the inlet is open and its regulation is failing. That requires the inlet to be disabled and safety procedures from the "measurement task" (see Subsection 7.6.4) should (and will) close it.

- The turbopump must be prepumped to operate. A pressure in the TOF below $1\,\text{hPa}$ indicates that the prepumping unit (the IDP3/2 pump) is working properly and therefore the turbopump can be enabled. Otherwise, it remains disabled.

- To enable the high voltages in the TOF, the following conditions have to be met:

    1. the pressures in the housings of the HV units (TPS and pulser) have to exceed $700\,\text{hPa}$ to avoid electrical sparks in them (Section 5.8);
    2. the pressure in the TOF has to be bellow $5.0 \times 10^{-6}\,\text{hPa}$, which is one of the requirements of the TOF mass spectrometry;
    3. the ambient pressure has to be below $200\,\text{hPa}$, to make measurements only above certain altitude.

- To enable high voltages in the IFS the pressures in its housings have to be above $700\,\text{hPa}$ to avoid electrical sparks inside the IFS (see Section 5.8).

The flowcharts of this task are shown in Figures A.2 and A.3.

---

[1] Enabling the unit means to set the appropriate boolean variable to `True` ("enable_unit = True"), disabling it, to `False` ("enable_unit = False")

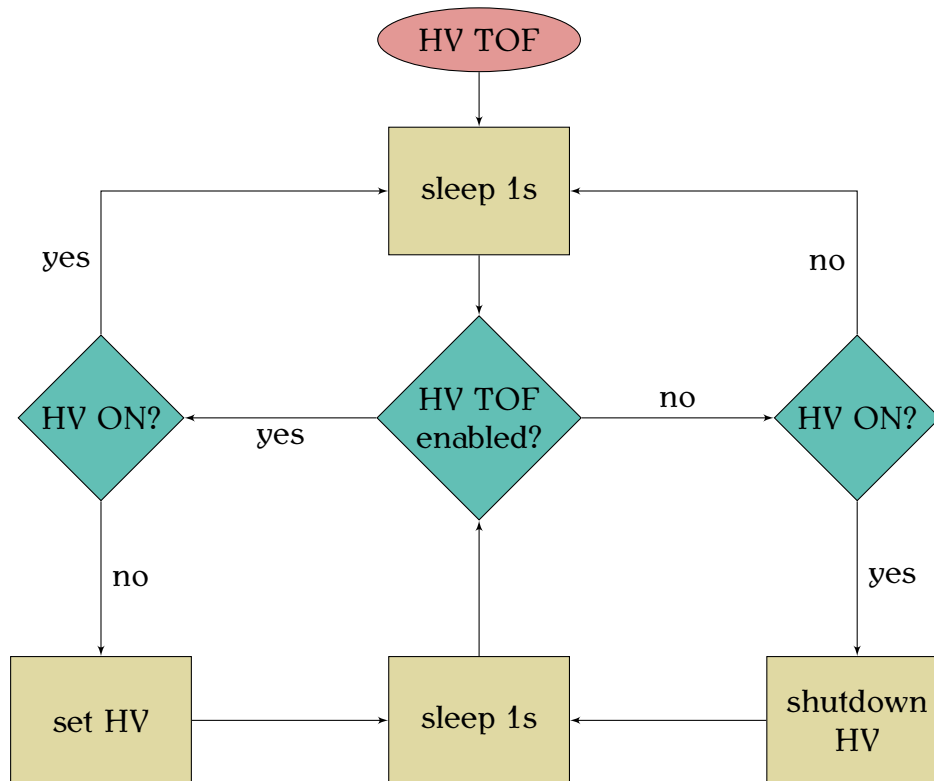### 7.6.3   TOF high voltage task, IFS high voltage task and turbopump task

Figure 7.3: Flowchart of TOF high voltage task

All these tasks follow a similar procedural logic. They check if their corresponding unit is enabled or not and take care of switching/keeping it on or switching/keeping it off accordingly.

"TOF high voltage task" (see Figure 7.3) follows this pattern exactly.

"IFS high voltage task" (see Figure A.1) in addition to switching on/off the HV of the ion source, starts/stops the necessary gas flow through the ion source.

"Turbopump task" (see Figure A.4) includes an additional check for overheating errors and a way to handle it. This check was introduced after the turbopump failed while FunMass was running inside of the wingpod on the ground for over an hour at a high ambient temperature (see Section 5.10). In case of overheating, the electronics of the turbopump switches off automatically without any warning or error message, and it does not start back up on once it gets colder, even though it remains powered. To bypass this potential problem, it is checked if the rotor of the turbopump is slowing down. If so, the task powers the pump off and after a ten minute break (enough to cool it down), the routine starts from the beginning. The pump is switched on again if still enabled.

7.6.4   Measurement task

During the flight, ambient air measurements (measurement mode MM) are periodically interrupted by the measurement of the background signal (blank mode BM) and two calibration modes (CMA, CMB), as discussed in Section 6.7. In addition to running this cycle of modes in the correct order and at the right time, safety procedures were introduced to this task to protect the instrument in case of the inlet malfunction.

The measurement task actually starts in the standby mode (S/BM) (Figure A.5), which will run as long as the inlet is disabled i.e. FunMass is not ready to make actual atmospheric measurements. During the S/BM, a small predefined flow of nitrogen runs through the calibration line. This flushes the system with pure dry gas while waiting until the inlet is enabled in the system monitor task. As soon as it is enabled, the flow of nitrogen will be stopped and the measurement mode (Figure A.6) will begin. From this moment on, the modes are rotated in the sequence MM, CMA (Figure A.7), BM (Figure A.8), CMB (Figure A.9) and back to MM. The MM is planned to run for 20 minutes and the CMA, BM and CMB for 40 seconds each. In the modes, which operate with the inlet being open (MM and CMA) together with the timer, a safety procedure is running, always ready to escape to the safe SB/M if the inlet gets disabled. This would also close the inlet during the final descent, going back to SB/M until the landing.

7.6.5   Independence of the tasks

The tasks described in Section 7.6.3 - 7.6.4 are bound to the system monitor task but independent from each other. If one of the units remains disabled due to a hardware or external problem, the corresponding task will not be allowed to take any actions. However all remaining tasks would run regardless of the failing unit. For example, if pressure in the TOF does not reach the threshold, TOF will not be enabled and high voltage would never be set in the corresponding task. Nevertheless the inlet would regulate and the ion source would run as well etc., which would allow us to gather information about the system and test other units even though no valid atmospheric measurements would be done. That is exactly what happened during the fifth flight where the turbopumps failed but the inlet finally opened for the first time confirming that the previous problems were fixed (see Section 5.10).

7.6.6   Event logger

Besides saving all instrument related data, the program needs to record actions done by itself for better understanding of its performance while autonomously operating. Python has an excellent built-in module `logging` [19], which allows to save entries of the running flow of the program into a log file and stream them simultaneously to the stdout (console output). Having log messages duplicated in the stdout is very convenient for laboratory tests. The logger is configured to yield log messages with an automatically generated timestamp and other service information about its origin such as the module name, line number in the file and the thread name.

First of all, such a log file allows to understand what was happening during the flight and which actions the program has taken. Second, it contains a lot of useful information which might be obtained without having to look deep into the main data file, e.g., an approximate time of take-off, a time when the aircraft switched from the GPU to engine power, etc. Finally, it allows to debug the code in case of any misbehavior.

For the data acquisition, Tofwerk AG has its own logger, which needs to be launched in the beginning by the program. It will automatically save all events of the TofDaqRecorder in a separate log file.
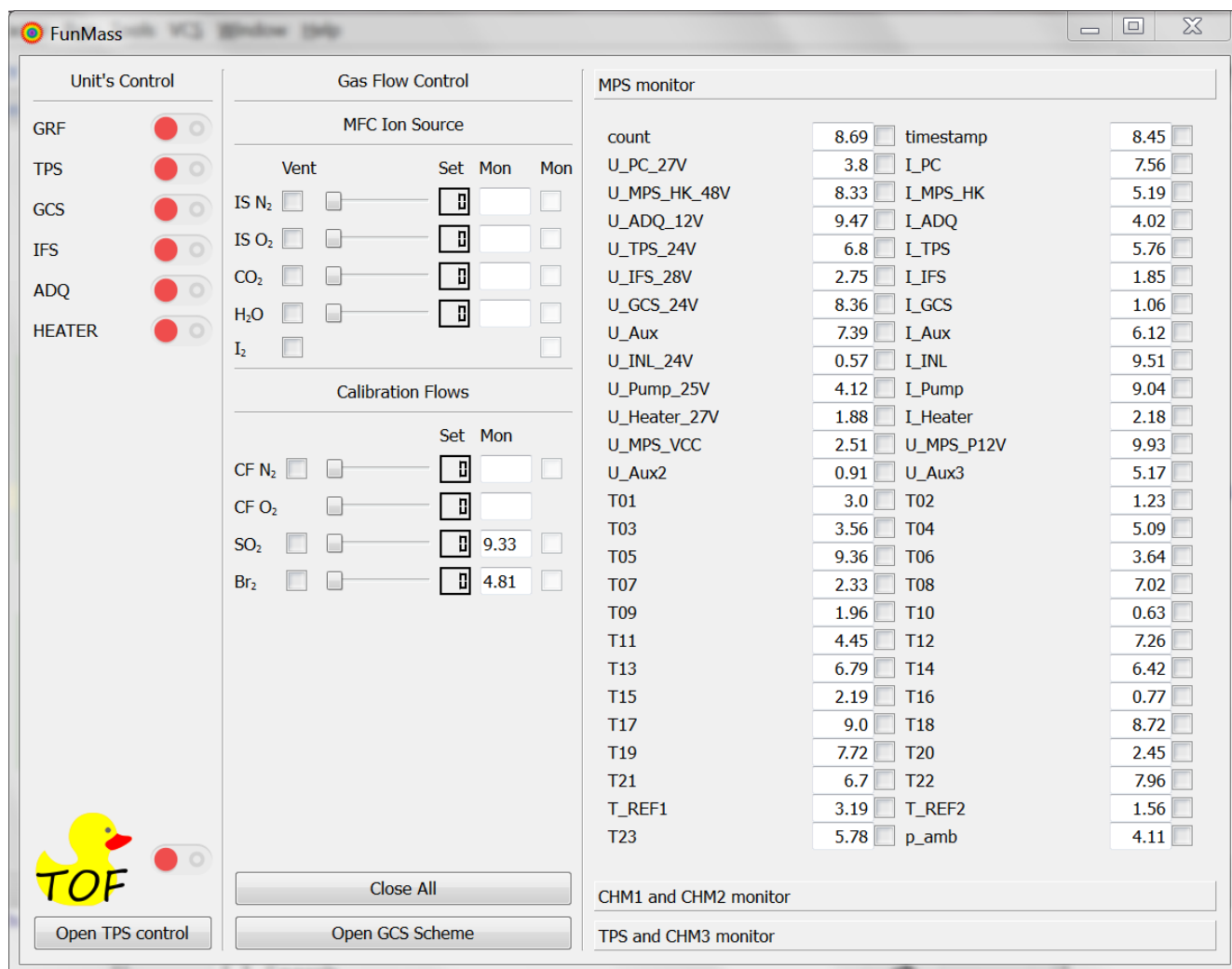
Figure 7.4: Screenshot of the main window of the GUI application for the FunMass instrument.

7.7 GUI application for FunMass

A GUI application was developed to operate the FunMass instrument during the various tests in the laboratory. For the back end of this application, the previously discussed module `funmass.py` is used, and for the GUI part (front end), the module `PyQt4`. `PyQt4` is a Python binding for the `Qt` (version 4) framework.

The GUI application significantly simplifies the user's communication with the instrument. Instead of having to remember all confusing commands of the MPS or using the corresponding methods from the `funmass.py` module in the command line interface like style, to power on/off any unit the user can just press the corresponding toggle switch (left panel in the Figure 7.4). To set gas flows, the horizontal sliders can be used (central panel in the Figure 7.4). The command to do so will be sent at the moment the slider is released. With the checkboxes, the solenoid valves in the gasdeck can be opened and closed. On the right panel (Figure 7.4), all housekeeping data can be monitored in real time. and the last 20 minutes of it can be ploted.

In the GUI mode, before the main window of the program is shown, the power status of all the units has to be checked and if any of the parts already has power, the program has to establish connection with it. This check is not necessary in the flight mode. But in the GUI mode, as a user could have quited the program previously without switching all parts off, this check is needed. This is done right after the GUI application is started, meanwhile a splash screen is shown to the user with the current output of the ongoing check. Units which have an ethernet connection with the PC are simply pinged to check their availability. For the ADQ, which is instead connected via USB, the list of connected USB devices will be checked using the `devcon.exe` utility from the Microsoft developer tools pack.

Another reliable way to inspect the power status of all units would be to check their voltage in the housekeeping data from the MPS. This approach is not used because for the logic of the program it is more important that the unit is available, rather than being just powered. Altogether it takes around ten seconds to start up the program before it is ready to go.

7.8 Results

A new software was developed for the FunMass instrument, which can run autonomously in the flight mode as well as be manually operated in the lab with the GUI application. The flight program performed flawlessly during the campaign, both executing the right sequence of operations in order to make atmospheric measurements, as well as taking care of all known potential threats to the instrument. Also, some hardware failures discovered in the course of the campaign (e.g. turbopump overheat) were addressed on the run by adapting the program in order to temporarily fix them. The program is equipped with data acquisition procedures that allow to store all instrumental and research data in one single file, simplifying the later analysis of it. The GUI application will probably remain in use in the lab as long as FunMass does. The software is built in an extensible way allowing for modifications and addition of new functions to the GUI app, as well as allowing for development of new autonomous modes with their own logic using the already existing blocks of code from the `funmass.py` module.

Chapter 8

FunMass results

In this Chapter the FunMass measurements during the campaign in Kathmandu, Nepal are presented and data consistency with other measurements is discussed. Some HNO_3 and HCN features obvious in the data sets are also discussed to show the scientific potential of the new CIMS data.

8.1 Measurements and meteorological considerations

In Kathmandu FunMass successfully acquired atmospheric data from two flights (see Section 5.10). In this chapter, only these two flights will be discussed. Figure 8.1 shows the time series of the 6th and 7th flights, performed on 06.08.2017 and 08.08.2017, respectively. Figure 8.2 shows actual flight tracks of these flights on a map (of the region).

8.1.1 Meteorological situation

During the campaign, prior to each flight, meteorological forecasts and predictions of atmospheric models are carefully analyzed in order to take advantage of the scientifically most interesting events and design optimal flight tracks.

Figure 8.3 shows forecasts of the CLaMS model for CO mixing ratios, a tracer of tropospheric air, at 100 hPa and 80 hPa for the dates of the 6th and 7th flights correspondingly, as well as the planned flight tracks.

The 6th flight was aimed at mainly observing convective outflow which occurs frequently below the tropopause. Therefore the flight altitude was chosen around 16 km towards a region of high convective activity towards the south-east (see Figure 8.3(a)). This flight also contributes to the objectives of the Asian Tropopause Aerosol Layer (ATAL) particle composition and formation. Flight 7 was aimed at exploring the vertical structure of the Asian monsoon anticyclone and also climbed up into the free stratosphere where elevated HCN had been detected by ACE FTS measurements amd reported by Randel et al. [73] and where enhanced HNO_3 levels also were expected.

To justify proper usage of the terms "troposphere" and "stratosphere" later in this chapter, the tropopause location during the 6th and 7th flight has to be placed. It can be located using the ambient temperature and geometric flight altitude from the avionic data of M-55 Geophysica, the corresponding vertical profiles are shown in Figure 8.4. The WMO defines the tropopause as [64] "the lowest level at which the lapse rate decreases to $2\,°C\,km^{-1}$ or less, provided that the average lapse rate between this level and all higher levels within 2 km does not exceed $2\,°C\,km^{-1}$". That situates the tropopause at around 16.3 km in the region where the 6th and 7th scientific flights took place according to Figure 8.4. It is very
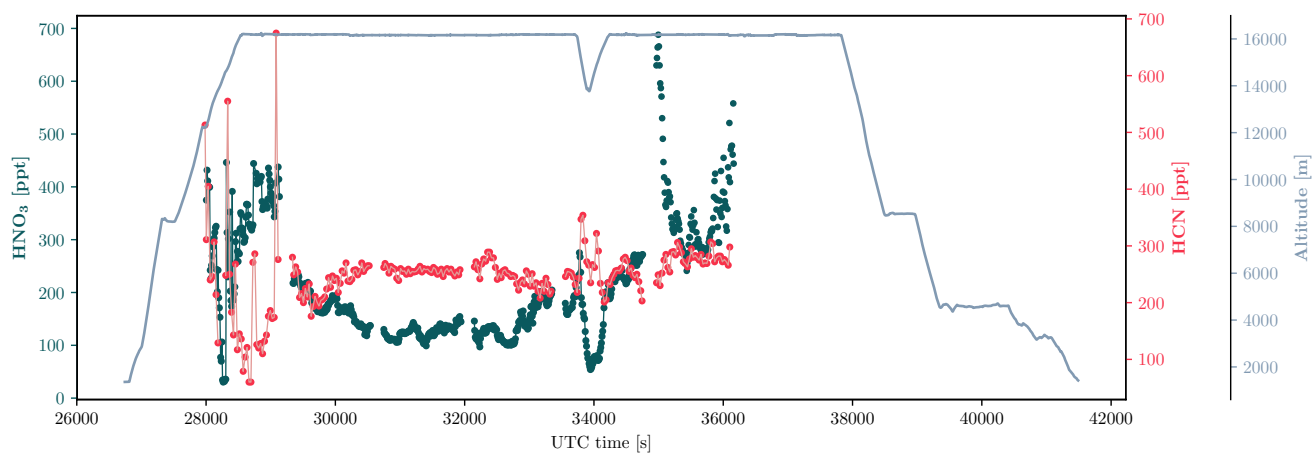
(a) 6th measurement flight on 06.08.2017.
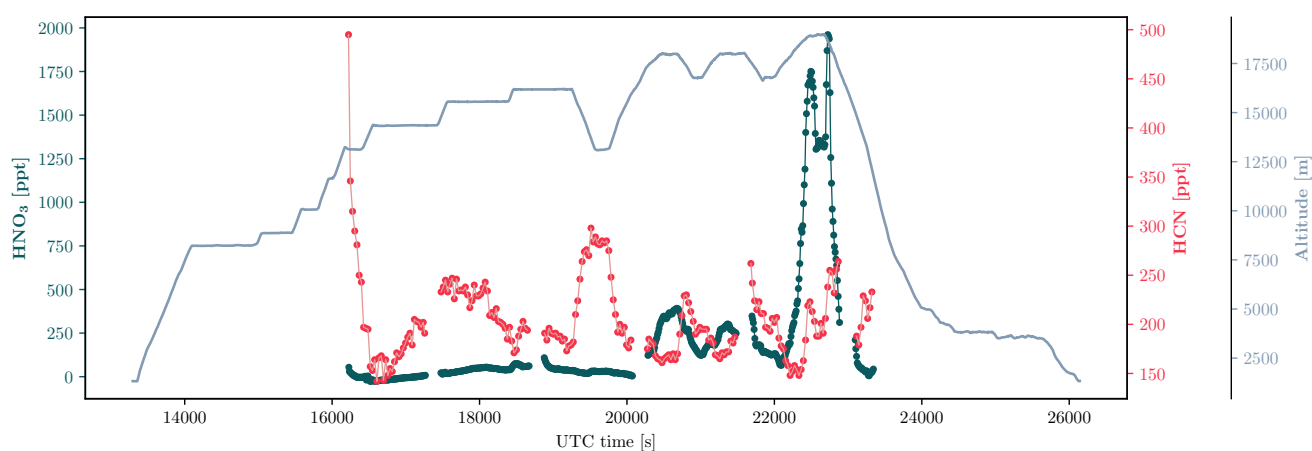
(b) 7th measurement flight on 08.08.2017.

Figure 8.1: Measurements of HNO_3 and HCN performed with FunMass during the campaign in Kathmandu, Nepal, 2017. Values of HNO_3 and HCN are averaged for $10\,s$ and $30\,s$ correspondingly. The geometric flight altitude was taken from the Geophysica avionic data.
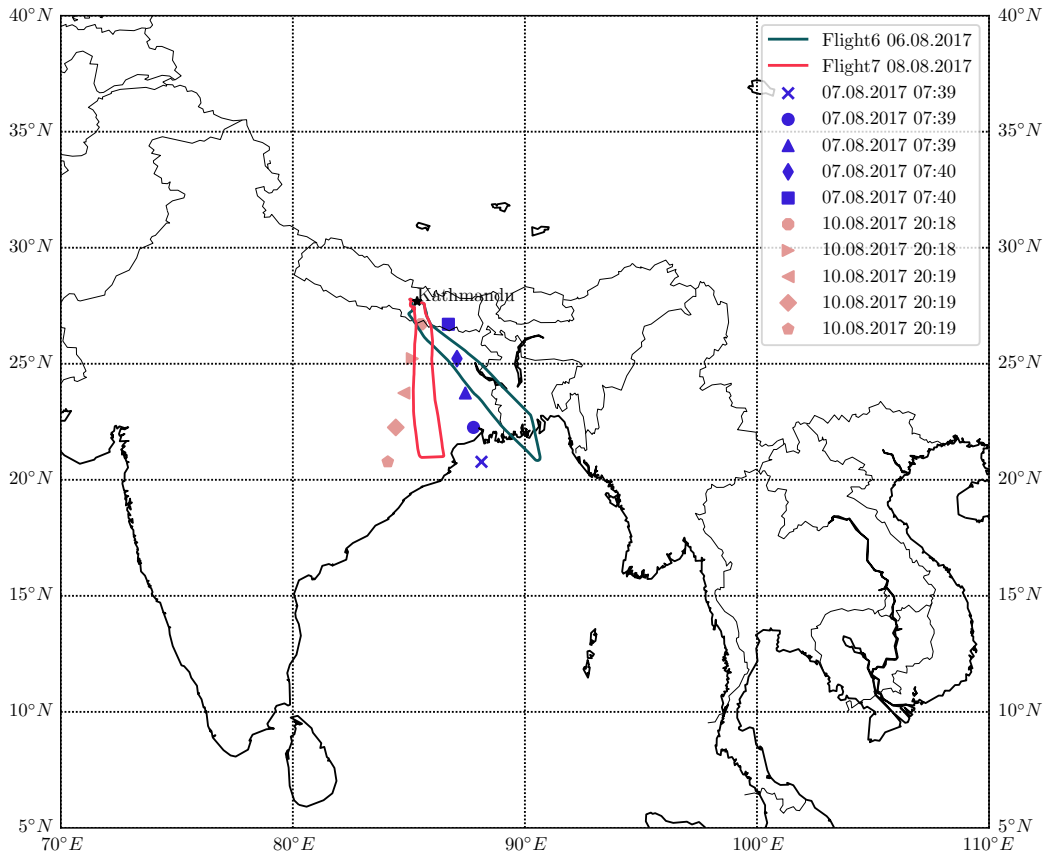
Figure 8.2: Actual flight tracks during the 6th (06.08.2017) and 7th (08.08.2017) flights from the avionic data. Measurement locations for the AURA-MLS datasets used for the inter-comparison with the FunMass data are also marked.
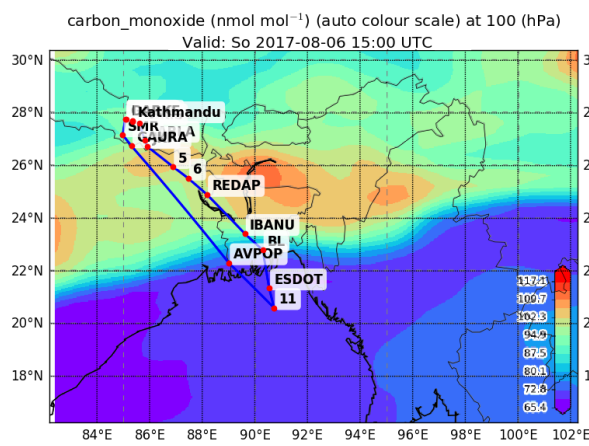
(a) Planned trajectory for flight 6 on 06.08.2017. CO mixing ratio at 100 hPa from the model.
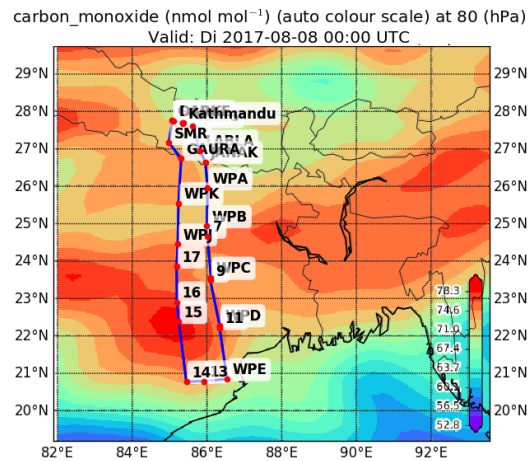
(b) Planned trajectory for flight 7 on 08.08.2017. CO mixing ratio at 80 hPa from the model.

Figure 8.3: Planed paths and meteorological forecasts for the 6th and 7th flight.
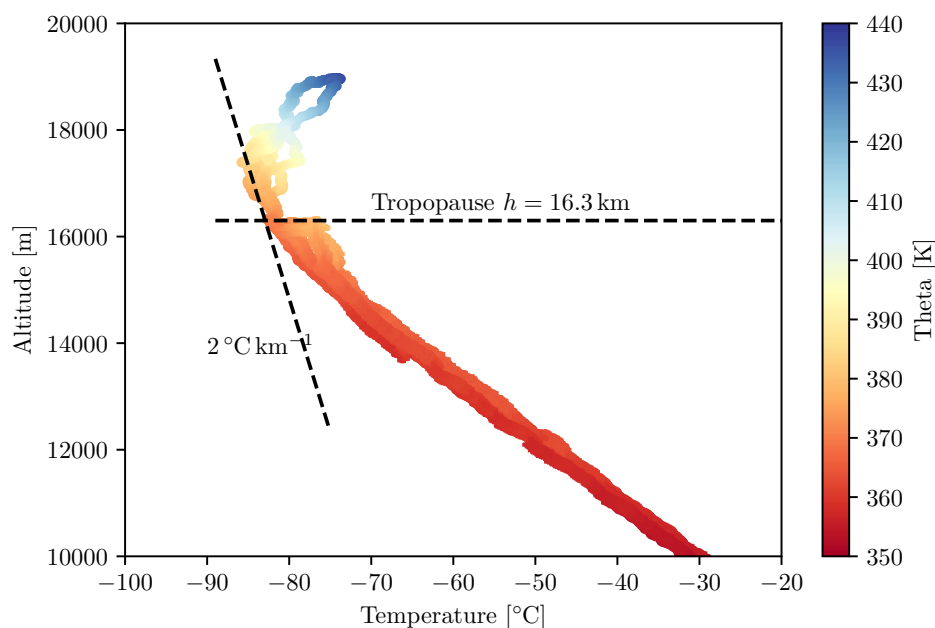
Figure 8.4:   Vertical profile of the ambient temperature during the 6th (06.08.2017) and 7th (08.08.2017) flights together with color-coded calculated potential temperature. Measurements were taken from the Geophysica avionic data.

consistent with the tropopause location widely used for this region at potential temperature of 380 K (see Figure 8.4).

8.2   Data consistency and preliminary results

8.2.1   HCN

The vertical profiles of HCN mixing ratio versus altitude and potential temperature are shown in Figures 8.5 and 8.6 respectively. During both flights, the mixing ratios of HCN mostly stayed within the range of 100 ppt to 300 ppt, which is consistent with earlier HCN observations. However, below the tropopause some spikes of up to 500 ppt have also been observed. The high variability of the data during the 6th flight at 16 km can be explained by the strong convective activity on this day transporting up air masses very recently influenced by e.g. biomass burning. On the long horizontal level flight tracks air masses with different origins (convective and non-convective) and histories are sampled probably generating this variability. Some more possible aspects will be discussed in Section 8.2.5.

Due to the high variability of HCN throughout the Asian monsoon anticyclone no clear vertical trend can be identified for the two flights. The negative gradient obvious in Figure 8.6 for the highest potential temperature levels above 423 K may represent the degrading HCN going deeper into the stratosphere.

8.2.2   HNO$_3$

The vertical profiles of HNO$_3$ mixing ratio versus altitude and potential temperature are shown in Figures 8.7 and 8.8 respectively. The profiles of the 6th and 7th flight in the

Figure 8.5: Vertical profiles of HCN from FunMass measurements during the flights on 06.08.2017 and 08.08.2017 are shown in the coordinates of geometric altitude. Values are averaged for 30 s. The tropopause height is determined from the avionic temperature measurements (see Figure 8.4).

Figure 8.6: Vertical profiles of HCN from FunMass measurements during the flights on 06.08.2017 and 08.08.2017 are shown in the coordinates of potential temperature Θ. Values are averaged for 30 s.
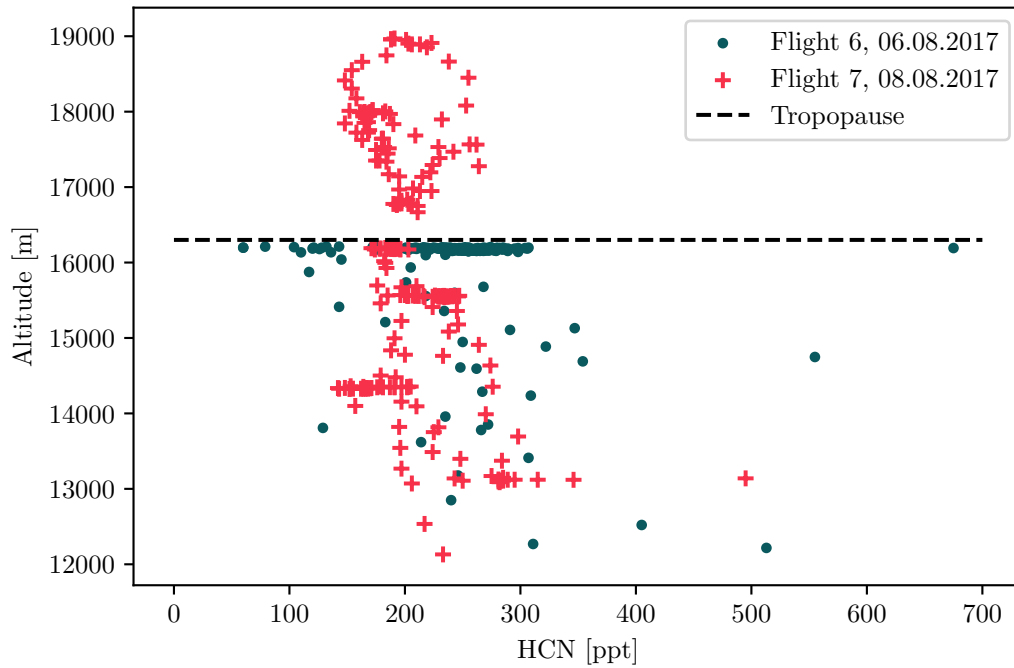
Vertical profile of HNO$_3$

Figure 8.7: Vertical profiles of HNO$_3$ from FunMass measurements during the flights on 06.08.2017 and 08.08.2017 are shown in the coordinates of geometric altitude. Values are averaged for 10 s. The tropopause height is determined from the avionic temperature measurements (see Figure 8.4).
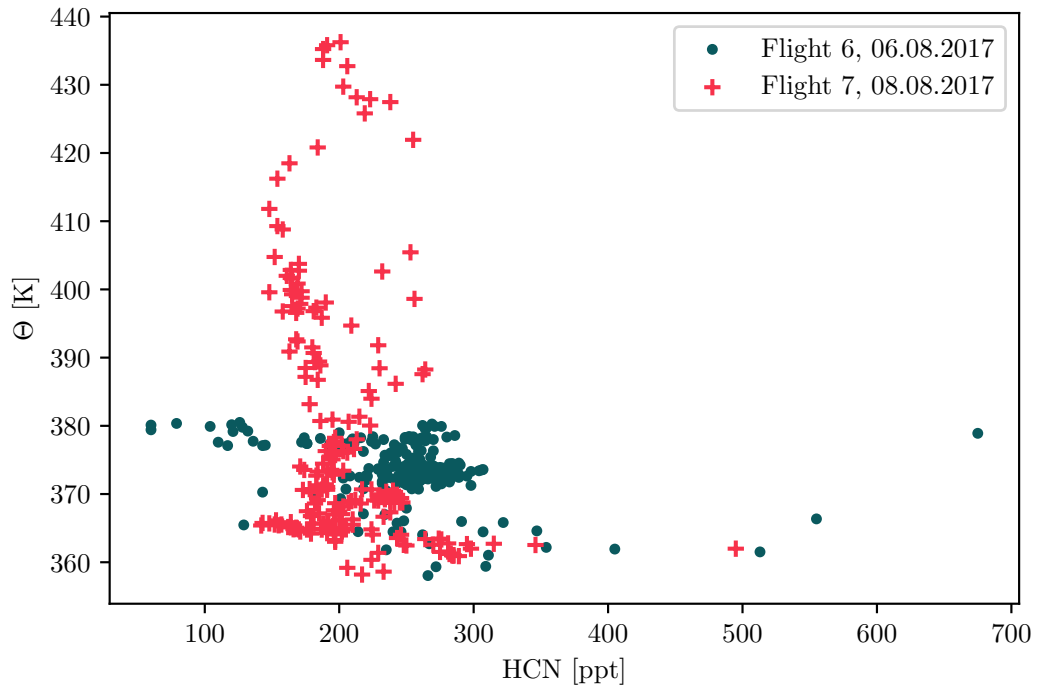
troposphere show significantly different behavior. During the 7th flight, the HNO$_3$ mixing ratios stayed fairly constant in the troposphere and below 100 ppt. Only one visible short spike up to 250 ppt at about 15 km was observed. On the contrary, in the 6th flight high variability of HNO$_3$ mixing ratios is observed along the whole measured vertical range up to the tropopause (similar to HCN but with no consistent correlation or anti-correlation). HNO$_3$ values up to 500 ppt were observed well below the tropopause and up to 700 ppt at the tropopause. The reasons for this high variability of the measured values during the 6th flight will be discussed in Sections 8.2.4 and 8.2.5.

In the stratospheric portion of the 7th flight, a local maximum 2 ppb of HNO$_3$ mixing ratio is observed at around 18.7 km, followed by a decrease to less than 1.3 ppb at around 19 km (Figure 8.7 and 8.8).

8.2.3   A first FunMass and AURA-MLS comparison

As described in Section 1.2 there are two satellite-based remote sensing instruments providing reasonably good measurements of HNO$_3$ and HCN in the UTLS region. Here it was decided to intercompare the FunMass measurements to the AURA-MLS instrument which is not so much affected by aerosol and clouds lower in the AMA and therefore provides a better comparison case with our measurements. The AURA-MLS provides over 3000 vertical profiles daily all over the globe.

The MLS data from 7th (from 07:39 to 07:40) and 10th (from 20:18 to 20:19) of August 2017 were selected as the most reasonable measurements for the intercomparison with the FunMass data because of their proximity to the flight tracks both in time and location, as illustrated in Figure 8.2. The comparison is shown in Figures 8.9 and 8.10 where also the
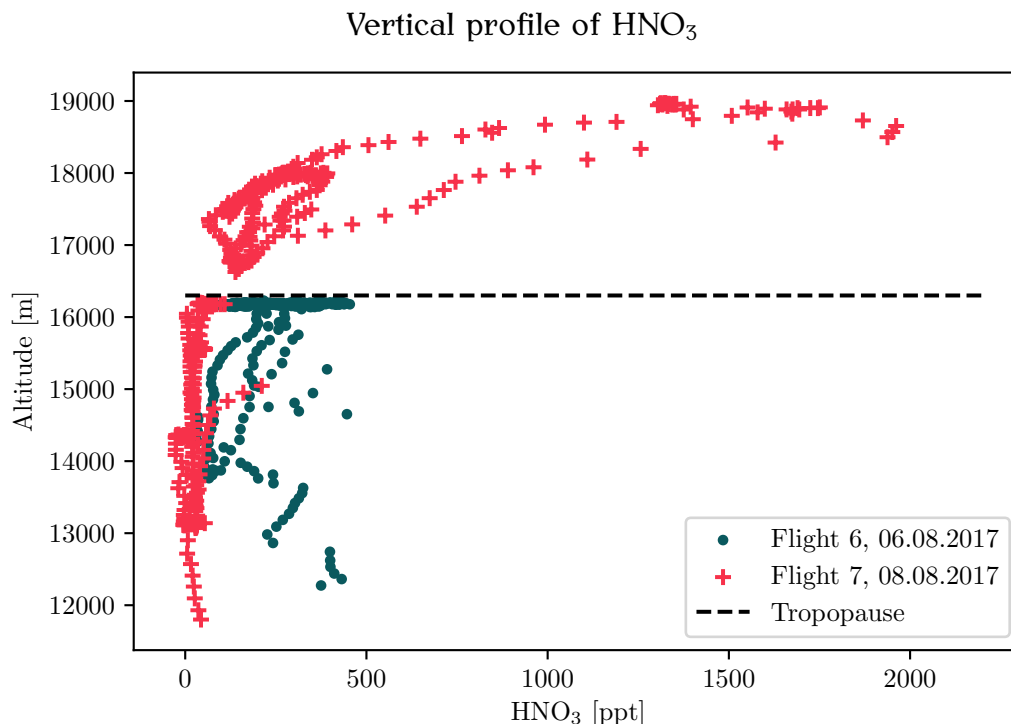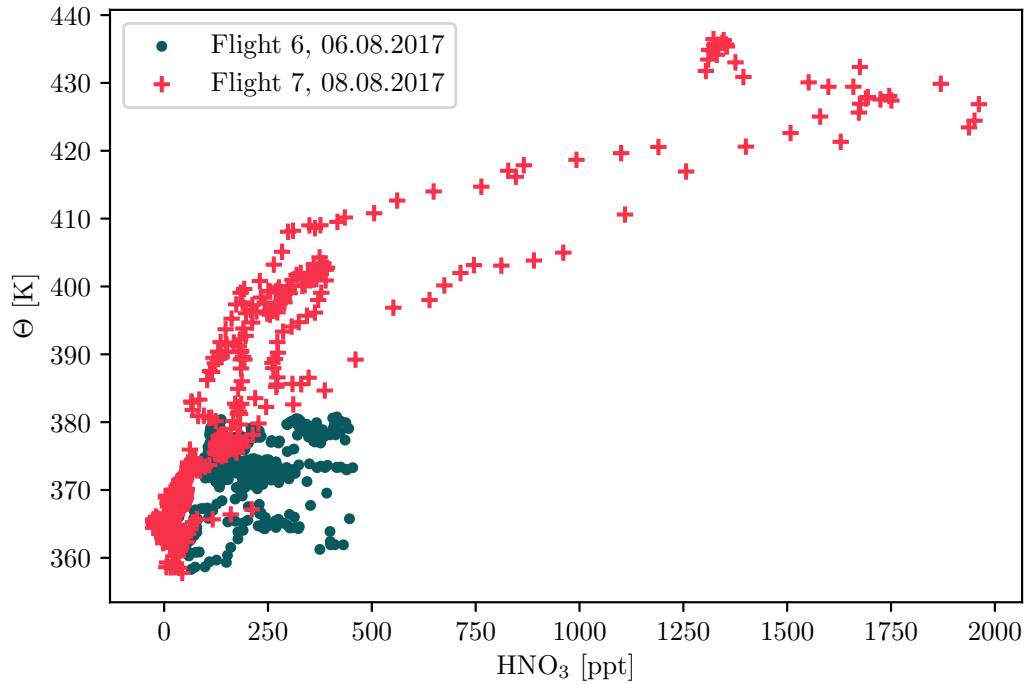
Figure 8.8: Vertical profiles of HNO$_3$ from FunMass measurements during the flights on 06.08.2017 and 08.08.2017 are shown in the coordinates of potential temperature Θ. Values are averaged for 10 s.

stratospheric MLS measurements are plotted to show the vertical evolution of the species above flight altitude. The markers and colors of the MLS data points are consistent with the ones used on the map in Figure 8.2. The 7th flight, which aimed to investigate the vertical structure of the Asian monsoon anticyclone, has a larger vertical overlap with the MLS data and therefore provides a better comparison. The MLS data show the maximum values for HNO$_3$ at the 150 hPa level for the measurements over the Bay of Bengal (blue circle and cross). At the same time FunMass measurements of HNO$_3$ show increased values for HNO$_3$ in this area and at comparable altitudes (flight 6) as well, both being caused most probably from lightning NOx generation. However, compared to the enhanced values observed in flight 6 average HNO$_3$ mixing ratios as observed by MLS at the 150 hPa level close to the bay of Bengal seem rather high. Higher up in the UTLS the FunMass and average MLS HNO$_3$ values agree quite well and much better than the error bars would suggest. For HCN also a very favorable comparison is found to the average MLS data, which however show very high error bars due to the low mixing ratios and resulting small signals involved, especially for the lowest levels. This also underlines the value of sensitive and accurate in-situ measurements to validate satellite data in these challenging environments. However, for a meaningful validation better statistics and closer spatial and temporal overlap of the aircraft measurements would be required with the much lower resolution satellite footprints which are on the order of 400 × 400 km horizontally and 3-4 km vertically. Compared to that, FunMass on board of M-55 Geophysica provides horizontal resolution around 100 m for 0.5 s average, and the vertical resolution depending on the ascent or descent rate of the aircraft may be as low as a few meters.
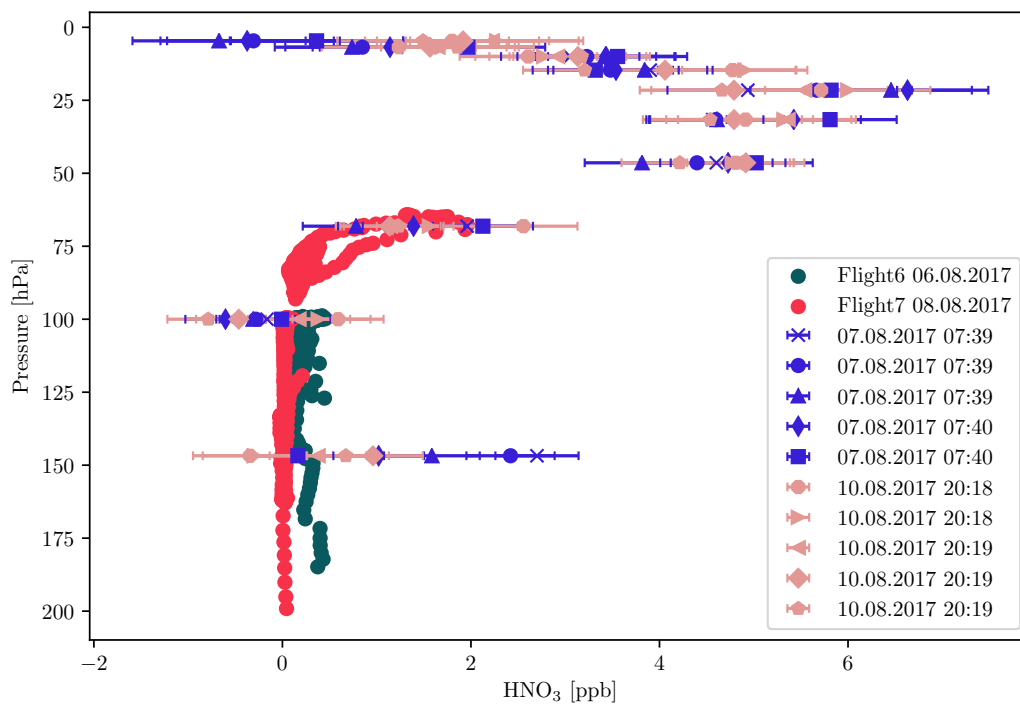
Figure 8.9: FunMass HNO₃ data compared to AURA-MLS measurements. FunMass data averaged for 10 s.
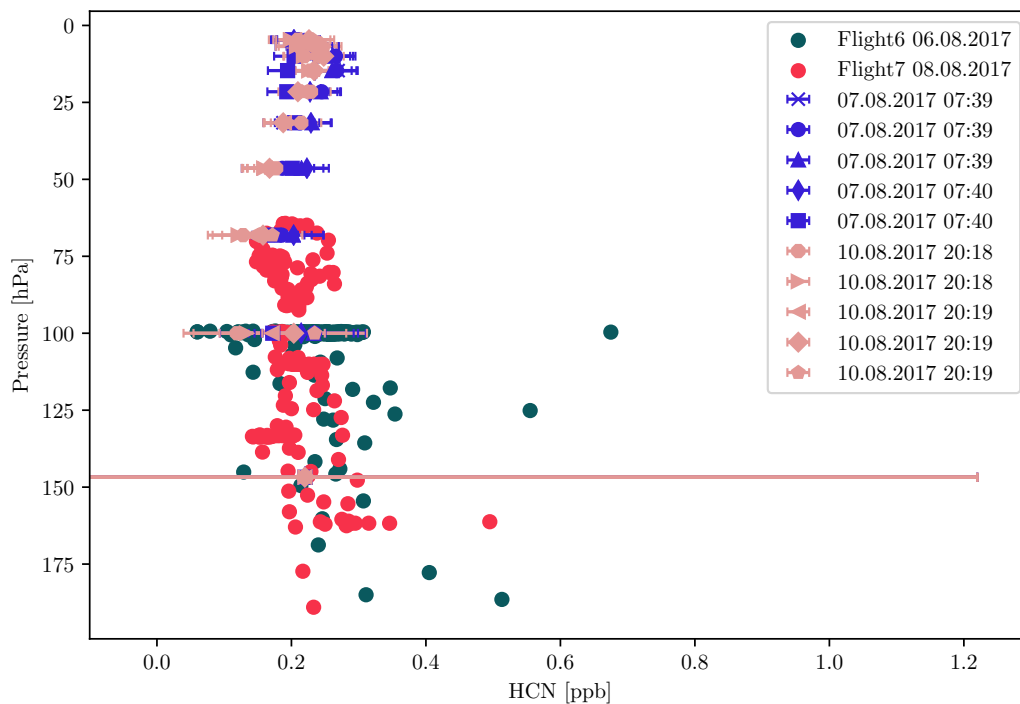

Figure 8.10: FunMass HCN data compared to AURA-MLS measurements. FunMass data averaged for 30 s. HCN value from AURA-MLS at 150 hPa has a symmetrical errorbar of ca. ±1 ppb, its left part is cut out.

8.2.4   HNO$_3$ - O$_3$ correlation

The primary source of most UTLS HNO$_3$ is nitrous oxide (N$_2$O) which is broken down by short-wave UV photolysis or reaction with O(1D) which both produces NO and higher nitrogen oxides (NOx). These in turn can form HNO$_3$. Similarly ozone is formed by the same spectral region of UV radiation via oxygen atoms in the Chapman cycle [8]. For this reason it is expected that a general correlation of HNO$_3$ and O$_3$ mixing ratios will be found with increasing altitude into the stratosphere at least to around 2 ppm O$_3$ (ca. 20 km) where photolysis starts to reduce HNO$_3$ significantly. Other sources and sinks of HNO$_3$ are formation from NOx produced in combustion, lightning NOx which may produce up to 80% of observed HNO$_3$ [53] and wash-out or condensation in particle formation. These cases will appear as outliers from the standard O$_3$ correlation.

The HNO$_3$ and O$_3$ time series from the 7th flight, recorded on board of M-55 Geophysica by FunMass and FOZAN [100] respectively are shown in Figure 8.11 which shows a stunning similarity of the HNO$_3$ and O$_3$ time series but also demonstrates the quality of the FunMass HNO$_3$ measurement in terms of time resolution and detail. FOZAN is a chemiluminescent ozone analyzer developed mainly in the Central Aerological Observatory (CAO), Dolgoprudny, Russia, and participating in the aircraft campaigns on board of the M-55 Geophysica since 1997, it is jointly operated with the Italian National Research Council (CNR).

HNO$_3$ and O$_3$ show a positive correlation (Figure 8.12). The latitude dependence of the slope of the HNO$_3$–O$_3$ correlation is discussed by Popp et al. [69] and Murphy et al. [59]. According to them, the correlation slope is higher at the poles and lower in the tropics. For the in-situ measurements done over Texas, USA (from 24 °N to 43 °N), Popp et al. [69] report the following correlation

$$[HNO_3] = 2.56 \times 10^{-3}[O_3] - 0.0922, \qquad (8.1)$$

with [HNO$_3$] and [O$_3$] expressed in ppb for the range 150 ppb $<$ [O$_3$] $<$ 1100 ppb.

The STRATOCLIM measurement campaign took place at almost the same latitudes as those of Texas (20 °N to 30 °N), however, transport in the AMA region may lead to a quite different correlation. However, Equation 8.1 was decided to be used for the measured O$_3$ and HNO$_3$ during this campaign as a reference. This relation is plotted in Figure 8.12 (black dashed line) for all O$_3$ measurements. Obviously, the vast majority of the data points for the O$_3$ mixing ratios below 250 ppb groups around a line with a somewhat lower slope (red dashed line in Figure 8.12), pointing to a slightly more "tropic" character of the observed air masses. However, another branch of air masses with seemingly much more "mid-latitude" character is also observed. These are mainly the data points observed on descent from the top altitude flight segment.

In the correlations given in Popp et al. [69] data below 150 ppb O$_3$ have not been included due to systematic enhancements in the HNO$_3$ values following lightning NOx production. We as well observe several clear outliers with enhanced HNO$_3$ from the linear trend in the troposphere at O$_3$ below 150 ppb (orange points in Figure 8.12 above the fitted line), which clearly seem to originate from lightning activity.

However, the good linearity of the vast majority of the data in the troposphere (Figure 8.12) even below 150 ppb of O$_3$ shows that during flight 7 almost no air masses with strong lightning events during the time interval of about 2-10 days back have been observed. Such events have most probably occurred in the air masses observed during flight 6 as obvious from the profile plots (Figure 8.7). But unfortunately no O$_3$ measurements are available due to malfunctioning of the FOZAN instrument in this flight. Therefore for the 6th flight, HNO$_3$–O$_3$ correlation cannot be investigated.

There is a quite smooth data segment showing "enhanced" HNO_3 located systematically above the Popp et al. [69] correlation. These data were acquired in the stratosphere during final descent from the highest flight segment. Their origin could also be attributed to down-mixed lightning signatures. It would need detailed chemical modeling to further explore this possibility. On the other hand these data portions may be signatures of inmixing from the mid-latitude stratosphere. To support either of these hypothesis, more data and further investigation are needed.

In flight 7, the O_3 profile shows a unique structure with the maximum at around 18.7 km - the same altitude as the HNO_3 maximum. Higher up, the HNO_3 as well as the O_3 decline again significantly. This is most obvious from the HNO_3 profile vs. potential temperature in Figure 8.8 and also from the expanded time series plot in Figure 8.11(b). For the O_3 measurements done by the FOZAN instrument this decrease of mixing ratio with altitude above 18.7 km was observed as well during the 8th flight. This indicates that this feature may not just be due to some isolated mixing event but may point to some general feature of the lower stratosphere above the AMA. Unfortunately, the aircraft was not scheduled to ascent to even higher altitude to observe the further vertical evolution of this feature, which probably will not be observable by satellite based remote-sensing instrumentation due to their low vertical resolution on the order of 2 km.

8.2.5   Lightning induced features in the FunMass measurements in Flight 6

Flight 6 was carried out on 06.08.2017 mainly at an altitude of 16 km slightly below the local tropopause in order to measure effects of strong local convection. High variability of HNO_3 and partly also HCN was observed (see Figures 8.7 and 8.5). In Figure 8.13 the zoomed-in HNO_3 and HCN time series for a part of the flight are shown. The first section of strongly elevated HNO_3 is observed mainly during ascent inside the anticyclone and the very first portion of the level flight (marked as region 6A in Fig. 8.13). The second region of enhanced HNO_3 (marked 6B) followed shortly after the aircraft finished the dive. Unfortunately, part of the section 6B FunMass measurement is interrupted by a calibration interval. Enhanced HNO_3 goes along with similar enhancements and spikes in the NO and NOy data measured by the SIOUX instrument, a two channel chemiluminescence nitrogen oxides analyzer [79] (not shown here). NOy of up to 7 ppb during ascent and 4 ppb at 16 km were observed [78]. Therefore, the HNO_3 signatures 6A and 6B were most likely generated from NOx resulting from lightning events in convective thunderstorms. Unfortunately, the SIOUX instrument failed shortly after the 16km level flight had been reached, therefore no direct comparison was possible for flight section 6B. Simultaneously to the enhanced HNO_3 significantly lower mixing ratios of HCN are obvious in both regions 6A and 6B. These may be explained by wash-out in heavy rain inside of the thunderstorms due to the good solubility of HCN in water. Rain is a known sink for HNO_3 too, but during the rain most probably there was almost no HNO_3 present yet, since it still had to be formed from the initially generated NO, which exhibits low solubility. The conversion to NO_2 and HNO_3 takes at least some hours. The proposed processes seem most obvious for the FunMass observations in flight 6, however, more work is needed to really establish these preliminary results. However, the high value of the highly sensitive and fast measurements of the FunMass instrument are clearly demonstrated.
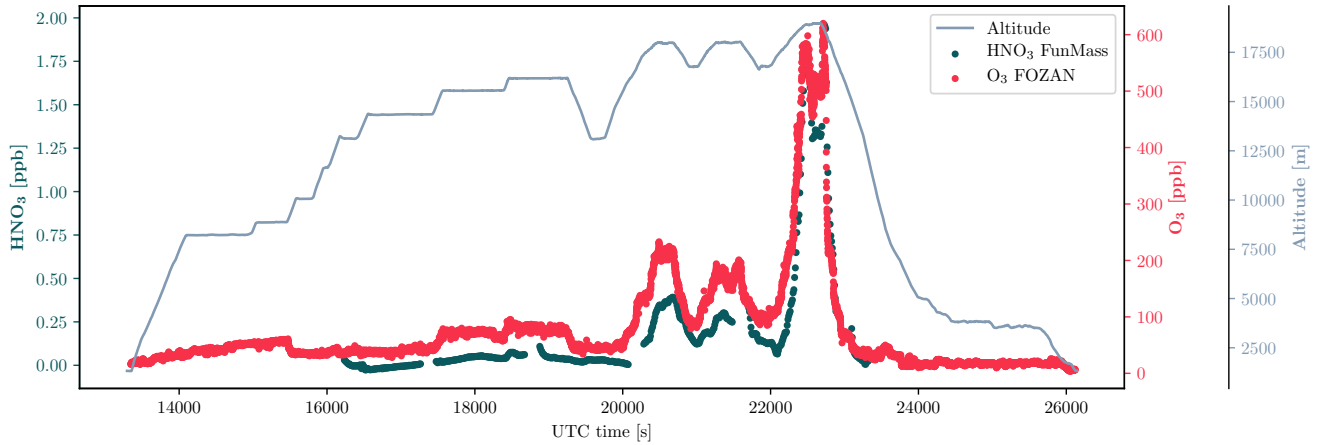
(a) 7th measurement flight on 08.08.2017.
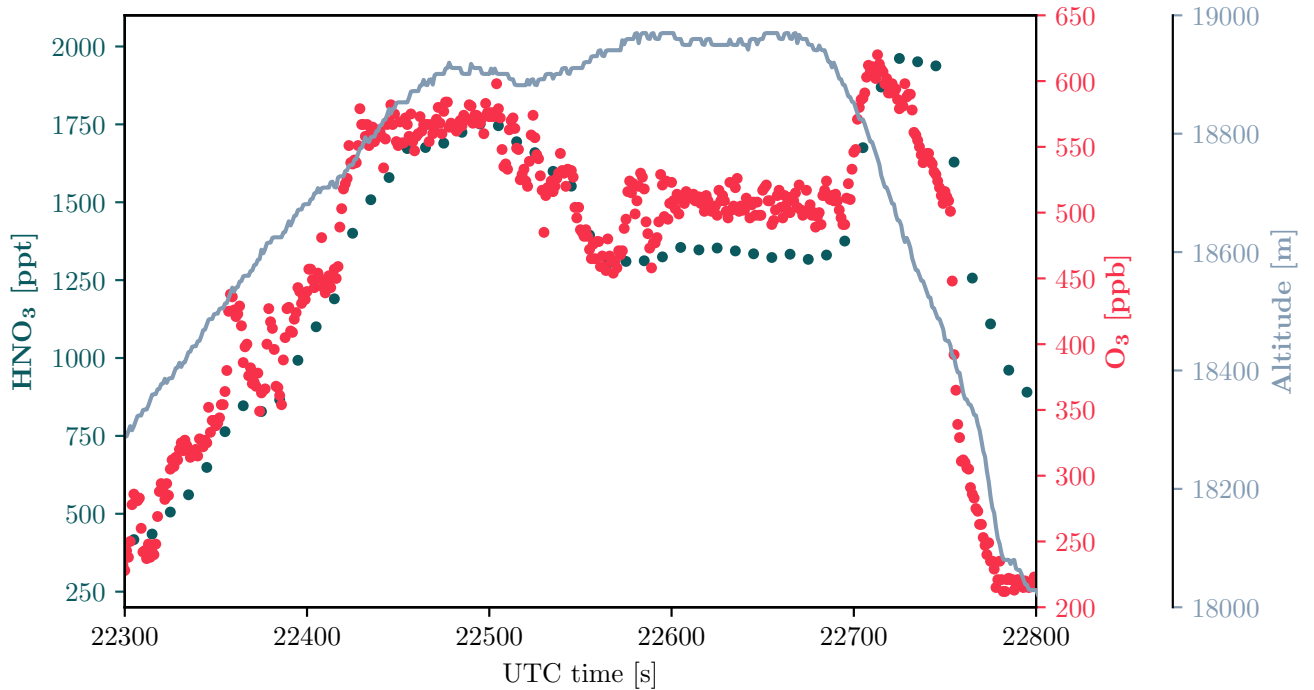
(b) High-altitude part of the 7th measurement flight on 08.08.2017.

Figure 8.11: Measurements of HNO_3 and O_3 during the 7th flight (08.08.2017) performed with FunMass and FOZAN respectively. Values from FunMass are averaged for 10 s. The flight altitude was taken from the Geophysica avionic data.
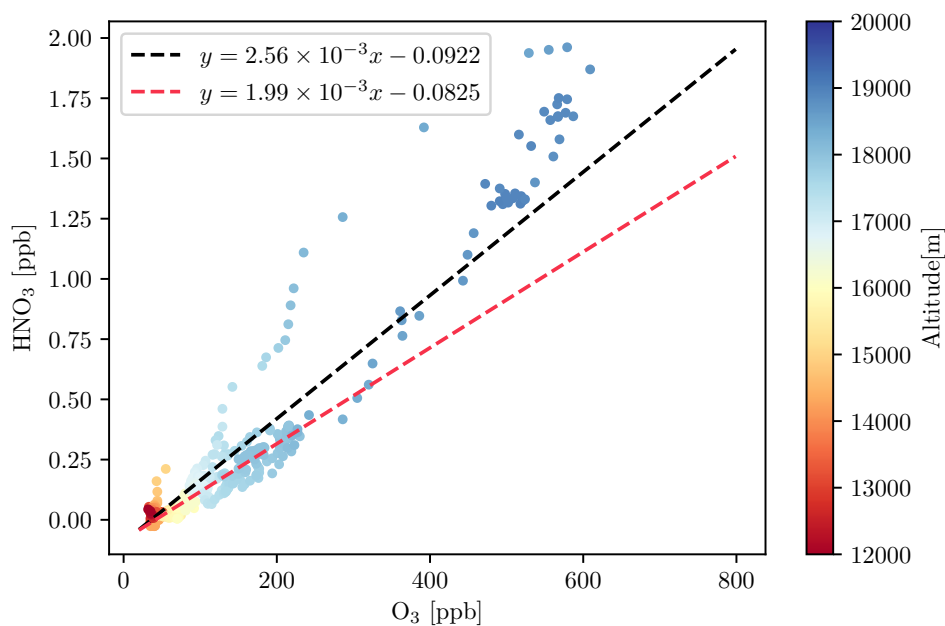
Figure 8.12: HNO$_3$ - O$_3$ correlation for the 7th flight on 08.08.2017. Measurements of HNO$_3$ and O$_3$ were performed with FunMass and FOZAN respectively. Values are averaged for 10 s. The dashed black line represents the expected dependence from Popp et al. [69]. The linear fit to the FunMass data (red dashed line) was done only for the following range: 150 ppb $\leq$ [O$_3$] $\leq$ 250 ppb and [HNO$_3$]$\leq$ 400 ppb.

8.3   Summary

The first successful measurements of HNO$_3$ and HCN with the FunMass instrument for flights 6 and 7 of the StratoClim campaign have been presented and some obvious features have been preliminarily discussed. A first comparison of the FunMass data with AURA-MLS measurements has been presented and shows a generally good agreement.

A stunning correlation of HNO$_3$ and O$_3$ measurements was observed during flight 7 and was compared to the analysis of Popp et al. [69]. Distinct features deviating from the correlation derived by Popp et al. [69] for similar latitudes were observed in both directions and possible causes have proposed as HNO$_3$ enhancements from lightning and in-mixing of mid-latitude stratospheric air.

The features qualitatively discussed in this chapter will be subject to further more refined studies including process models. However, the preliminary results strongly underline the scientific potential of the high-quality data sets obtained in flights 6 and 7 by the newly developed FunMass instrument.
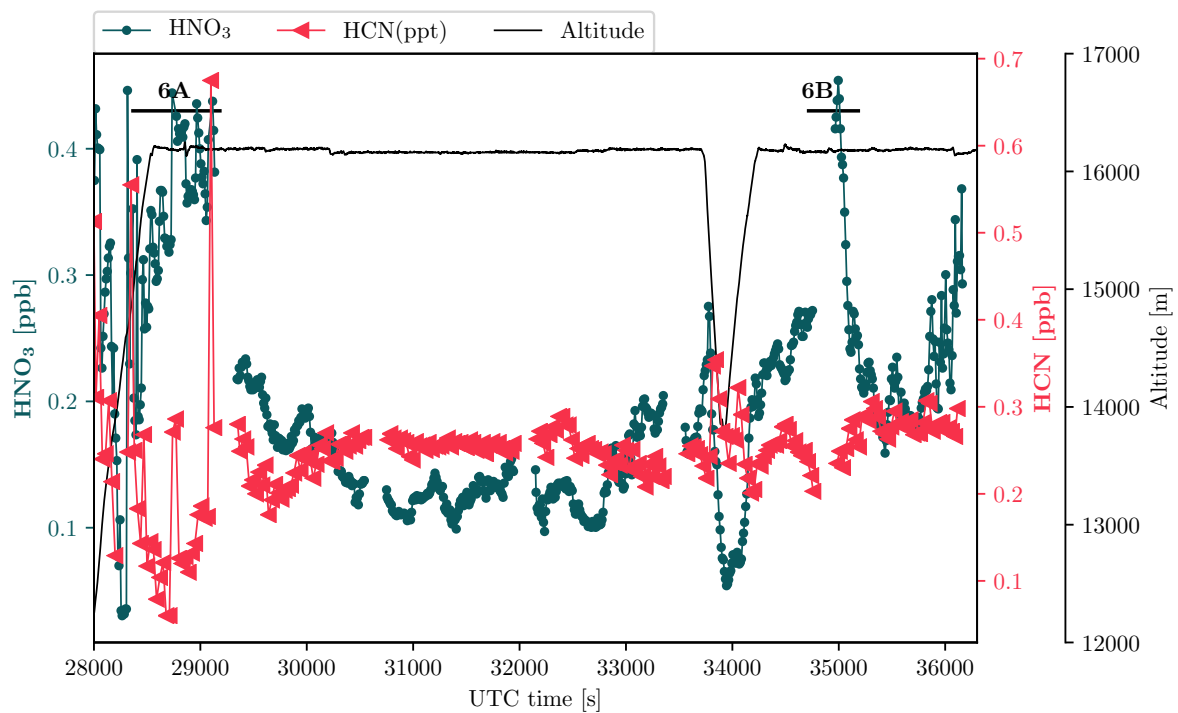
Figure 8.13: Blow-up of Figure 8.1(a) showing the FunMass measurements o HNO₃ (green circles) and HCN (green triangles) during the 6th flight on 06.08.2017. The geometric altitude (black line) was taken from the Geophysica avionic data. Values of HNO₃ and HCN are averaged for 10 s and 30 s correspondingly. Two regions of clearly enhanced HNO₃ values are marked and are discussed in the text.

Chapter 9

Conclusions and outlook

During this work a new versatile airborne chemical ionization time-of-flight mass spectrometer was developed, named FunMass. It was designed to simultaneously measure different trace gases in the UTLS region on board of the high-altitude research aircraft M-55 Geophysica (service ceiling 21.5 km). To our knowledge, FunMass is the first airborne TOF MS which is operated in the stratosphere without a pressurized housing around it, being exposed to low ambient pressures down to 50 hPa, which is challenging due to the high voltage requirements of TOF instruments but leads to considerable space and weight reduction.

To better quantify and understand dynamical and chemical processes in the atmosphere, high quality measurements of ultra trace gases are crucial. CIMS is a very sensitive measurement technique, which renders it favorable for the measurements of the low mixing ratios of trace gases in the UTLS. The vast majority of current CIMS instruments employed for these measurements are using variations of quadrupole mass analyzers, which in fact become rather slow if they are aiming for simultaneous measurements of several different species and have to monitor several peaks. The TOF mass analyzers are completely deprived of this disadvantage and capable of providing a complete mass spectrum for a wide range of masses at rates even faster than reasonable for airborne measurements, allowing to reduce spatial resolution easily down to several meters. On the other hand, TOF mass analyzers have to be operated at much lower pressure than quadrupole ones. Therefore a TOF MS instrument has to be equipped with a more complex pressure reducing transfer stage, which cannot be done completely without adversely affecting the sensitivity. To improve transmission of ions in the transfer stage from the IMR region to the TOF mass analyzer, i.e. to improve sensitivity of the instrument, ion funnels can be used, which can provide excellent ion transmission even at pressures above 1 hPa [1]. The concept of a transfer stage with an ion funnel developed for the laboratory prototype [1] has been integrated into the flight instrument. Another important and unique detail of FunMass is a versatile dielectric barrier discharge ion source, replacing the widely used radioactive ion source, which can hardly be deployed on international flight campaigns.

For all parts of the instrument developed at FZJ, software drivers have been written in order to centrally control the complex system from the main program via a network of control boards. The commercial TOF analyzer is also centrally controlled by the program. In order to allow fully autonomous operation on board of M-55 Geophysica, a flight mode consisting of over 20 parallel threads was developed and thoroughly tested. The flight program powers up and down and controls all the units and cycles them through measurement, background, and calibration sequences over flight. It also contains functions to handle abnormal situations and protect the equipment from potential damage during the

flight. In addition, to simplify tests and usage of the instrument in the lab, a GUI application was developed. All software was written in a modular way, which simplifies the addition of new features, as well as the development of autonomous modes for completely new measurement scenarios.

Before the first fully operational deployment on board of M-55 Geophysica, all parts of FunMass individually and later the whole instrument were tested in a climate chamber to ensure safe and proper operation at low ambient temperatures and pressures. All temperature sensitive units were supplied with proper heating, and the risk of unwanted sparks and dangerous discharges in and around the critical HV devices was minimized at the hardware level. In addition, software safety procedures were implemented to further minimize this risk of using high voltages at low pressures, which could destroy the instrument and even cause a fire hazard.

FunMass was calibrated in the lab for all targeted species, employing a setup with high accuracy permeation devices. It is also equipped with an in-flight calibration unit for at least one of the species in order to verify lab calibration and ensure accurate measurements. FunMass has been carefully characterized for HNO_3, SO_2 and HCN measurements in CO_3^- ionization mode. It shows outstanding sensitivity towards HNO_3 and SO_2, which translates into very low detection limits. Even at $0.5\,s$ average, for SO_2 we report a detection limit very similar to the best among CIMS instruments, and for HNO_3 almost one order of magnitude better.

The first fully operational deployment of the FunMass instrument on board of M-55 Geophysica happened in July 2017 in Kathmandu, Nepal within the STRATOCLIM aircraft campaign. In spite of issues with the regulating ambient air inlet first successful measurements of UTLS HNO_3 and HCN by the FunMass instrument have been acquired in this work. The data show very interesting features that are preliminarily discussed in the light of relevant processes in the Asian monsoon anticyclone. First intercomparisons of the FunMass measurements with data from other in-situ instruments on board of M-55 Geophysica and data from satellite-based remote sensing instruments show very good agreement.

9.1   Outlook

FunMass now is a fully characterized and operational instrument, which already proved its ability to measure HNO_3 and HCN in the UTLS region on board of M-55 Geophysica. Nevertheless, some improvements and modifications are advised or already in the process of implementation:

- For further deployments on board of M-55 Geophysica, the thermal problems of the ambient air inlet have to be reliably resolved.

- The SO_2 measurement and the online calibration remain to be tested and proven in flight.

- A new HCN permeation device with lower permeation rate is needed to calibrate the instrument in the range of the relevant atmospheric HCN mixing ratios (currently being tested).

- Optimize and characterize the instrument to perform with reagent ions different from CO_3^- (including positive chemical ionization), potentially measuring other species with high sensitivity.

- A DBD ion source with different geometry may improve mixing of analyte air and the reagent ions in the IMR region and further improve sensitivity (currently being tested).

- Transition of the FunMass software to Python 3 is needed, since the support for Python 2 ends in 2020;

- The instrument should favorably be adapted to new measurement platforms and can also be further used for ground based ambient air and environmental chamber measurements.

Bibliography

[1] Sascha Albrecht. *Development of a highly sensitive and versatile mass spectrometer system for laboratory and atmospheric measurements.* PhD thesis, University of Wuppertal,Wuppertal, 2014.

[2] J. G. ANDERSON, D. W. TOOHEY, and W. H. BRUNE. Free radicals within the antarctic vortex: The role of CFCs in antarctic ozone loss. *Science*, 251(4989):39–46, jan 1991. doi: 10.1126/science.251.4989.39.

[3] Susan T. Arnold, Robert A. Morris, A. A. Viggiano, and John T. Jayne. Ion chemistry relevant for chemical ionization detection of SO_3. *Journal of Geophysical Research*, 100(D7):14141, 1995. doi: 10.1029/95jd01004.

[4] T. S. Bates, B. K. Lamb, A. Guenther, J. Dignon, and R. E. Stoiber. Sulfur emissions to the atmosphere from natural sourees. *Journal of Atmospheric Chemistry*, 14(1-4): 315–337, apr 1992. doi: 10.1007/bf00115242.

[5] Arthur T. Benjamin and Jennifer Quinn. *Proofs that Really Count (Dolciani Mathematical Expositions).* American Mathematical Society, 2003. ISBN 978-0-88385-333-7.

[6] T. H. Bertram, J. R. Kimmel, T. A. Crisp, O. S. Ryder, R. L. N. Yatavelli, J. A. Thornton, M. J. Cubison, M. Gonin, and D. R. Worsnop. A field-deployable, chemical ionization time-of-flight mass spectrometer. *Atmospheric Measurement Techniques*, 4(7):1471–1479, jul 2011. doi: 10.5194/amt-4-1471-2011.

[7] Philip R. Bevington. Data reduction and error analysis for the physical sciences. *Journal of the American Statistical Association*, 67(337):249, mar 1972. doi: 10.2307/2284752.

[8] Guy P. Brasseur and Susan Solomon. *Aeronomy of the Middle Atmosphere.* Springer-Verlag, 1986. doi: 10.1007/1-4020-3824-0.

[9] M. Le Breton, M. R. McGillen, J. B. A. Muller, A. Bacak, D. E. Shallcross, P. Xiao, L. G. Huey, D. Tanner, H. Coe, and C. J. Percival. Airborne observations of formic acid using a chemical ionization mass spectrometer. *Atmospheric Measurement Techniques*, 5 (12):3029–3039, dec 2012. doi: 10.5194/amt-5-3029-2012.

[10] Shaun Burke. Regression and calibration, statistics and data analysis, 2018.

[11] Javier Hidalgo Carrio. Allan variance analysis, 2015. URL `https://cran.r-project.org/web/packages/allanvar/allanvar.pdf`.

[12] J.S. Coursey, D.J. Schwab, J.J. Tsai, and R.A. Dragoset. Atomic weights and isotopic compositions (version 4.1). National Institute of Standards and Technology, Gaithersburg, MD, http://physics.nist.gov/Comp, 2015. URL `http://physics.nist.gov/Comp`.

[13] Paul J. Crutzen. The possible importance of CSO for the sulfate layer of the stratosphere. *Geophysical Research Letters*, 3(2):73–76, feb 1976. doi: 10.1029/gl003i002p00073.

[14] John G. Dillard. Negative ion mass spectrometry. *Chemical Reviews*, 73(6):589–643, dec 1973. doi: 10.1021/cr60286a002.

[15] F. L. Eisele and D. J. Tanner. Ion-assisted tropospheric OH measurements. *Journal of Geophysical Research*, 96(D5):9295, 1991. doi: 10.1029/91jd00198.

[16] Andreas Engel. Institute for Atmospheric and Environmental Sciences, Goethe-University Frankfurt, Germany. Private communication, 2018.

[17] F.C. Fehsenfeld and C.J. Howard. Ion chemistry of HNO_3 and NO_2. *BULLETIN OF THE AMERICAN PHYSICAL SOCIETY*, 20(2):239, 1975. ISSN 0003-0503.

[18] V. Fiedler, F. Arnold, S. Ludmann, A. Minikin, T. Hamburger, L. Pirjola, A. Dörnbrack, and H. Schlager. African biomass burning plumes over the atlantic: aircraft based measurements and implications for H_2SO_4 and HNO_3 mediated smoke particle activation. *Atmospheric Chemistry and Physics*, 11(7):3211–3225, apr 2011. doi: 10.5194/acp-11-3211-2011.

[19] Python Software Foundation. Python language reference. https://www.python.org/, 2018. URL `https://www.python.org/`.

[20] C. W. Gear. The automatic integration of ordinary differential equations. *Communications of the ACM*, 14(3):176–179, mar 1971. doi: 10.1145/362566.362571.

[21] Dieter Gerlich. Inhomogeneous RF fields: A versatile tool for the study of processes with slow ions. In *Advances in Chemical Physics*, pages 1–176. John Wiley & Sons, Inc., mar 2007. doi: 10.1002/9780470141397.ch1.

[22] N. Glatthor, M. Höpfner, G. P. Stiller, T. von Clarmann, B. Funke, S. Lossow, E. Eckert, U. Grabowski, S. Kellmann, A. Linden, K. A. Walker, and A. Wiegele. Seasonal and interannual variations in HCN amounts in the upper troposphere and lower stratosphere observed by MIPAS. *Atmospheric Chemistry and Physics*, 15(2):563–582, jan 2015. doi: 10.5194/acp-15-563-2015.

[23] Anton A. Goloborodko, Lev I. Levitsky, Mark V. Ivanov, and Mikhail V. Gorshkov. Pyteomics—a python framework for exploratory data analysis and rapid software prototyping in proteomics. *Journal of The American Society for Mass Spectrometry*, 24(2):301–304, jan 2013. doi: 10.1007/s13361-012-0516-6.

[24] Jurgen H Gross. *Mass Spectrometry: A Textbook*. Springer, 2011. ISBN 978-3-642-10709-2. URL `https://www.amazon.com/Mass-Spectrometry-Textbook-J%C3%BCrgen-Gross/dp/3642107095?SubscriptionId=0JYN1NVW651KCA56C102&tag=techkie-20&linkCode=xm2&camp=2025&creative=165953&creativeASIN=3642107095`.

[25] HDF Group. HDF5, 2017. URL `https://support.hdfgroup.org/HDF5/whatishdf5.html`.

[26] M. Hanke, B. Umann, J. Uecker, F. Arnold, and H. Bunz. Atmospheric measurements of gas-phase HNO_3 and SO_2 using chemical ionization mass spectrometry during the MINATROC field campaign 2000 on monte cimone. *Atmospheric Chemistry and Physics*, 3(2):417–436, apr 2003. doi: 10.5194/acp-3-417-2003.

[27] Trevor Hastie, Robert Tibshirani, and Jerome Friedman. *Elements of Statistical Learning*. Springer New York, 2013. URL https://www.ebook.de/de/product/25193600/trevor_hastie_robert_tibshirani_jerome_friedman_elements_of_statistical_learning.html.

[28] Roman Held, Josef Goette, Marcel Jacomet, Christian Tanner, Marc Gonin, and Martin Tanner. High-speed hardware algorithm for continuous mode time-of-flight mass spectrometry. In *2012 IEEE 3rd Latin American Symposium on Circuits and Systems (LASCAS)*. IEEE, feb 2012. doi: 10.1109/lascas.2012.6180315.

[29] David Hemmendinger. Object-oriented programming, 2018. URL https://www.britannica.com/technology/object-oriented-programming.

[30] D. J. Hofmann. Increase in the stratospheric background sulfuric acid aerosol mass in the past 10 years. *Science*, 248(4958):996–1000, may 1990. doi: 10.1126/science.248.4958.996.

[31] Rupert Holzinger, Carsten Warneke, Armin Hansel, Alfons Jordan, Werner Lindinger, Dieter H. Scharffe, Gunnar Schade, and Paul J. Crutzen. Biomass burning as a source of formaldehyde, acetaldehyde, methanol, acetone, acetonitrile, and hydrogen cyanide. *Geophysical Research Letters*, 26(8):1161–1164, apr 1999. doi: 10.1029/1999gl900156.

[32] M. Höpfner, N. Glatthor, U. Grabowski, S. Kellmann, M. Kiefer, A. Linden, J. Orphal, G. Stiller, T. von Clarmann, B. Funke, and C. D. Boone. Sulfur dioxide (SO_2) as observed by MIPAS/envisat: temporal development and spatial distribution at 15–45 km altitude. *Atmospheric Chemistry and Physics*, 13(20):10405–10423, oct 2013. doi: 10.5194/acp-13-10405-2013.

[33] M. Höpfner, C. D. Boone, B. Funke, N. Glatthor, U. Grabowski, A. Günther, S. Kellmann, M. Kiefer, A. Linden, S. Lossow, H. C. Pumphrey, W. G. Read, A. Roiger, G. Stiller, H. Schlager, T. von Clarmann, and K. Wissmüller. Sulfur dioxide (SO_2) from MIPAS in the upper troposphere and lower stratosphere 2002–2012. *Atmospheric Chemistry and Physics*, 15(12):7017–7037, jun 2015. doi: 10.5194/acp-15-7017-2015.

[34] L. Gregory Huey. Measurement of trace atmospheric species by chemical ionization mass spectrometry: Speciation of reactive nitrogen and future directions. *Mass Spectrometry Reviews*, 26(2):166–184, 2007. doi: 10.1002/mas.20118.

[35] L. Gregory Huey, David R. Hanson, and Carleton J. Howard. Reactions of SF6- and i- with atmospheric trace gases. *The Journal of Physical Chemistry*, 99(14):5001–5008, apr 1995. doi: 10.1021/j100014a021.

[36] L.G. Huey, D.J. Tanner, D.L. Slusher, J.E. Dibb, R. Arimoto, G. Chen, D. Davis, M.P. Buhr, J.B. Nowak, R.L. Mauldin, F.L. Eisele, and E. Kosciuch. CIMS measurements of HNO_3 andSO_2 at the south pole during ISCAT 2000. *Atmospheric Environment*, 38(32):5411–5421, oct 2004. doi: 10.1016/j.atmosenv.2004.04.037.

[37] IAGOS-AISBL. In-service aircraft for a global observing system (IAGOS). https://www.iagos.org/, 2018.

[38] IPCC. *Climate Change 2013 - The Physical Science Basis*. Cambridge University Press, 2013. doi: 10.1017/cbo9781107415324.

[39] Salvatore Ipsale. Fine Metrology, Italy. Private communication, 2017.

[40] Eric Jones, Travis Oliphant, Pearu Peterson, et al. SciPy: Open source scientific tools for Python. http://www.scipy.org/, 2001–2018. URL http://www.scipy.org/.

[41] Christian E. Junge, Charles W. Chagnon, and James E. Manson. STRATOSPHERIC AEROSOLS. *Journal of Meteorology*, 18(1):81–108, feb 1961. doi: 10.1175/ 1520-0469(1961)018<0081:sa>2.0.co;2.

[42] Tina Jurkat, Stefan Kaufmann, Christiane Voigt, Dominik Schäuble, Philipp Jeßberger, and Helmut Ziereis. The airborne mass spectrometer AIMS – part 2: Measurements of trace gases with stratospheric or tropospheric origin in the UTLS. *Atmospheric Measurement Techniques*, 9(4):1907–1923, apr 2016. doi: 10.5194/amt-9-1907-2016.

[43] Taeman Kim, Aleksey V. Tolmachev, Richard Harkewicz, David C. Prior, Gordon Anderson, Harold R. Udseth, Richard D. Smith, Thomas H. Bailey, Sergey Rakov, and Jean H. Futrell. Design and implementation of a new electrodynamic ion funnel. *Analytical Chemistry*, 72(10):2247–2255, may 2000. doi: 10.1021/ac991412x.

[44] Corinna Kloss. *Carbonyl Sulde in the Stratosphere: airborne instrument development and satellite based data analysis*. PhD thesis, University of Wuppertal,Wuppertal, 2017.

[45] Franziska Kämmerer. Chemical ionisation mass spectrometry with a time of flight detector (cims-tof) measurements in support of the calibration of the airborne "FunMass" instrument, 2018.

[46] Stefanie Kremser, Larry W. Thomason, Marc von Hobe, Markus Hermann, Terry Deshler, Claudia Timmreck, Matthew Toohey, Andrea Stenke, Joshua P. Schwarz, Ralf Weigel, Stephan Fueglistaler, Fred J. Prata, Jean-Paul Vernier, Hans Schlager, John E. Barnes, Juan-Carlos Antuña-Marrero, Duncan Fairlie, Mathias Palm, Emmanuel Mahieu, Justus Notholt, Markus Rex, Christine Bingen, Filip Vanhellemont, Adam Bourassa, John M. C. Plane, Daniel Klocke, Simon A. Carn, Lieven Clarisse, Thomas Trickl, Ryan Neely, Alexander D. James, Landon Rieger, James C. Wilson, and Brian Meland. Stratospheric aerosol-observations, processes, and impact on climate. *Reviews of Geophysics*, 54(2):278–335, may 2016. doi: 10.1002/2015rg000511.

[47] H.H. Ku. Notes on the use of propagation of error formulas. *Journal of Research of the National Bureau of Standards, Section C: Engineering and Instrumentation*, 70C(4):263, oct 1966. doi: 10.6028/jres.070c.025.

[48] A. Lambert, W. G. Read, N. J. Livesey, M. L. Santee, G. L. Manney, L. Froidevaux, D. L. Wu, M. J. Schwartz, H. C. Pumphrey, C. Jimenez, G. E. Nedoluha, R. E. Cofield, D. T. Cuddy, W. H. Daffer, B. J. Drouin, R. A. Fuller, R. F. Jarnot, B. W. Knosp, H. M. Pickett, V. S. Perun, W. V. Snyder, P. C. Stek, R. P. Thurstans, P. A. Wagner, J. W. Waters, K. W. Jucks, G. C. Toon, R. A. Stachnik, P. F. Bernath, C. D. Boone, K. A. Walker, J. Urban, D. Murtagh, J. W. Elkins, and E. Atlas. Validation of the aura microwave limb sounder middle atmosphere water vapor and nitrous oxide measurements. *Journal of Geophysical Research*, 112(D24), dec 2007. doi: 10.1029/2007jd008724.

[49] Ben H. Lee, Felipe D. Lopez-Hilfiker, Claudia Mohr, Theo Kurtén, Douglas R. Worsnop, and Joel A. Thornton. An iodide-adduct high-resolution time-of-flight

chemical-ionization mass spectrometer: Application to atmospheric inorganic and organic compounds. *Environmental Science & Technology*, 48(11):6309–6317, may 2014. doi: 10.1021/es500362a.

[50] Q. Li, P. I. Palmer, H. C. Pumphrey, P. Bernath, and E. Mahieu. What drives the observed variability of HCN in the troposphere and lower stratosphere? *Atmospheric Chemistry and Physics Discussions*, 9(3):10883–10912, may 2009. doi: 10.5194/acpd-9-10883-2009.

[51] Qinbin Li, Daniel J. Jacob, Isabelle Bey, Robert M. Yantosca, Yongjing Zhao, Yutaka Kondo, and Justus Notholt. Atmospheric hydrogen cyanide (HCN): Biomass burning source, ocean sink? *Geophysical Research Letters*, 27(3):357–360, feb 2000. doi: 10.1029/1999gl010935.

[52] B.A. Mamyrin. Laser assisted reflectron time-of-flight mass spectrometry. *International Journal of Mass Spectrometry and Ion Processes*, 131:1–19, feb 1994. doi: 10.1016/0168-1176(93)03891-o.

[53] Randall V. Martin, Bastien Sauvage, Ian Folkins, Christopher E. Sioris, Christopher Boone, Peter Bernath, and Jerry Ziemke. Space-based constraints on the production of nitric oxide by lightning. *Journal of Geophysical Research*, 112(D9), may 2007. doi: 10.1029/2006jd007831.

[54] R. L. Mauldin, D. J. Tanner, and F. L. Eisele. A new chemical ionization mass spectrometer technique for the fast measurement of gas phase nitric acid in the atmosphere. *Journal of Geophysical Research: Atmospheres*, 103(D3):3361–3367, feb 1998. doi: 10.1029/97jd02212.

[55] R. L. Mauldin, D. J. Tanner, J. A. Heath, B. J. Huebert, and F. L. Eisele. Observations of h2so4and MSA during PEM-tropics-a. *Journal of Geophysical Research: Atmospheres*, 104(D5):5801–5816, mar 1999. doi: 10.1029/98jd02612.

[56] O. Möhler, T. Reiner, and F. Arnold. The formation of SO_5^- by gas phase ion–molecule reactions. *The Journal of Chemical Physics*, 97(11):8233–8239, dec 1992. doi: 10.1063/1.463394.

[57] M. Müller, T. Mikoviny, S. Feil, S. Haidacher, G. Hanel, E. Hartungen, A. Jordan, L. Märk, P. Mutschlechner, R. Schottkowsky, P. Sulzer, J. H. Crawford, and A. Wisthaler. A compact PTR-ToF-MS instrument for airborne measurements of volatile organic compounds at high spatiotemporal resolution. *Atmospheric Measurement Techniques*, 7(11):3763–3772, nov 2014. doi: 10.5194/amt-7-3763-2014.

[58] M. S. B. Munson and F. H. Field. Chemical ionization mass spectrometry. i. general introduction. *Journal of the American Chemical Society*, 88(12):2621–2630, jun 1966. doi: 10.1021/ja00964a001.

[59] D. M. Murphy, D. W. Fahey, M. H. Proffitt, S. C. Liu, K. R. Chan, C. S. Eubank, S. R. Kawa, and K. K. Kelly. Reactive nitrogen and its correlation with ozone in the lower stratosphere and upper troposphere. *Journal of Geophysical Research: Atmospheres*, 98(D5):8751–8773, may 1993. doi: 10.1029/92jd00681.

[60] Kermit K. Murray, Robert K. Boyd, Marcos N. Eberlin, G. John Langley, Liang Li, and Yasuhide Naito. Definitions of terms relating to mass spectrometry (IUPAC recommendations 2013). *Pure and Applied Chemistry*, 85(7):1515–1609, jun 2013. doi: 10.1351/pac-rec-06-04-06.

[61] NASA. Scientific balloons. https://www.nasa.gov/scientific-balloons/types-of-balloons, 2018.

[62] J. A. Neuman, L. G. Huey, T. B. Ryerson, and D. W. Fahey. Study of inlet materials for sampling atmospheric nitric acid. *Environmental Science & Technology*, 33(7): 1133–1136, apr 1999. doi: 10.1021/es980767f.

[63] A. E. O'Keeffe and G. C. Ortman. Primary standards for trace gas analysis. *Analytical Chemistry*, 38(6):760–763, may 1966. doi: 10.1021/ac60238a022.

[64] WMO (World Meteorological Organization). *Scientific Assessment of Ozone Depletion: 2014.* 2014.

[65] Luc Patiny and Alain Borel. ChemCalc: A building block for tomorrow's chemical infrastructure. *Journal of Chemical Information and Modeling*, 53(5):1223–1228, apr 2013. doi: 10.1021/ci300563h.

[66] Thomas Peter and Jens-Uwe Grooss. Chapter 4. polar stratospheric clouds and sulfate aerosol particles: Microphysics, denitrification and heterogeneous chemistry. In *Stratospheric Ozone Depletion and Climate Change*, pages 108–144. Royal Society of Chemistry, 2011. doi: 10.1039/9781849733182-00108.

[67] Joseph P. Pinto, Richard P. Turco, and Owen B. Toon. Self-limiting physical and chemical effects in volcanic eruption clouds. *Journal of Geophysical Research*, 94 (D8):11165, 1989. doi: 10.1029/jd094id08p11165.

[68] Benoit Plet. TofWerk AG, Thun, Switzerland. Private communication, 2017.

[69] P. J. Popp, T. P. Marcy, R. S. Gao, L. A. Watts, D. W. Fahey, E. C. Richard, S. J. Oltmans, M. L. Santee, N. J. Livesey, L. Froidevaux, B. Sen, G. C. Toon, K. A. Walker, C. D. Boone, and P. F. Bernath. Stratospheric correlation between nitric acid and ozone. *Journal of Geophysical Research*, 114(D3), feb 2009. doi: 10.1029/2008jd010875.

[70] R. W. Portmann, J. S. Daniel, and A. R. Ravishankara. Stratospheric ozone depletion due to nitrous oxide: influences of other gases. *Philosophical Transactions of the Royal Society B: Biological Sciences*, 367(1593):1256–1264, mar 2012. doi: 10.1098/rstb.2011.0377.

[71] R Core Team. *R: A Language and Environment for Statistical Computing.* R Foundation for Statistical Computing, Vienna, Austria, 2013. URL `http://www.R-project.org/`.

[72] Yuri P. Raizer. *Gas Discharge Physics.* Springer, 2011. ISBN 978-3642647604. URL `https://www.amazon.com/Gas-Discharge-Physics-Yuri-Raizer/dp/364264760X?SubscriptionId=0JYN1NVW651KCA56C102&tag=techkie-20&linkCode=xm2&camp=2025&creative=165953&creativeASIN=364264760X`.

[73] W. J. Randel, M. Park, L. Emmons, D. Kinnison, P. Bernath, K. A. Walker, C. Boone, and H. Pumphrey. Asian monsoon transport of pollution to the stratosphere. *Science*, 328(5978):611–613, mar 2010. doi: 10.1126/science.1182274.

[74] Thomas Reiner, Ottmar Möhler, and Frank Arnold. Improved atmospheric trace gas measurements with an aircraft-based tandem mass spectrometer: Ion identification by mass-selected fragmentation studies. *Journal of Geophysical Research: Atmospheres*, 103(D23):31309–31320, dec 1998. doi: 10.1029/1998jd100003.

[75] T. B. Ryerson, L. G. Huey, K. Knapp, J. A. Neuman, D. D. Parrish, D. T. Sueper, and F. C. Fehsenfeld. Design and initial characterization of an inlet for gas-phase NOy measurements from aircraft. *Journal of Geophysical Research: Atmospheres*, 104 (D5):5483–5492, mar 1999. doi: 10.1029/1998jd100087.

[76] D. Salcedo, P.W. Villalta, V. Varutbangkul, J.C. Wormhoudt, R.C. Miake-Lye, D.R. Worsnop, J.O. Ballenthin, W.F. Thorn, A.A. Viggiano, T.M. Miller, R.C. Flagan, and J.H. Seinfeld. Effect of relative humidity on the detection of sulfur dioxide and sulfuric acid using a chemical ionization mass spectrometer. *International Journal of Mass Spectrometry*, 231(1):17–30, jan 2004. doi: 10.1016/j.ijms.2003.09.005.

[77] Javier Sanchez, David J. Tanner, Dexian Chen, L. Gregory Huey, and Nga L. Ng. A new technique for the direct detection of HO_2 radicals using bromide chemical ionization mass spectrometry (br-CIMS): initial characterization. *Atmospheric Measurement Techniques*, 9(8):3851–3861, aug 2016. doi: 10.5194/amt-9-3851-2016.

[78] Hans Schlager. Dlr, germany. Private communication.

[79] Jenca Schmitt. *Aufbau und Erprobung eines in-situ NO/NOy-Mess-Systems am Höhenforschungsflugzeug M55-Geophysica.* PhD thesis, December 2003. URL http://nbn-resolving.de/urn:nbn:de:bvb:19-20960.

[80] J. Schneider, V. Bürger, and F. Arnold. Methyl cyanide and hydrogen cyanide measurements in the lower stratosphere: Implications for methyl cyanide sources and sinks. *Journal of Geophysical Research: Atmospheres*, 102(D21):25501–25506, nov 1997. doi: 10.1029/97jd02364.

[81] J. Schneider, F. Arnold, V. Bürger, B. Droste-Franke, F. Grimm, G. Kirchner, M. Klemm, T. Stilp, K.-H. Wohlfrom, P. Siegmund, and P. F. J. van Velthoven. Nitric acid (HNO3) in the upper troposphere and lower stratosphere at midlatitudes: New results from aircraft-based mass spectrometric measurements. *Journal of Geophysical Research: Atmospheres*, 103(D19):25337–25343, oct 1998. doi: 10.1029/98jd02240.

[82] U. Schumann and H. Huntrieser. The global lightning-induced nitrogen oxides source. *Atmospheric Chemistry and Physics Discussions*, 7(1):2623–2818, feb 2007. doi: 10. 5194/acpd-7-2623-2007.

[83] John V. Seeley, Robert A. Morris, and A. A. Viggiano. Rate constants for the reactions of $CO_3^-(H_2O)_{n=0-5}$ + SO_2: Implications for CIMS detection of SO_2. *Geophysical Research Letters*, 24(11):1379–1382, jun 1997. doi: 10.1029/97gl01323.

[84] Jan D. Skalny, Juraj Orszagh, Nigel J. Mason, J. Alan Rees, Yolanda Aranda-Gonzalvo, and Terry D. Whitmore. Mass spectrometric study of negative ions extracted from point to plane negative corona discharge in ambient air at atmospheric pressure.

International Journal of Mass Spectrometry, 272(1):12–21, apr 2008. doi: 10.1016/j. ijms.2007.12.012.

[85] Brett Slatkin. *Effective Python*. Pearson Technology Group, 2015. URL `https://www. ebook.de/de/product/23675438/brett_slatkin_effective_python.html`.

[86] D. L. Slusher. *Techniques for measuring pernitric acid, peroxyacyl nitrates, and dinitrogen pentoxide by chemical ionization mass spectrometry*. PhD thesis, Georgia Institute of Technology, Atlanta, USA, 2003.

[87] David Stone. Calibration and linear regression analysis: A self-guided tutorial. part 2 – the calibration curve, correlation coefficient and confidence limits. URL `http://www.chem.utoronto.ca/coursenotes/analsci/LinRegr2a.pdf`.

[88] K. A. Tereszchuk, G. González Abad, C. Clerbaux, J. Hadji-Lazaro, D. Hurtmans, P.-F. Coheur, and P. F. Bernath. ACE-FTS observations of pyrogenic trace species in boreal biomass burning plumes during BORTAS. *Atmospheric Chemistry and Physics*, 13 (9):4529–4541, may 2013. doi: 10.5194/acp-13-4529-2013.

[89] Donald C. Thornton. Fast airborne sulfur dioxide measurements by atmospheric pressure ionization mass spectrometry (APIMS). *Journal of Geophysical Research*, 107(D22), 2002. doi: 10.1029/2002jd002289.

[90] TofWerk AG. *Reference Guide for TOF-CIMS Instrument*, 2016.

[91] B. Umann, F. Arnold, C. Schaal, M. Hanke, J. Uecker, H. Aufmhoff, Y. Balkanski, and R. Van Dingenen. Interaction of mineral dust with gas phase nitric acid and sulfur dioxide during the MINATROC II field campaign: First estimate of the uptake coefficient HNO3 from atmospheric data. *Journal of Geophysical Research*, 110(D22), 2005. doi: 10.1029/2005jd005906.

[92] SilcoTek USA. Silcotek coatings. `https://www.silcotek.com/`, 2018.

[93] Claire Vallance. *An Introduction to Chemical Kinetics*. IOP Publishing, 2017. doi: 10.1088/978-1-6817-4664-7.

[94] A. A. Viggiano, John V. Seeley, Paul L. Mundis, John S. Williamson, and Robert A. Morris. Rate constants for the reactions of $XO_3^-(H_2O)_n$ (X = C, HC, and N) and $NO_3^-(HNO_3)_n$ with H_2SO_4: Implications for atmospheric detection of H_2SO_4. *The Journal of Physical Chemistry A*, 101(44):8275–8278, oct 1997. doi: 10.1021/jp971768h.

[95] A. A. Viggiano, D. E. Hunton, Thomas M. Miller, and John O. Ballenthin. In situ measurements of hydrogen cyanide in the upper troposphere/lower stratosphere during arctic spring 2000. *Journal of Geophysical Research: Atmospheres*, 107(D5):SOL 47–1–SOL 47–6, mar 2002. doi: 10.1029/2001jd001033.

[96] M. von Hobe, A. Afchine, J. Barthel, H. Franke, S. Hrechanyy, N. Spelten, V. Tan, U. Winkler, and F. Stroh. HALOX: An Instrument for the In-situ Measurement of ClO Dimer and Chlorine Nitrate. In *EGS - AGU - EUG Joint Assembly*, page 3111, April 2003.

[97] M. von Hobe, J.-U. Grooß, R. Müller, S. Hrechanyy, U. Winkler, and F. Stroh. A re-evaluation of the ClO/Cl_2O_2 equilibrium constant based on stratospheric in-situ observations. *Atmospheric Chemistry and Physics*, 5(3):693–702, mar 2005. doi: 10.5194/acp-5-693-2005.

[98] Marc von Hobe, Nicole Spelten, Corinna Kloss, Yun Li, Talat Khattatov, and Fred Stroh. A compact low cost permeation oven. Manuscript in preparation, 2018.

[99] P. Werle, R. Muecke, and F. Slemr. The limits of signal averaging in atmospheric trace-gas monitoring by tunable diode-laser absorption spectroscopy (TDLAS). *Applied Physics B Photophysics and Laser Chemistry*, 57(2):131–139, aug 1993. doi: 10.1007/bf00425997.

[100] V. Yushkov, A. Oulanovsky, N. Lechenuk, I. Roudakov, K. Arshinov, F. Tikhonov, L. Stefanutti, F. Ravegnani, U. Bonafé, and T. Georgiadis. A chemiluminescent analyzer for stratospheric measurements of the ozone concentration (FOZAN). *Journal of Atmospheric and Oceanic Technology*, 16(10):1345–1350, oct 1999. doi: 10.1175/1520-0426(1999)016<1345:acafsm>2.0.co;2.

[101] ZEA-1. Mechanical certificate of the FunMass instrument RTCA/DO-160G. Available by request (Fred Stroh, f.stroh@fz-juelich.de), 2016.

[102] ZEA-2. Electromagnetic compatibility certificate of the FunMass instrument RTC-DO160E (category M). Available by request (Fred Stroh, f.stroh@fz-juelich.de), 2016.

[103] Jun Zheng, Alexei Khalizov, Lin Wang, and Renyi Zhang. Atmospheric pressure-ion drift chemical ionization mass spectrometry for detection of trace gas species. *Analytical Chemistry*, 82(17):7302–7308, sep 2010. doi: 10.1021/ac101253n.

Acknowledgments

I would like to thank all people with whom I worked in Forschungszentrum Jülich, especially to:

- Dr. Fred Stroh, my scientific adviser, for guiding me throughout all these years and being an excellent supervisor with endless energy and research ideas;

- Prof. Dr. Martin Riese, head of the institute where this work was done, giving me the opportunity to work in FZJ and for supervising my work there. I am also thankful for the invitation to the summer school in Sochi 2016;

- Prof. Dr. Thorsten Benter, who kindly agreed to be the second reviewer of this work;

- Dr. Sascha Albrecht, who developed the CIMS TOF lab prototype upon which FunMass is mainly based;

- Yun Li (soon to be Dr. Li), with whom I spent a lot of excellent teamwork time in the lab while conducting various tests;

- Dr. Marc von Hobe, for the development of the equipment used to calibrate FunMass;

- Vicheith Tan and Axel Schönfeld, for the development and 24/7 support of the electronics of FunMass;

- Armin Afchine, for conducting fluid dynamics simulations for FunMass;

- Dr. Heinz Rongen and Markus Dick for the development and optimization of the electronics for the ion funnel and ion source;

- Jochen Barthel, who put a lot afford in the mechanical design of the FunMass instrument on all stages of the development;

- Christian Tanner from TofWerk AG, who kindly was helping with TOF/TPS related problems arising in the process of the software development of FunMass;

- Nicole Spelten, who helped in the development of the gasdeck;

- Anneliese Richter, for being an absolutely irreplaceable person in the lab;

- Dr. Christian Rolf, with whom I shared the office from the first day, for helping me to adapt to FZJ and Germany;

- Dr. Anne Luebke and Dina Khordakova with whom in different time I shared the office in FZJ, for their recomforting company;

Appendix A
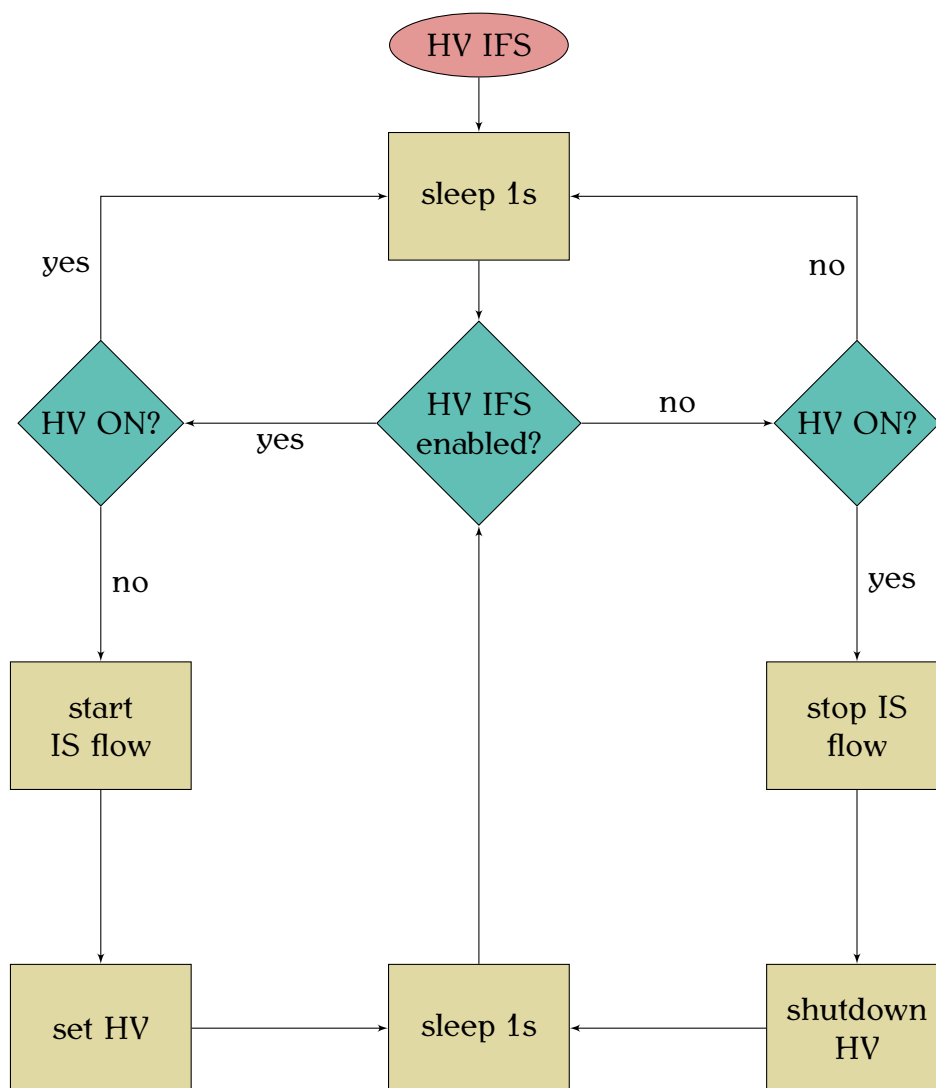
Flowcharts for the FunMass software
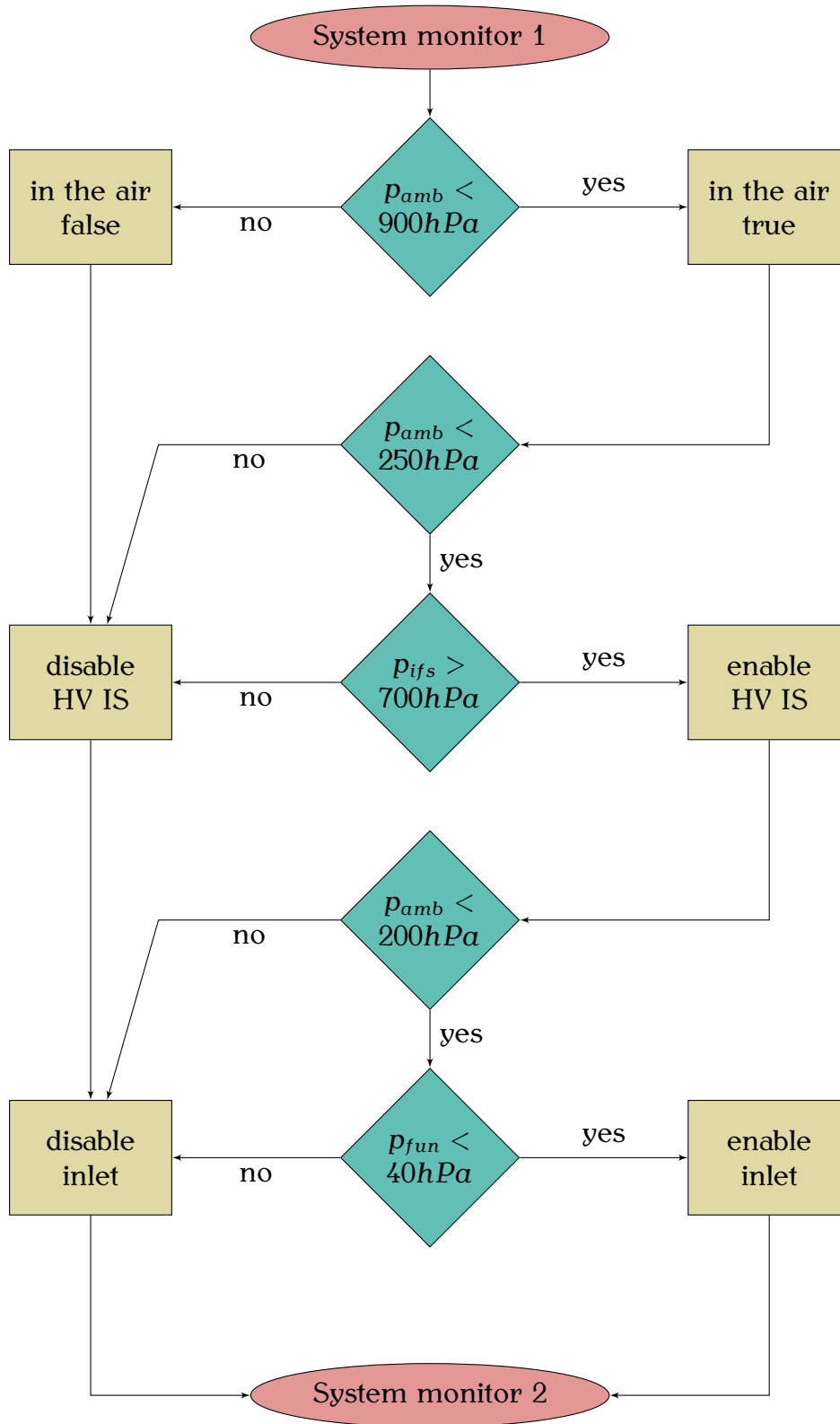

Figure A.1: IFS high voltage task.

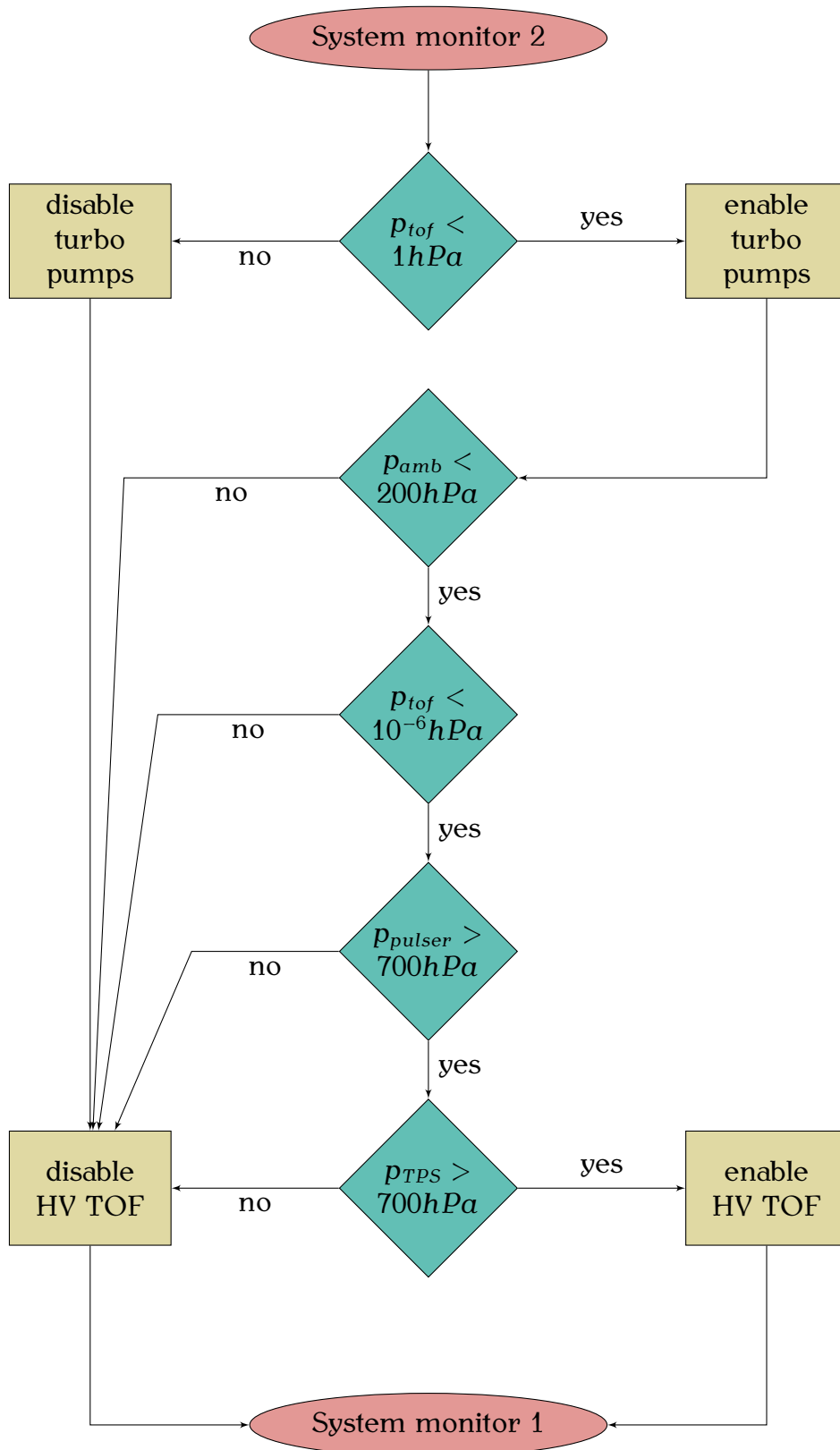Figure A.2: System monitor task. Part 1 out of 2.

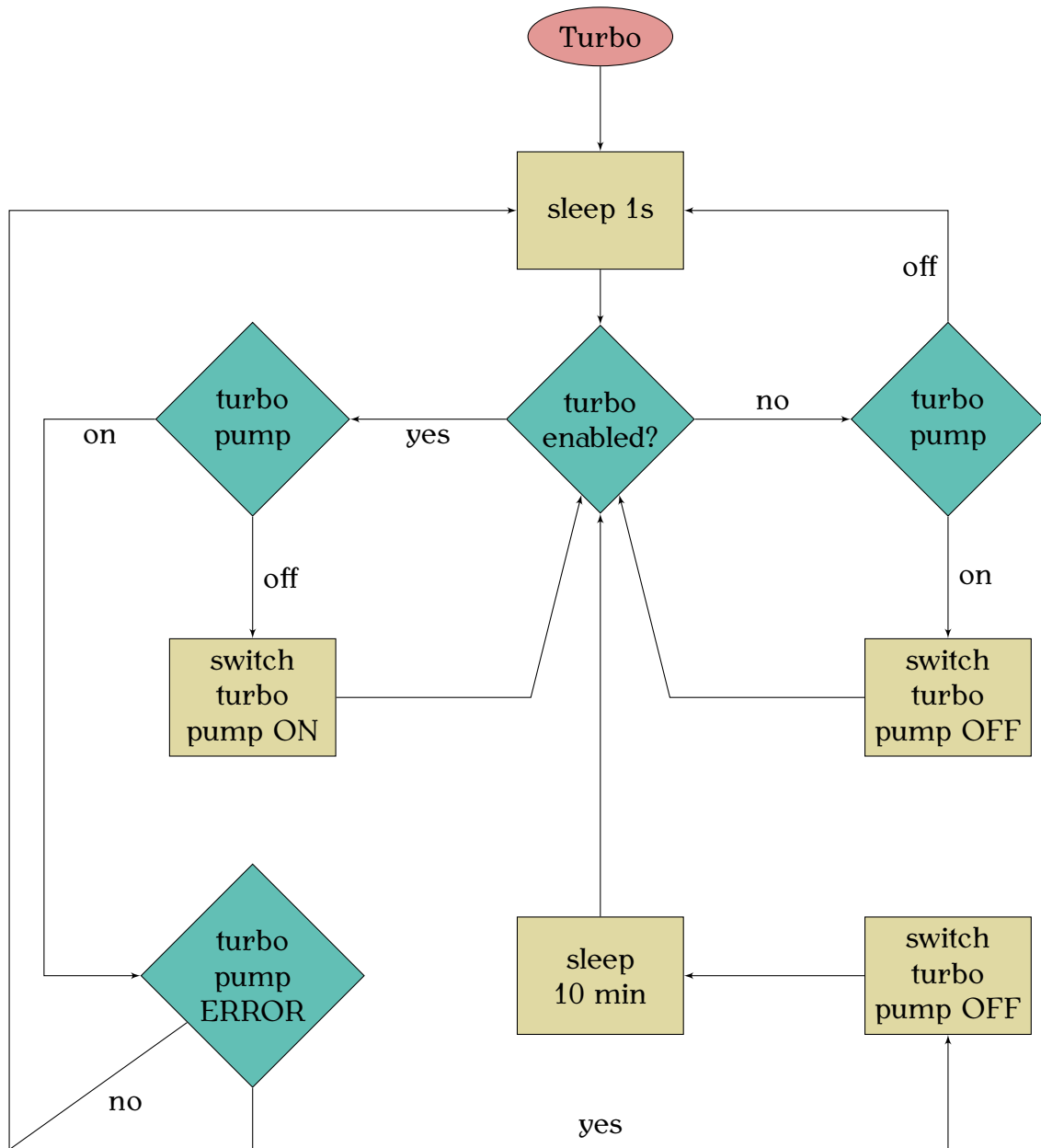Figure A.3: System monitor task. Part 2 out of 2.
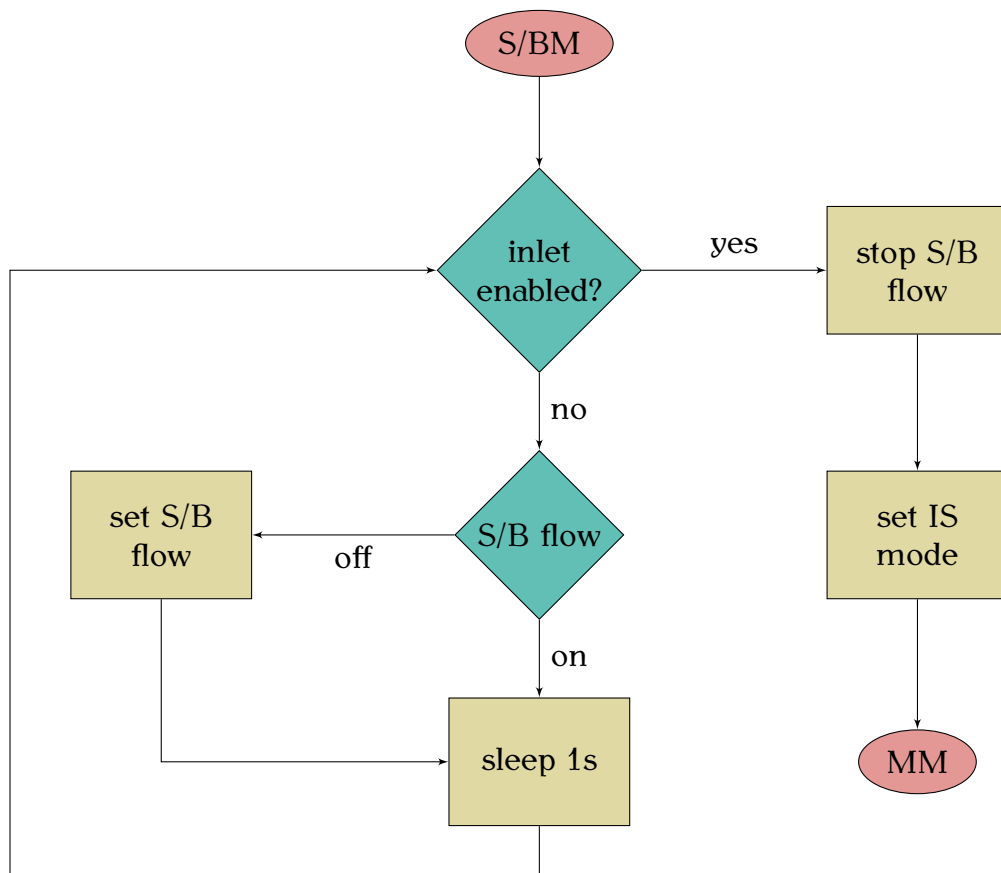
Figure A.4: Turbo pump task.
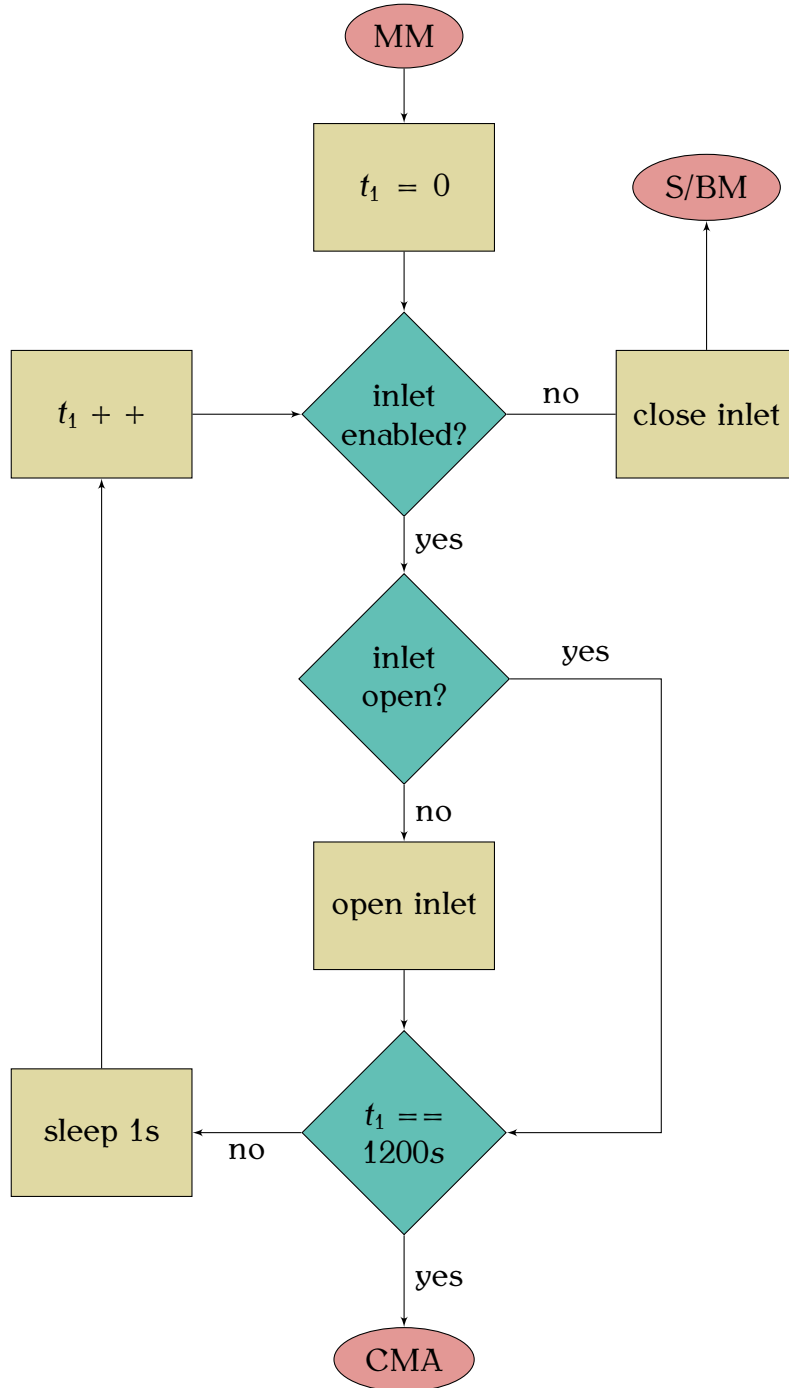
Figure A.5: Standby mode S/BM.

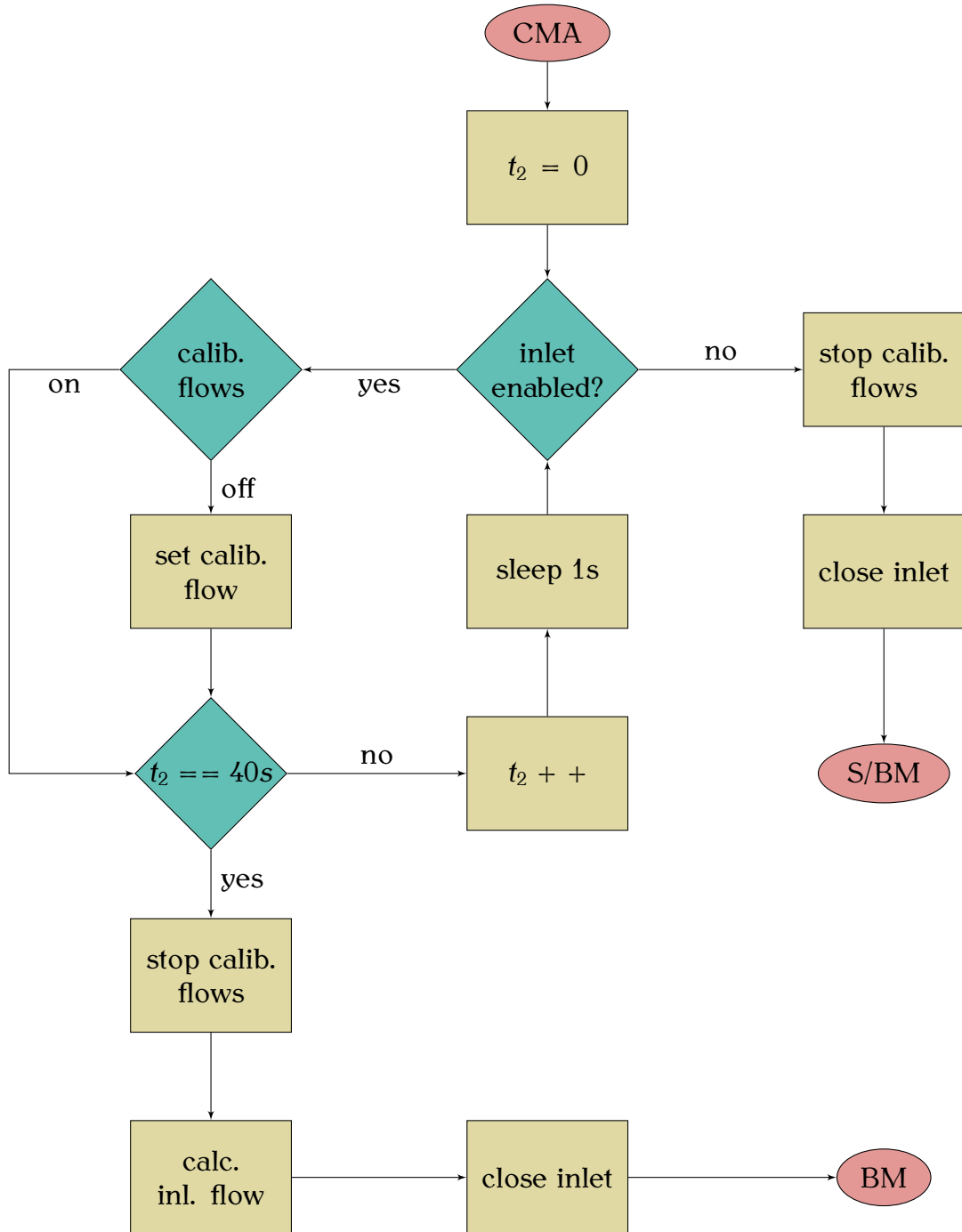Figure A.6: Flow chart of the measurement mode MM.
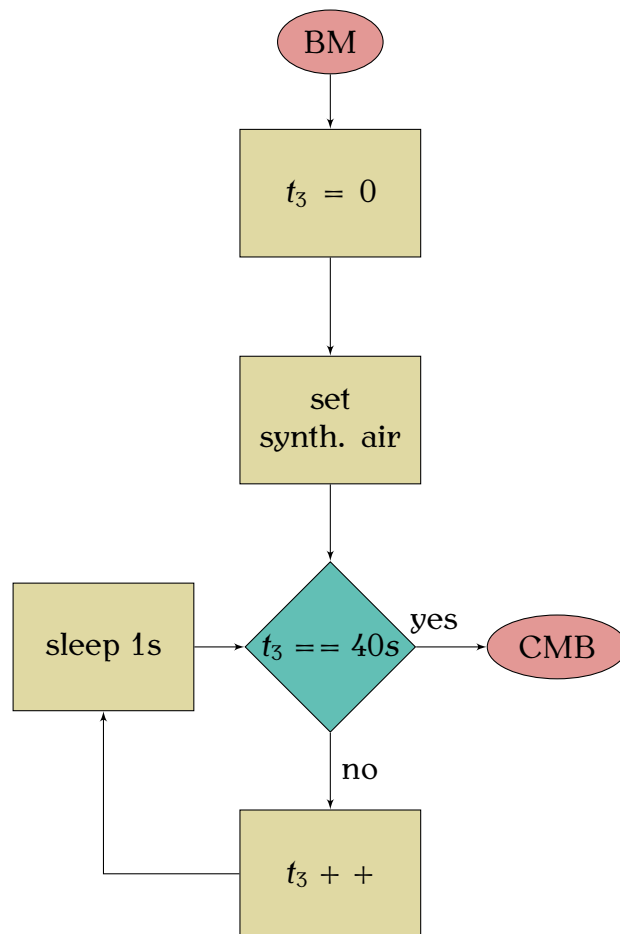
Figure A.7: Calibration mode A CMA.
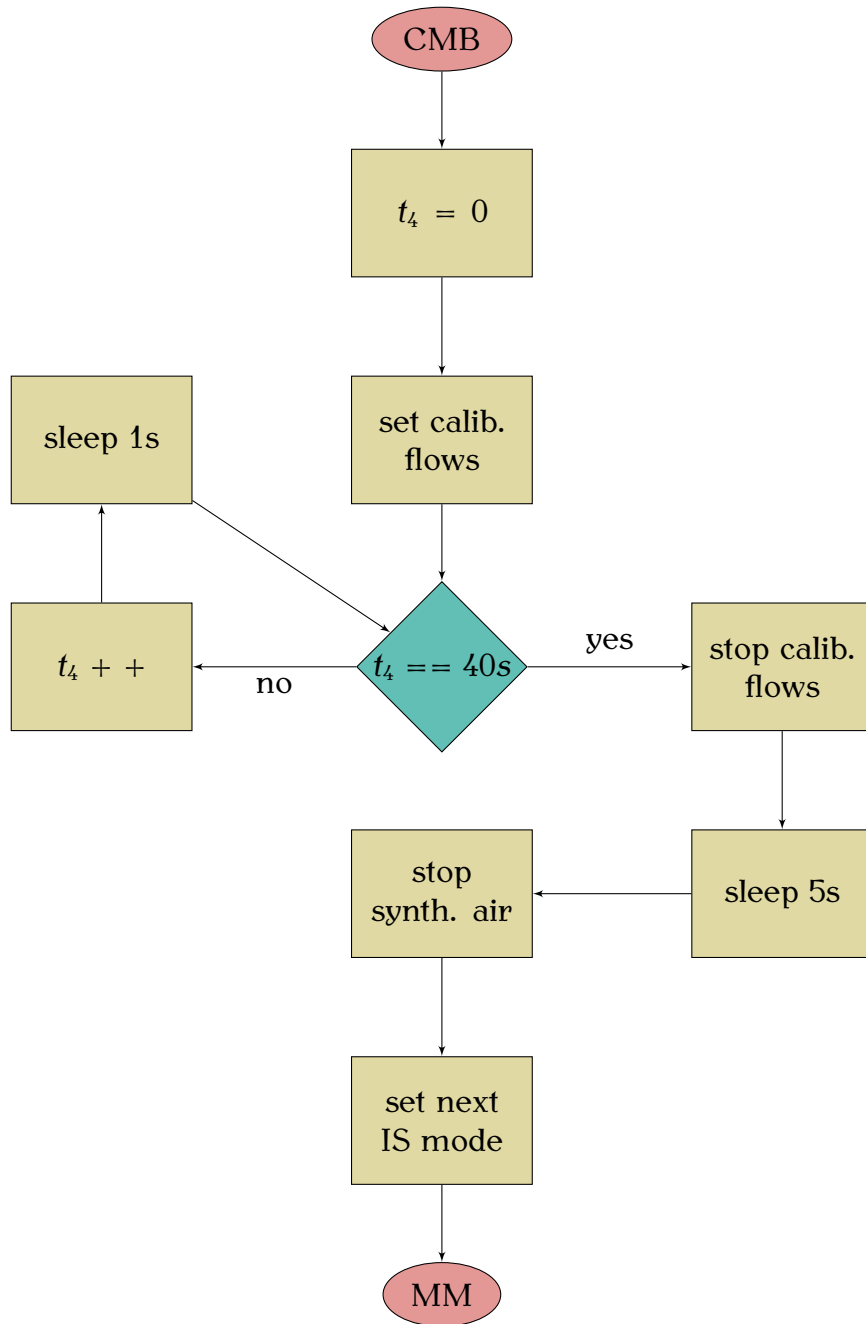
Figure A.8: Background measurements. Blank mode BM.

Figure A.9: Calibration mode B CMB.

Appendix B

Multithreading in Python

B.1 Example of unsafe multithreading

```python
# tested in python 3.6.5
import threading
import time


i = 0


def increment():
    # this function increments global var i 1000000 times
    global i
    for _ in range(1000000):
        i += 1


th1 = threading.Thread(target=increment)
th2 = threading.Thread(target=increment)
th1.start()
th2.start()
time.sleep(2) # wait till threads are finished
print('i should be 2000000, found i = %i' % i)
>>>
i should be 2000000, found i = 1279542
```

The example above is supposed to increment the global variable i by 2×10^6 in two threads parallel by 1×10^6 in each thread. The code executes without any error messages but yields an unexpected result. The troubled moment is that the simple command $i+ = 1$ (i.e. $i = i + 1$) contains four bytecode instructions inside (i.e. this command can be interrupted):

- loads the global variable i onto the stack (LOAD_GLOBAL)

- pushes constant 1 onto the stack (LOAD_CONST)

- implements in-place $i = 1 + i$ (INPLACE_ADD)

- stores new value as a global variable i (STORE_GLOBAL)

The approximate scenario of miscalculations is explained below. The first thread `th1` loads value of the variable i, is interrupted by the second thread `th2`. `th2` gets time to increment i once or several times stores the new value. `th1` takes over of the program exactly where it was interrupted, but still has an old value of i and increments the old i, again stores it to i. Everything that `th2` has done in between is getting lost. In the next section this problem is addressed with the usage of a lock, to make the command $i+ = 1$ free of interruptions. B.2.

B.2 Example of safe multithreading

```python
# tested in python 3.6.5
import threading
import time


i = 0
lock = threading.Lock()


def increment():
    # this function increments global var i 1000000 times
    global i, lock
    for _ in range(1000000):
        with lock:
            i += 1
th1 = threading.Thread(target=increment)
th2 = threading.Thread(target=increment)
th1.start()
th2.start()
time.sleep(2) # wait till threads are finished
print('i should be 2000000, found i = %i' % i)
>>>
i should be 2000000, found i = 2000000
```

Appendix C

Python listings

C.1 Contribution to pyteomics

```python
import itertools
from pandas import DataFrame
from pyteomics import mass
'''
This module extends functionality of pyteomics library with function all_isotoplogues(molecular_formula), which returns
a data frame with all isotoplogues of given molecule with their exact masses and abundances
'''


def tuple2sum_str(tuple_or_list):
    result = ''
    for element in tuple_or_list:
        result += element
    return result


def composition2str(composition):
    formula = ''
    for k, v in composition.items():
        if v != 1:
            formula += k + str(v)
        else:
            formula += k
    return formula


def all_isotopologues(formula):
    """
    :param formula: str H2SO4
    :return:
    """
    composition = mass.Composition(formula)
    dict_elem_isotopes = {}
    for element in composition:
        isotopes = mass.nist_mass[element]
        isotopes = {k: v for k, v in isotopes.items() if k*v[1] != 0}    # deletes from the dict first element with
        # average mass with abundance 1 and delete all isotopes with abundance 0
        list_isotopes = [element + '[' + str(k) + ']' for k in isotopes]
        dict_elem_isotopes.update({element: list_isotopes})
    _all_isotopologues = []
    for element, list_isotopes in dict_elem_isotopes.items():
        n = composition[element]
        list_comb_element_n = []
        for elementXn in itertools.combinations_with_replacement(list_isotopes, n):
            str_element_n = tuple2sum_str(elementXn)
            list_comb_element_n.append(str_element_n)
        _all_isotopologues.append(list_comb_element_n)
    masses, abundances, index = [], [], []
    for isotopologue in list(itertools.product(*_all_isotopologues)):
        str_isotopologue = tuple2sum_str(isotopologue)
        masses.append(mass.calculate_mass(str_isotopologue))
        abundances.append(mass.isotopic_composition_abundance(str_isotopologue))
        index.append(composition2str(mass.Composition(str_isotopologue)))
    data_frame = DataFrame({'Mass': masses, 'Abundance': abundances, 'Formula': formula}, index=index,
                           columns=['Mass', 'Abundance', 'Formula'])
    return data_frame.sort_values(by='Abundance', ascending=False)
```

C.2 FunMass software

The full source code of the FunMass software or parts of it can be requested from Talat Khattatov (t.khattatov@gmail.com) or Fred Stroh (f.stroh@fz-juelich.de).